UNIVERSITY OF ADELAIDE

PHYSICS DEPARTMENT

THESIS FOR THE DEGREE OF MASTER OF SCIENCE

INFRARED ABSORPTION IN THIN METALLIC FILMS

K.C. Liddiard, B.Sc. (Hons)
Research Scientist
Australian Defence Scientific Service

WEAPONS RESEARCH ESTABLISHMENT,
SALISBURY, SOUTH AUSTRALIA

1973

TABLE OF CONTENTS

LIST OF TABLES

LIST OF FIGURES

29. Emissivity of nickel films

30. Absorptance and transmittance of nickel films

31. Structure of formvar substrates

32. Structure of collodion substrates

33. Influence of collodion substrates in electron microscopy

34. Structure of gold films 1

35. Structure of gold films 2

36. Structure of nichrome films

37. Structure of nickel films

38. Stress in nickel film on formvar substrate

39. Thermal rise time measurement. Oscilloscope display

40. Thermal rise time for a gold absorber film

41. Thermal rise time for a nickel absorber film

42. Steady state temperature rise. Gold absorber film

43. Steady state temperature rise. Nickel absorber film

SUMMARY

This thesis describes research studies on the absorption of infrared radiation in thin metallic films. Thin films of nickel, gold and a nickel-chromium alloy were vacuum deposited on to freely-supported polymer membrane substrates. It is intended that these films will comprise the radiation receiver element of high performance infrared detectors.

The research is broadly divided into two main areas of study. These are the infrared optical properties of the selected metal films, and thermal properties relevant to the absorption process such as temperature rise, thermal rise time and thermal spread in the plane of the film. The thermal characteristics are of fundamental importance in infrared detector research, because they determine sensitivity, speed of response and optical image quality.

The first part of the thesis is concerned with a theoretical analysis of the thermal and infrared optical properties of metallic absorber films, and includes a resume of nucleation and growth phenomenon in vacuum deposited metal films. This is followed by a description of measurement techniques and the apparatus used for the preparation of metal films, and then a detailed discussion of experimental results. Careful consideration was given to the influence of deposition parameters, and a study was made of the structure of the films using conventional bright field electron microscopy. Finally, the experimental results are compared with theoretical predictions.

In general, good agreement was found between the theoretical analysis and the measured optical and thermal properties of the selected metal absorber films. This encouraging result enables us to predict the most suitable metal, and the optimum deposition parameters, to satisfy specific requirements in infrared detector research.

STATEMENT

I herewith state that this thesis does not contain any material which has been accepted for the award of any other degree or diploma in any University and that, to the best of my knowledge and belief, the thesis contains no material previously published or written by any other person, except when due reference is made in the text of the thesis.

1. INTRODUCTION

This thesis describes research into the physics of the absorption of infrared radiation in thin metallic films vacuum deposited on to plastic membrane substrates. The aim of the project was to deduce, from fundamental considerations, the desired properties and optimum method of preparation of a simple and efficient infrared absorbing film, which would form the radiation receiver element of a thermal infrared detector.

It is emphasised that the thesis is not concerned explicitly with the study of infrared detectors; nevertheless we should bear in mind the project motivation expressed above, as this must inevitably influence the direction along which research should proceed. It is therefore desirable that we briefly consider the various factors which influence the performance of the thermal detector.

Thermal infrared detectors are distinguished by the common characteristic that the heating effect of the incident infrared radiation causes a measurable change in some physical property of the detector. The temperature sensitive property may be any one of an extensive list of physical parameters, e.g., electrical resistance or capacitance, mechanical flexure, thermoelectric power, expansion of a gas, vapour pressure, optical reflectance, etc. The detector itself is comprised of three basic components, namely an infrared absorber, a temperature sensitive element and a suitable substrate or mechanical support. Depending on the detector type, the individual components need not be discrete; thus the temperature sensitive element may also function as a substrate for the absorber.

In this thesis we consider an important group of detectors in which the infrared absorber is deposited on to a thin self-supporting pellicle. This group includes the thin film resistance bolometer, the dielectric bolometer and various types of infrared imaging sensors. We will be concerned only with the infrared absorber component of the detector. No mention will be made

explicitly of the temperature sensitive component, nor of methods of signal processing. It is important to note, however, that the optical and thermal theory presented in the thesis can be extended to include the temperature sensitive element, and hence may be used to predict the performance of this particular group of detectors.

The first requirement of an efficient thermal detector is that the change with temperature of the relevant temperature sensitive physical property (its 'temperature coefficient') should be of sufficient magnitude to permit the detection of the desired signal level. Two additional factors influence the performance of the thermal detector :

(a) the temperature rise following radiation exposure must be as high as possible, and

(b) the thermal rise time must be sufficiently fast to achieve the desired information rate.

These factors are strongly related to the physical characteristics of the infrared absorber element, and must therefore be considered in this project.

As we would expect, the most suitable metallic film must have an absorptance approaching theoretical maximum. It should also be electrically stable and thermally uniform. Furthermore, if the film is to be supported in vacuo, and suffers surface heat loss solely by radiation exchange with its nearby background, then in order that it may respond rapidly to changes in incident radiant energy, it must possess minimum thermal capacitance. It will be shown that this last requirement is met by the thinnest possible film satisfying the desired optical properties.

In addition to radiation exchange, the absorber film will also suffer heat loss through thermal conduction to the support on which the film is mounted. This thermal spread in the plane of the film will cause a reduction in the speed of response, but also a decrease in the average temperature rise of the absorber

element. The magnitude of the effect depends on the thermal conductivity of the absorber and again on film thickness. Thermal spread will become increasingly significant as the size of the absorber element becomes smaller. In practice, the absorber element of an infrared detector would normally have a surface area of $1mm^2$ or less; therefore the modifications to the thermal properties of an absorber film due to a reduction in surface dimensions should also be considered in this study.

We should note here that the need to keep both thermal capacitance and lateral heat spread to a minimum is the main reason for the selection of thin metallic films for many detector applications, in preference to other well known types of infrared absorbers.

The use of thin plastic substrates is particularly appropriate for experimental investigations because of ease of preparation and high infrared transmission. However, these films do contribute substantially to the overall thermal capacitance; hence in the ideal situation the metallic absorber films should be self-supporting. Unfortunately, with the exception of the metal film resistance bolometer detector (which is self-absorbing), this ideal has no practical value, because a temperature sensitive material will always be required. Nevertheless, experience has shown that we should seek one further property, namely that the metallic film should be structurally continuous.

The research described in the thesis is broadly divided into two main areas of study. These are the optical properties of metallic absorber films in the 8 to 14 μm wavelength region of the electromagnetic spectrum, specifically the response to blackbody radiation near ambient temperature; and thermal properties relevant to the absorption process such as temperature rise due to the absorbed radiation, thermal rise time and lateral heat spread. Thermal properties are discussed in the opening sections. A theory is established which gives the relationship between various thermal parameters, subsequently

leading to the selection of a suitable type of metal for experimental studies. This is followed by a summary of the electromagnetic theory of infrared absorption in metallic films, underlining the fundamental relationship between optical absorption and electrical conductivity.

In view of the importance of electrical conductivity, which is structure dependent, and the desire to achieve structural continuity, some thought should also be accorded to the mechanism of film formation. A brief resume is therefore given of the nucleation and growth process in vacuum deposited metallic films. From our current understanding of the physics of this phenomenon we are able to place further emphasis on the particular choice of metals selected for study.

Based on the theoretical considerations mentioned above, nickel was eventually chosen for detailed experimental investigation. Some results are also included, for comparison purposes, of a brief study of gold and a nickel-chromium alloy.

The final sections of the thesis are devoted to a description of the apparatus used to prepare the metallic films and a detailed account of the experimental results. The experimental investigation is mainly concerned with the dependence of the optical and thermal properties of nickel films on conditions of evaporation, thickness, electrical conductivity and film structure. The results are compared with theoretical predictions.

Symbols used for physical quantities are in accordance with British Standards, except in radiometry where symbols are based on widely accepted notation. This has caused duplication in some instances. However, care has been taken to avoid duplication in the same Sections of the thesis. SI units are used throughout, except for length which is expressed in cm. This is in accord with common practice in infrared technology. As a consequence, density is given in $g.cm^{-3}$. Other submultiples, permissible under the Standard, are

used where convenient for the expression of physical data.

2. THERMAL PROPERTIES OF THIN METALLIC FILMS

2.1 Thermal theory of a thin film infrared absorber

The temperature distribution in the plane of a thin solid film in vacuo depends upon thermal balance between conduction loss to the mounts on which the film is supported, surface radiation exchange with the nearby surroundings and the rate of generation of heat within the film. Since the metallic films considered in this thesis are extremely thin, we can assume that the temperature is independent of thickness and the problem then reduces to that of a solution to the two-dimensional equation of heat conduction in a thin metallic plate with radiation loss at its surface. For the present we may ignore the plastic membrane substrate; its influence can be introduced without loss of generality at a later stage.

If the film has a rectangular area, lying on the x-y plane, then the temperature at any point can, in principle, be determined from the solution to the equation :

$$\rho c \frac{\partial T}{\partial t} = K\left[\frac{\partial^2 T}{\partial x^2} + \frac{\partial^2 T}{\partial y^2}\right] - F(T) + B(x,y,t) \qquad (1)$$

where T = absolute temperature (^oK) at x,y,t

t = time (second)

K = thermal conductivity ($W.cm^{-1}\ ^oK^{-1}$)

ρ = density ($g.cm^{-3}$)

c = specific heat ($J.g^{-1}\ ^oK^{-1}$)

F(T)= surface flux loss per unit volume due to radiation exchange ($W.cm^{-3}$)

B(x,y,t)= rate of generation of heat within the film ($W.cm^{-3}$)

For a film of circular surface area, the heat equation can be expressed in plane polar co-ordinates on carrying out the usual trans-

formations.

As it stands, full solutions to equation (1) are not easily obtained. In particular, there is no exact solution to this problem for surface radiation loss according to the Stefan-Boltzmann fourth power law. In practice, however, we find that suitable approximations can be made which yield solutions of sufficient accuracy for many applications. The most important simplification is the assumption of a linear radiation law, as explained below.

2.1.1 Surface radiation loss

The net energy loss from a thin plate due to Lambertian radiation (i.e., radiance constant with angle) from each surface into a background at temperature $T_o(^oK)$ is given by the Stefan-Boltzmann law, which may be expressed in the form :

$$P_s = 2A_s\sigma\varepsilon(T^4-T_o^4) \text{ watt} \qquad (2)$$

where A_s is the surface area (cm^2), ε is the total emissivity (considered here to be the same for both surfaces), and σ is the Stefan-Boltzmann constant (5.67×10^{-12} W cm^{-2} $^oK^{-1}$).

Equation (2) may be approximated by a Taylor series expansion :

$$P_s = 2\ A_s\sigma\varepsilon\left[4T_o^3(T-T_o)+6T_o^2(T-T_o)^2+\right] \ldots\ldots \qquad (3)$$

Hence for small values of (T-To)

$$P_s \simeq 8A_s\sigma\varepsilon T_o^3(T-T_o) \qquad (4)$$

This equation is often written in the form

$$P_s = G\ \Delta T. \qquad (5)$$

G is called the thermal surface conductance, and, for the problem we are considering, is given by

$$G = 8A_s\sigma\varepsilon T_o^3 \qquad W.(^oK)^{-1} \qquad (6)$$

It is easily shown that for a background temperature T_o of 300^oK the error incurred by the use of the linear radiation loss

approximation is 2.5% when the temperature difference $(T-T_o)$ is 5 deg K rising to 28% for a temperature difference of 50 deg K. In this investigation we will not consider values of $(T-T_o)$ greater than several degrees.

2.1.2 Absorbed radiant energy

The second simplification we can make to the heat conduction equation is in our selection of the form for the expression $B(x,y,t)$. This quantity is just the absorbed energy due to radiant power incident on the metallic film from some remote infrared source. We shall assume that this radiant power is absorbed uniformly throughout the film, and that the radiation exposure is long compared to the thermal time constant of the film.

The assumption of a constant value for $B(x,y,t)$ in no way detracts from the study of the thermal properties of the metallic films. It is of interest to note that in the practical application of infrared detectors any form of modulation of the incident radiant is usually chosen to have a period which is greater than the detector response time. In the present study, the only advantage to be gained by the use of modulated radiation is in the estimation of thermal rise time; but this can just as easily be determined from a step function form of incident irradiation.

2.1.3 Absorber geometry

The final simplification lies in the choice of the surface geometry of the metallic film. There are two geometries of particular interest in this investigation:

(a) In most of the experimental study films are supported on circular mounting rings. In this case, the thermal contours in the film should be radially symmetric. If the diameter

of the film is sufficiently large, then lateral conduction loss to the mounting rings is predominant only over a region near the film boundary which may be approximated by one-dimensional heat flow, and the temperature at the centre of the film then depends only on radiation exchange with the background.

(b) An important concept associated with the practical applications of infrared radiation detectors is that the absorber element should be as small as possible. It is therefore of considerable interest to examine the mechanism of lateral spread of heat in thin metallic films of small surface area. In this study it will be sufficient to consider the flow of heat in a rectangular film supported at two opposing edges by a solid heat sink at temperature $T_o(^oK)$. If we assume that the film is both homogeneous and isotropic we can then quite reasonably reduce the problem to one of linear heat flow along the length of the film between the supports.

2.1.4 The one-dimensional heat equation

The simplifications we may now apply to the general heat equation (1) arising from the discussions of the preceding sub-sections enable us to deduce nearly all of the thermal properties relevant to this study. We shall find that many of the results are applicable to various film geometries. The validity of the results will be demonstrated in a later section by solving the equivalent equation in plane polar coordinates.

Let us assume that a rectangular metallic film of length ℓ and width w, with its length parallel to the x-axis, is freely supported in vacuo at $x = 0, \ell$ by a solid heat sink at temperature

$T_o(^oK)$. The film loses heat from both surfaces by radiation to its nearby background, which for simplicity we shall also consider to be also at temperature $T_o(^oK)$. Hence in thermal equilibrium the temperature of the film is T_o. At time t = 0, the film absorbs a small quantity of energy ΔP watt uniformly throughout its surface due to irradiation from a distant infrared source, causing its temperature to rise by a small amount $\Delta T(^oK)$. ΔT in general will be a function of both x and t. If we write

$$T = T_o + \Delta T \tag{7}$$

then equation (1) may be expressed in the form :

$$\frac{\partial \Delta T}{\partial t} = \frac{K}{\rho c} \cdot \left[\frac{\partial^2 \Delta T}{\partial x^2} + \frac{\partial^2 \Delta T}{\partial y^2} \right] - \frac{G \Delta T}{\rho c v} + \frac{\Delta P}{\rho c v}$$

$$\Delta T = 0; \; t = 0 \tag{8}$$

$$\Delta T = 0; \; x = 0, \ell$$

where $v(cm^{-3})$ is the volume of the absorber element. For simplicity we rewrite equation (8) in the form

$$\frac{\partial \Delta T}{\partial t} = \kappa \frac{\partial^2 \Delta T}{\partial x^2} - \alpha \Delta T + \beta, \tag{9}$$

where

$$\kappa = \frac{K}{\rho c},$$

$$\alpha = \frac{G}{\rho c v},$$

$$\beta = \frac{\Delta P}{\rho c v},$$

and we have assumed isothermal conditions perpendicular to the x-axis, so that $\frac{\partial}{\partial y} = 0$. κ is often referred to as the diffusivity.

Equation (9) is readily solved for the temperature rise, ΔT, by means of established analytical methods (ref. 1). Before proceeding, however, let us first consider an important parameter,

the thermal capacitance of the film, which appears implicitly in the above equations.

2.2 Thermal capacitance

The thermal capacitance of the thin absorbing film is, by definition,

$$C = \rho c v$$

$$= \rho c A_s t \quad (J^{o}K^{-1}) \tag{10}$$

whence

$$\kappa = \frac{KA_s t}{C}$$

$$\alpha = \frac{G}{C}$$

$$\beta = \frac{\Delta P}{C} \tag{11}$$

where t is the film thickness. In keeping with convention t is used for both time and thickness. Since time appears only in the differential equations and their immediate solutions and thickness does not appear explicitly in the same equations, no confusion should arise from this duplication.

The importance of the thermal capacitance is, as we shall see, that it determines the extent to which the film stores heat, and hence its ability to respond to fluctuations in incident radiation. The concept of a simple thermal capacitance may also, in certain circumstances, be extended to a multilayer film.

2.2.1 Application to composite films

Let us now consider a composite film consisting of several layers of different materials, each layer having its own characteristic value of ρ and c. Then providing the temperature at any time and at any given coordinate (x,y) in the plane of the film is assumed to be independent of thickness, i.e., is the same at all points through the film, the total thermal capacitance is :

$$C = A_s \ (\rho_1 c_1 t_1 + \rho_1 c_2 \ t_2 + \rho_3 c_3 t_3 + \ldots.) \tag{12}$$

The concept of a 'lumped' thermal capacitance simply means that a rise in temperature is transmitted from the upper to the lower surfaces of the composite film in a time very much less than the thermal rise time of the entire film. It can be readily shown that this is indeed the case for very thin films of thickness small compared to the surface dimensions.

Carslaw and Jaeger (reference 1, page 100) have considered the case of heat transfer across a slab, one face of which is held at a constant temperature and the other face thermally insulated. This example approximates a thin metallic absorber film deposited onto a plastic membrane in vacuo, for here we may assume that the membrane represents the slab, one surface of which is instantaneously raised to the absorber temperature. A simple calculation shows that for a film thickness of 1000Å the opposite face of the membrane rises to absorber temperature in a time less than 1 μs, which is negligible compared to the typical thermal time constant.

2.2.2 Lateral thermal conductance

The assumption of a lumped thermal capacitance also enables us to extend the diffusivity to include composite films. The quantity Kt may be referred to as the lateral thermal conductance of a thin film (ref. 2). From the above discussion, it is evident that we can substitute in equation (11)

$$Kt = K_1 t_1 + K_2 t_2 + K_3 t_3 + \ldots\ldots \qquad (13)$$

where $K_1, K_2, K_3, \ldots$ are the thermal conductivities of the component layers of the composite film. Hence heat diffuses uniformly along the film as if it had a single diffusivity determined by equations (11), (12) and (13).

2.3 Temperature rise due to absorbed radiation

Provided the assumption of a lumped thermal capacitance is valid, the solution to equation (9) for the temperature rise in the absorber film is applicable to both the metallic film by itself and the absorber-membrane composite film. Note, however, that if the emissivity is not the same for both sides of the composite film, then equation (6) must be multiplied by $(\varepsilon_1 + \varepsilon_2)/2$, where ε_1, ε_2 are the emissivities of the two surfaces.

Equation (9) is readily solved (see, e.g. ref. 1) by letting

$$\Delta T = \Delta T_1 + \Delta T_2 \tag{14}$$

where ΔT_1 is time independent and satisfies

$$\kappa \frac{d^2 \Delta T_1}{dx^2} - \alpha \Delta T_1 + \beta = 0$$
$$\Delta T_1 = 0; \quad x = 0, \ell \tag{15}$$

and ΔT_2 is a function of both x and t and satisfies

$$\frac{\partial \Delta T_2}{\partial t} = \kappa \frac{\partial^2 \Delta T_2}{\partial x^2} - \alpha \Delta T_2$$
$$\Delta T_2 = 0; \quad x = 0, \ell \tag{16}$$
$$\Delta T_2 = \Delta T \; ; \; t = 0$$

The solution to the time independent equation (15) represents the important case of steady state temperature and deserves detailed examination.

2.3.1 Steady state solution

When the time is large compared to the thermal time constant of the film, equation (15) yields the steady state solution :

$$\Delta T_S = \frac{\beta}{\alpha} \left[1 - \frac{\sinh \mu x - \sinh \mu(\ell - x)}{\sinh \mu \ell} \right] \tag{17}$$

where $\mu = \sqrt{\frac{\alpha}{\kappa}}$

It follows that the maximum temperature rise for a film of finite length occurs at the mid point, when

$$\Delta T_m = \frac{\beta}{\alpha} \left(1 - \operatorname{sech} \frac{\mu \ell}{2}\right) \tag{18}$$

The ratio β/α has particular significance. If the film was not terminated at $x = \ell$, but was of infinite length, then the solution to the steady state conduction equation would be :

$$\Delta T = \frac{\beta}{\alpha} \left(1 - e^{-\mu x}\right) \tag{19}$$

Thus, in this case, when x is large the temperature rise attains the theoretical maximum value

$$\Delta T_o = \frac{\beta}{\alpha} \tag{20}$$

$$= \frac{\Delta P}{G}$$

It is evident from equation (18) that the temperature at the centre of a finite film approaches the maximum value when ℓ is large. Also, if the absorbed energy ΔP is due to an incident infrared irradiance of H_o ($W.cm^{-2}$) then from equation (6) it follows that the maximum temperature rise is independent of both emissivity and area, and for a given value of T_o depends only on the magnitude of H_o.

2.3.2 Average temperature rise

When lateral conduction loss to the film supports is significant it is often of value to estimate the average temperature rise under steady state conditions. This is given by

$$\Delta T_a = \frac{1}{\ell} \cdot \int_o^{\ell} \Delta T_s dx \tag{21}$$

Carrying out the integration we find that

$$\Delta T_a = \Delta T_o \cdot \left[1 - \frac{2}{\mu \ell} \left(\frac{\cosh \mu \ell - 1}{\sinh \mu \ell} \right)\right] \tag{22}$$

The average temperature rise approaches the maximum value when ℓ is large or, for a given length, when $1/\mu$ is small.

2.3.3 Time dependent temperature rise

On solving equation (16) and adding equation (17) we arrive at the full solution of the heat conduction equation :

$$\Delta T = \Delta T_S - 4 \frac{\Delta T_O}{\pi} \sum_{n=1}^{\infty} \frac{\ell^2 \mu^2}{(2n-1)\left[(2n-1)^2\pi^2+\ell^2\mu^2\right]} . \sin \frac{(2n-1)\pi x}{\ell} . \exp . \left[-\alpha t - t\left\{\kappa (2n-1)^2 \frac{\pi^2}{\ell^2}\right\}\right] \quad (23)$$

This is a slowly convergent series and in order to obtain sufficiently accurate estimates of temperature rise, use was made of a digital computer. Some results are included in the analysis of typical thin film absorbers in Section 2.7.

The time dependent average temperature rise is obtained by integration of equation (23). Term-by-term integration is valid in this case, and the solution is in the same form as equation (23) with ΔT_s replaced by ΔT_a, with the sine term replaced by $1/(2n-1)$ and each term of the series multiplied by $2/\pi$.

2.4 Thermal rise time

We have seen above that when ℓ is sufficiently large the mid-point temperature approaches the maximum value ΔT_O, the temperature rise attained for an infinitely long film. The same result would be achieved for a finite film if there were not lateral conduction loss. For this special case of uniform temperature, equation (9) becomes

$$\frac{\partial \Delta T}{\partial t} + \alpha \Delta T = \beta \quad (24)$$

with the solution

$$\Delta T = \Delta T_O \left(1-e^{-\alpha t}\right) \quad (25)$$

By analogy to the electrical theory of RC circuits we define a thermal time constant

$$\tau = 1/\alpha \qquad (26)$$
$$= \frac{C}{G}$$

which is the time taken for the temperature to rise to (1-1/e) of the final maximum value. The analogy is often taken further by defining the reciprocal of G to be the thermal resistance.

Equation (26) is quite general (see e.g., reference 3). It is applicable to other surface loss mechanisms, such as solid or gaseous conductive heat loss, although in these cases the expressions for both the thermal conductance and thermal capacitance are often quite complex and the concept of a simple time constant may no longer apply. The important point to note, however, is that if the thermal surface conductance is increased in order to improve the response of the absorber to changes in incident radiation there inevitably follows a decrease in temperature rise. This is the well known compromise between the sensitivity and speed of response of infrared detectors.

The above considerations demonstrate that when radiation exchange is the predominant surface loss mechanism the only effective means of obtaining a small value of τ is to seek minimum thermal capacitance. Hence since the value of the product ρc does not vary greatly for most materials (typically 2 to 4 $J.cm^{-3}\ {}^{o}K^{-1}$) the only remaining avenue is to ensure that the film is as thin as possible. In arriving at this conclusion we should also observe that the value of τ is independent of area.

When lateral conduction loss to the film supports is significant the temporal dependence of the temperature rise in the film must be determined from equation (23). The foregoing discussion nevertheless demonstrates that when the length of the film is large, the temperature rise and rate of response at the centre of the film is closely approximated by equations (20) and (26).

2.5 Thermal spread

In the same way that we characterize an absorber film by its maximum temperature rise and response time, we can also introduce another parameter which is a measure of lateral spread of heat in the film. From the solution for an infinitely long film (equation (19) above), it is seen that the distance from the film support over which the temperature rises to (1-1/e) of the maximum value is simply $1/\mu$. We define a thermal spread or space constant X, such that

$$X = 1/\mu$$

$$= \sqrt{\frac{K}{\alpha}} \qquad (27)$$

$$= \sqrt{\frac{KA_S t}{G}}$$

This useful concept has been employed widely by fellow members of the author's laboratory as a figure of merit for the spread of heat in thin absorber films. It is applicable to composite films (provided the lumped parameter approximation is valid),and is a readily measured quantity.

It follows from the definition of the thermal surface conductance G that the space constant is independent of surface area. For a given surface loss, therefore, X is dependent only on the thermal conductivity and thickness of the film (or component films). Unfortunately metals are typified by extremely high values of thermal conductivity, and hence we must again conclude that the absorber film should be as thin as possible. By comparison, the contribution to the thermal spread due to the plastic substrate film is almost negligible, because its thermal conductivity is small and its thickness is comparable with that of the metal film.

A numerical estimate of the thermal spread constant provides a simple and useful means of predicting how large the absorber film must be in order to avoid significant loss of heat to nearby heat sinks. Thus, from

equation (18), the centre of the film rises to (1-1/e) of the maximum temperature when

$$\operatorname{sech} \frac{\ell}{2X} = e^{-1}$$

i.e. when

$$\ell \simeq 3.3X \tag{28}$$

The average temperature rises to the same value when

$$\ell \simeq 5X \tag{29}$$

The centre point temperature rises to 90% of the maximum value when length of the film is $6X$.

2.6 Solution in plane polar coordinates

The above treatment based on a one-dimensional approximation of the heat conduction equation is dependent upon several simplifying assumptions which tend to cast some degree of doubt on the generality of the final results. In particular, since we are primarily concerned in this study with the analysis of the properties of circular films of fairly small dimensions, it is desirable to test the validity of the theory by seeking a solution of the heat conduction equation in plane polar coordinates.

On carrying out the usual transformations we obtain :

$$\frac{\partial \Delta T}{\partial t} = \kappa\left[\frac{\partial^2 \Delta T}{\partial r^2} + \frac{1}{r}\frac{\partial \Delta T}{\partial r} + \frac{1}{r^2}\frac{\partial^2 \Delta T}{\partial \theta^2}\right] - \alpha\Delta T + \beta \tag{30}$$

where r is the radial coordinate and θ is the azimuthal angle. From the obvious symmetry of the problem we may ignore θ, so that under steady state conditions, equation (30) becomes :

$$\kappa\left[\frac{d^2\Delta T}{dr^2} + \frac{1}{r}\frac{d\Delta T}{dr}\right] - \alpha\Delta T + \beta = 0 \tag{31}$$

We require the temperature rise to be finite at the origin and zero at the edge of the film.

A solution is obtained on making the substitution :

$$\phi = \alpha\Delta T - \beta, \tag{32}$$

whence

$$r^2\frac{d^2\phi}{dr^2} + r\frac{d\phi}{dr} - r^2\mu^2\phi = 0, \tag{33}$$

and $\mu=\sqrt{\alpha/\kappa}$ as before. Equation (32) is in the form of the modified Bessel Equation of zero order and parameter μ. The solution is

$$\phi= C_1I_o(\mu r) + C_2K_o(\mu r) \tag{34}$$

where C_1 and C_2 are constants. Thus the solution to equation (31) is :

$$\Delta T = \frac{1}{\mu^2}\left[C_1I_o(\mu r) + C_2K_o(\mu r) + \frac{\beta}{\kappa}\right] \tag{35}$$

Since the temperature rise cannot be infinite at the centre of the film C_2 must be zero, and the remaining boundary condition provides that

$$C_1 = -\frac{\beta}{\kappa}\frac{1}{I_o(\mu a)} \tag{36}$$

where a is the radius of the film. The final solution, is therefore :

$$\Delta T_s = \Delta T_o\cdot\left[1-\frac{I_o(\mu r)}{I_o(\mu a)}\right] \tag{37}$$

ΔT_o is just the optimum temperature rise obtained in the earlier theory.

2.6.1 Maximum temperature rise

The maximum temperature rise occurs at the centre of the film where r is zero. $I_o(\mu r)$ is then unity by definition, whence

$$\Delta T_m = \Delta T_o\left[1-\frac{1}{I_o(\mu a)}\right] \tag{38}$$

It follows from the trend of I_o that the temperature rise approaches the maximum possible value ΔT_o at the centre of the film when the radius is large compared with the space constant $\chi = 1/\mu$. However, when this is not the case, the centre temperature rises to (1-1/e) of the maximum possible value when

$$I_o(\mu a) = e \qquad (39)$$

$$2a \simeq 4.5X$$

Thus the diameter of a circular film should be roughly 1.5 times larger than the length of a rectangular strip in order to reach the same temperature.

2.6.2 Temperature rise near the boundary

In order to compare the temperature rise near the boundary of a circular film with that of a rectangular film, it is convenient to carry out the substitution :

$$r = a - \Delta r$$

whence

$$\Delta T = \Delta T_o \cdot \left[1 - \frac{I_o(\mu(a-\Delta r))}{I_o(\mu a)}\right] \qquad (40)$$

If we let

$$a = \zeta \Delta r$$

and

$$\Delta r = 1/\mu$$

then

$$\Delta T = \Delta T_o \cdot \left[1 - \frac{I_o(\zeta-1)}{I_o(\zeta)}\right] \qquad (41)$$

From readily available tables for $e^{-z} \cdot I_o(z)$ it is easily shown that

$$\Delta T \to \Delta T_o \left(1 - \frac{1}{e}\right), \quad \zeta >> 1, \qquad (42)$$

which is the same result obtained when $X=1/\mu$ in the theory of Section 2.5.

This simple treatment suggests that when the film diameter is large compared to the thermal spread constant, the temperature distribution across the film is adequately described by one-dimensional theory. The results of the introductory problem

presented in Section 2.7 support this conclusion.

2.7 Thermal analysis of a typical thin film infrared absorber

2.7.1 Considerations in the selection of a suitable absorber element

We have now reached a stage where sufficient theory has been established to enable us to predict the thermal characteristics of a thin metallic film upon absorption of infrared radiation. Initially the author is interested in the selection of an infrared absorber which would eventually prove suitable for use in infrared radiation detectors. The final selection of this absorber element cannot be based entirely on thermal properties, as consideration must also be given to other factors such as ease of preparation, structure, stability and repeatability. An understanding of the thermal properties is, however, quite essential as there are certain fundamental conditions which must be met, as we have seen in the preceding discussions.

On the other hand, since the computations must, in the first instance, be based on known bulk values of thermal conductivity, specific heat and density, we cannot concede the validity of the results if these basic properties differ from the bulk when in the thin film form. The estimation of the thermal conductivity and the product of specific heat and density, from practical measurement of the thermal rise time and lateral thermal spread, is indeed a most important part of this research project. The results of the thermal analysis enable us to predict with confidence the conditions under which these measurements are valid, and conversely, the measured quantities enable us to make more accurate predictions.

In order to illustrate the application of thermal analysis to the study of thin film infrared absorbers, a problem has been constructed

representative of the conditions likely to be encountered in practice. It is assumed that this typical infrared absorber element consists of a thin metallic film vacuum deposited on to a freely-supported plastic film stretched across a gap in a perfect heat sink mounted in vacuo. The analysis is divided into three parts, as follows :

(a) The computation of the temperature rise of a rectangular absorber element when the dimensions are so small that there is a substantial lateral thermal loss to the heat sink.

(b) The extension of part (a) to an absorber of much larger dimensions, typical of the specimens used in the experimental section of the project.

(c) A comparison between the results of parts (a) and (b) and the computations for an absorber of circular area and similar size.

We will assume in each case that the thickness t_1 of the metallic film is 100Å and its emissivity 0.5, and that the thickness of the plastic film is 500Å. The reason for the selection of an emissivity of 0.5 will become evident in Section 3 of the thesis. The emissivity of a plastic film of the given thickness is typically less than 0.02. Hence it does not significantly contribute to the overall absorption (see also Section 3.4.2).

It is also assumed that Kirchoff's Law can be applied (see Section 3.1), i.e., the emissivity of the metallic absorber is equal to its absorptance. This pre-supposes a Lambertian radiation law, which we have already assumed in Section 2.1.1.

Gold, nickel and nichrome have been selected for inclusion in

this analysis. These are representative of high, medium and low thermal conductivity absorber materials. Nichrome is a nickel-chromium alloy. The particular alloy chosen for study has the composition 80Ni:20Cr. A number of metals have in fact been investigated, but their inclusion in the thermal analysis yields little further information.

The bulk thermal properties of the selected materials are listed in Table 1. The values shown for the substrate material are typical of many thermoplastics.

TABLE 1. BULK THERMAL PROPERTIES OF SELECTED ABSORBER MATERIALS

	ρ $g.cm^{-3}$	c $J.(g.^{o}C)^{-1}$	ρc $J.cm^{-3}.{}^{o}C^{-1}$	K $W.(cm.^{o}C)^{-1}$
Gold	19.3	0.130	2.5	3.0
Nickel	8.8	0.440	3.87	0.595
Nichrome	8.2	0.420	3.44	0.11
Thermoplastic substrate	1.5	1.5	2.25	0.002

A FORTRAN program incorporating the thermal equations of the preceding subsections has been prepared by the author for an I.B.M. 7090 Computer. This program was used to derive the results of the thermal problem now described.

2.7.2 Incident infrared radiation

Whilst it is not necessary for the purpose of this analysis to determine an accurate value of the incremental power, ΔP_o, incident on the infrared absorber, an estimate of the radiant power intercepted from a typical source of infrared radiation is of particular interest. Such an estimate is required in the experimental investigation of infrared absorption as it enables

us to predict the rise in absorber temperature for a given rise in source temperature.

Let the infrared radiation source be a blackbody Lambertian radiator of area A situated at a distance R from the absorber element. Blackbody radiation can be very nearly realised in practice by means of specially shaped cavities. These cavity sources are widely used in radiometric research.

If the temperature of the source rises above ambient by an incremental amount ΔT_S, then it is easily shown from radiometric theory that the corresponding incremental change in source radiance at $300^{o}K$ is given by

$$\Delta N = 2.02 \times 10^{-4} \Delta T_S \quad (W.cm^{-2} sr^{-1}) \tag{43}$$

The irradiance at the absorber is

$$\Delta H = \frac{A}{R^2} \Delta N , \qquad (W.cm^{-2}) \tag{44}$$

assuming there is no transmission loss in the intervening atmosphere.

If the absorber element is placed in the focal plane of an optical system of focal ratio F_o, so that the source more than fills the field of view, then the incremental irradiance at the focal surface is :

$$\Delta H_o = \frac{\tau_o \pi \Delta N}{4 F_o^2} \tag{45}$$

where τ_o is the transmission of the optical system.

The absorbed radiant power is

$$\Delta P = \varepsilon \Delta H_o A_S \tag{46}$$

where ε is the absorber emissivity and A_S the surface area. In practice it becomes difficult to achieve a focal ratio much less than unity. Thus for an f/1 optical system of transmission 0.9, and an absorber emissivity 0.5, the absorbed power is

$$\Delta P = 1.44 \times 10^{-5} \varepsilon A_S \Delta T_S \tag{47}$$

for a source at temperature $300^{o}K$.

2.7.3 Temperature rise for a small rectangular absorber element

This is part (a) of the thermal problem outlined above. Let the length of the absorber be 0.1 cm.

The maximum temperature rise assuming loss of heat from the film by radiation only, is determined from equations (6), (20) and (46). Thus :

$$\Delta T_o = \Delta P/G$$

$$= \frac{\Delta H_o}{8\sigma T_o^3} \qquad (48)$$

For the incident radiant power given by equation (47),

$$\Delta T_o = 0.1176^{o}K \text{ (or } ^{o}C)$$

when

$$\Delta T_s = 1^{o}K$$

Thus in the ideal situation a rise in source temperature of approximately $8.5^{o}C$ is required to raise the absorber temperature by $1^{o}C$.

It is important to note that the maximum temperature is independent of both surface area and emissivity. It also does not depend on the type of absorber material. However, if we are to observe the rise in temperature over a reasonable period of time, then we must seek a sensible thermal response time. On assuming a lumped thermal capacitance, equations (12) and (26) give the thermal time constant

$$\tau = \frac{\rho_1 c_1 t_1 + \rho_2 c_2 t_2}{8\sigma\epsilon T_o^3} \qquad (49)$$

where $\rho_1 c_1$ and $\rho_2 c_2$ refer to the metal and plastic substrate respectively. Hence we require an absorber film of high emissivity. However, we cannot infer from equation (49) which is the best

absorber, only that it - and the plastic substrate - should be as thin as possible.

Now let us consider the influence of conduction loss.

The thermal phenomenon which determines the choice of a particular metal for a small absorber element is the lateral thermal spread. Again assuming lumped parameters we find from equations (13) and (27) that the thermal spread constant for the composite film is given by :

$$\chi = \sqrt{\frac{K_1 t_1 + K_2 t_2}{8\sigma\varepsilon T_o^3}} \qquad (50)$$

Thus, as we might expect, the lateral spread of heat is strongly dependent on the thermal conductivity of the metallic component. Table 1 shows that the contribution due to the plastic substrate is small in comparison (provided it is sufficiently thin). Again we note the dependence on film thickness.

As we have already seen the temperature rise in the film does not attain the theoretical maximum value ΔT_o unless the length is large compared to χ. That this is not the case in the present example is evident from the computation of both the temperature rise at the centre of the film and the average temperature rise, which are tabulated for the selected materials, together with the computed thermal time constants and thermal spread constants, in Table 2. The table shows that only the nichrome absorber,which has a low thermal conductivity, meets the conditions of equations (28) and (29). Nichrome is, in fact, a most useful infrared absorber, but for reasons we will see later, it is not always the most suitable material.

TABLE 2. COMPUTED THERMAL PARAMETERS

Absorber	τ (ms)	x (μm)	ℓ/χ	$\Delta T_m/\Delta T_o$	$\Delta T_a/\Delta T_o$
Gold	22.47	701.2	1.43	0.21	0.14
Nickel	24.7	314.4	3.18	0.61	0.42
Nichrome	24.00	140.0	7.14	0.94	0.72
Film length			0.1 cm.		
Absorber thickness			100Å		
Substrate thickness			500Å		

It is interesting to note that in the absence of the plastic substrate, i.e., for a self-supporting absorber element, the value of τ is very much smaller (e.g. for nickel it is only 5 ms) whereas the temperature rise and thermal spread are essentially unchanged. Therefore, from the thermal point of view, the only significant influence of the plastic support film is its contribution to the thermal capacitance of the composite film.

The steady state temperature rise along the film, computed from equation (17) for the three absorber materials, is plotted in figure 1. These curves readily demonstrate that it is wise to avoid high conductivity metals such as gold unless the absorber dimensions are quite large; whilst it is almost certainly necessary to choose a low conductivity material such as nichrome for very small absorbers. On the other hand, another interesting result emerges when we plot the time dependent temperature rise (equation (23)). Figure 2 illustrates this computation for nickel; it shows that steady state conditions are almost realised when the time exceeds $\tau/2$. This is not so for nichrome, as is evident from figure 3. Figure 3 shows the time dependent average temperature rise for the selected metallic absorbers. It is clearly seen that the

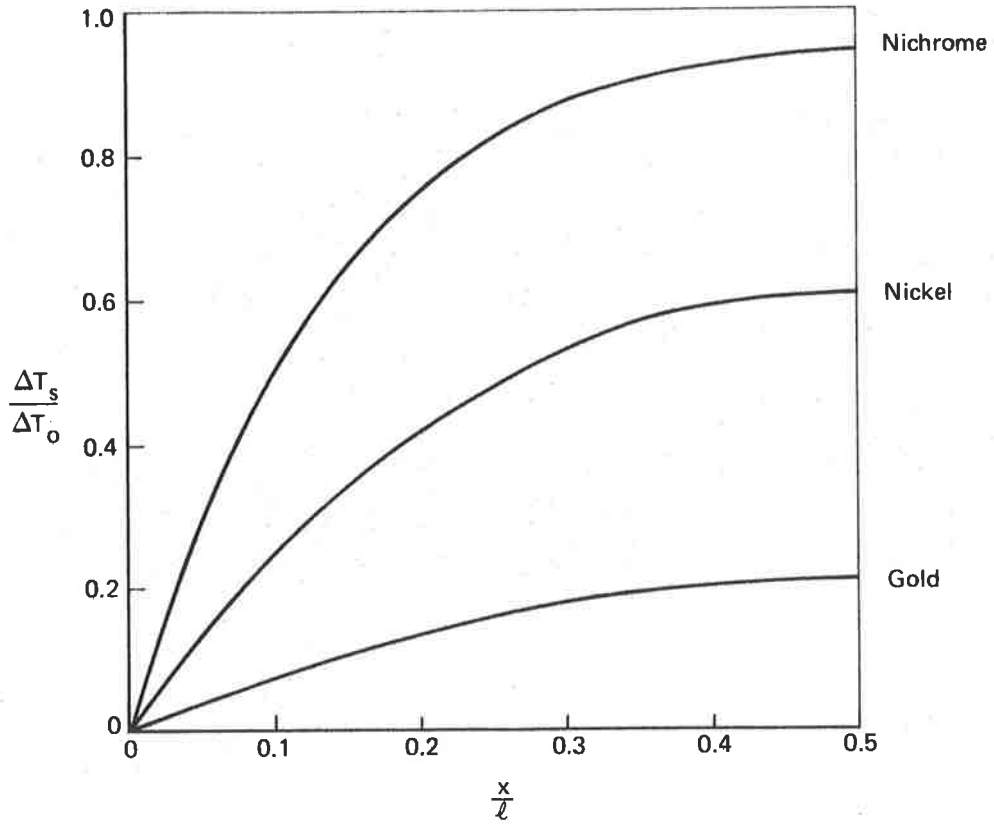

Figure 1. Steady state temperature rise. Selected metallic absorbers

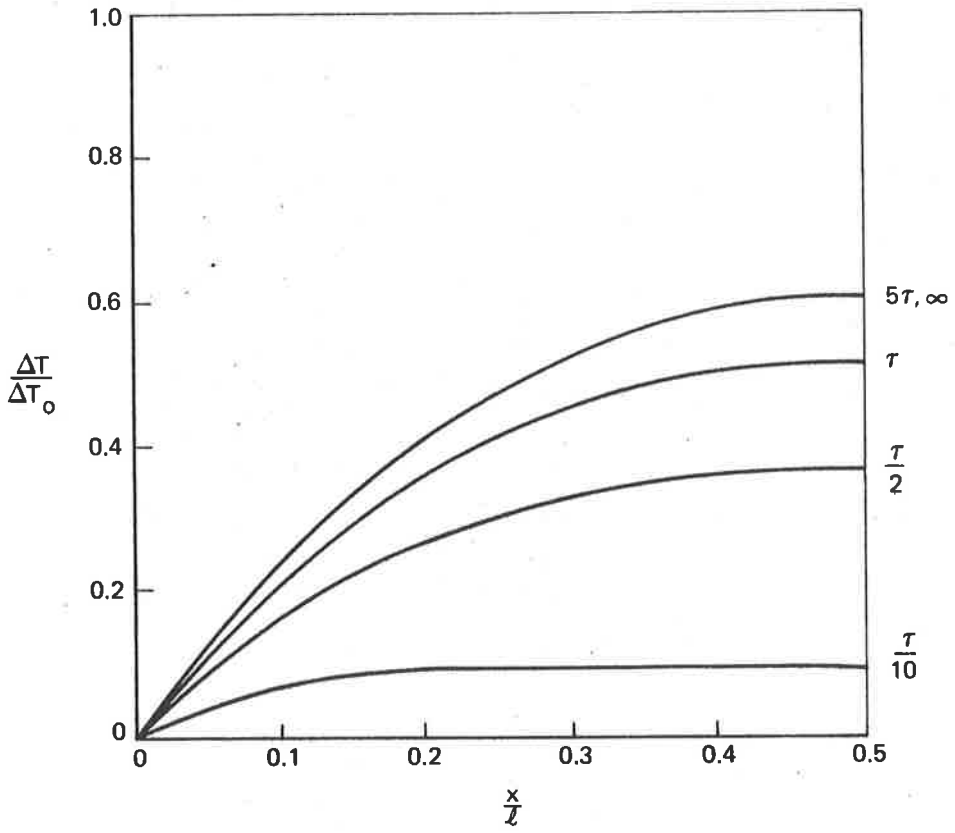

Figure 2. Time dependent temperature rise. Nickel absorber

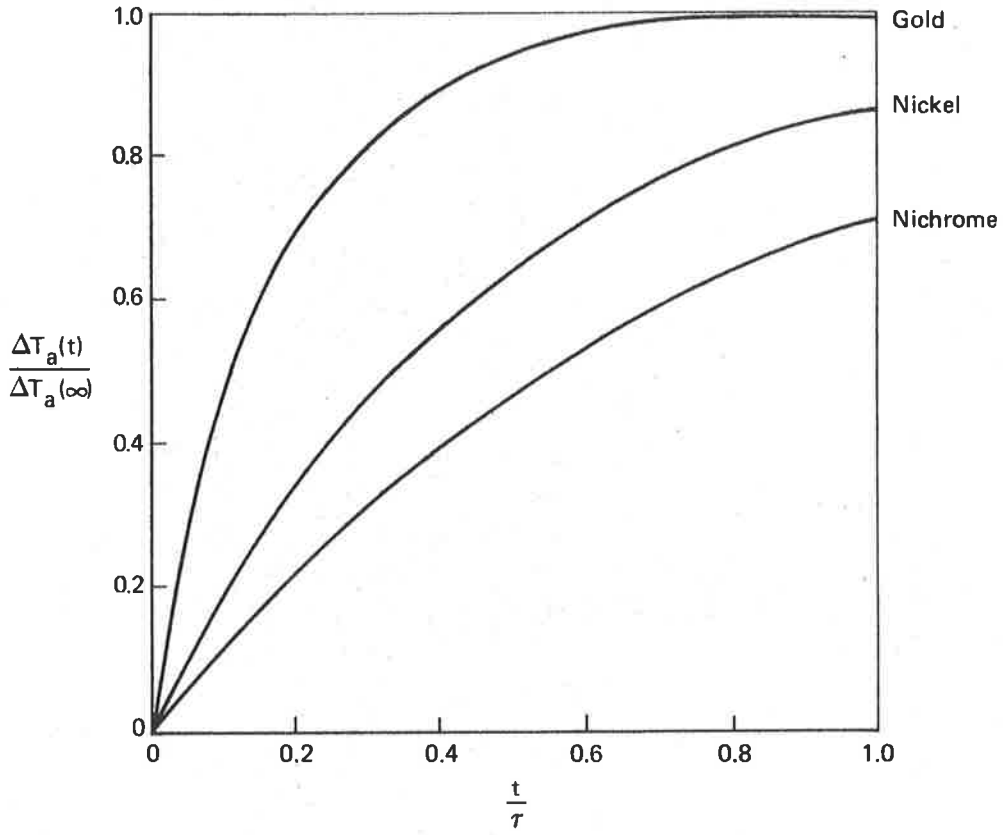

Figure 3. Time dependent average temperature rise. Selected metallic absorbers

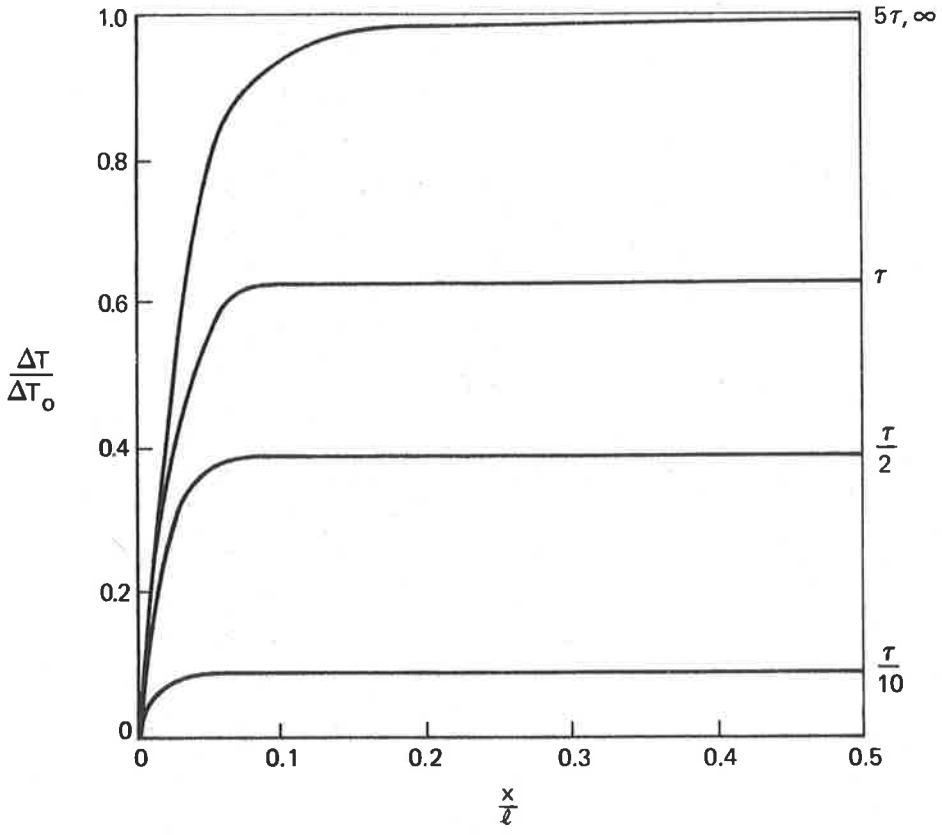

Figure 4. Time dependent temperature rise. Large area nickel absorber

temperature rise is much faster for materials of higher thermal conductivity, although the actual magnitude of the temperature rise is lower. This result is relevant to the study of infrared detectors where it is often desirable to sacrifice sensitivity for speed of response. In such a case a compromise is necessary.

2.7.4 Temperature rise for a large absorber element

In this section we extend the above analysis by increasing the length of the absorber to 1.0 cm. This change does not alter the values of τ and χ; however, it is now found that

$\ell = 14.3\chi$ for gold

$\ell = 31.8\chi$ for nickel, and

$\ell = 71.5\chi$ for nichrome.

Thus in all cases, the temperature rise at the centre of the film approaches the theoretical maximum value ΔT_o. The time dependent results for nickel are illustrated in figure 4. The absorber is now sufficiently large to approximate the conditions for an infinite film, as evident from the observed rise in temperature to (1-1/e) of the maximum value in time τ. The temperature will rise to 99.995% of its maximum possible value in time 5τ and when this condition is reached the value of χ can be read off the x-axis at the (1-1/e) ordinate.

These results are of particular significance in this project for it is evident that the thermal time constant can be determined experimentally by a simple radiometric measurement of the temperature rise at the central region of the film, whilst the thermal spread constant can be estimated from the output trace of a scanning radiometer under steady state conditions. These measurements in turn provide data for the computation of the thin film ρc product and the

thermal conductivity.

2.7.5 Absorbers of circular area

In concluding this theoretical study we now examine the remaining variable discussed in Section 2.1, the surface geometry of the absorber film. Circular elements are widely used in infrared radiometry - including the experimental sections of this study, and hence are of special interest. The above theoretical problem is readily extended to absorbers of circular symmetry by making use of the solutions in plane polar coordinates derived in Section 2.6.

A direct comparison with the results for a small rectangular strip is obtained by selecting an absorber diameter, 2a, of 0.1 cm. The steady state temperature rise for the selected absorber metals, computer from equation (37), is illustrated in figure 5. It can be seen that lateral conduction loss is more significant for a circular film. In this particular example, the maximum temperature rise is 56%, 70% and 92% of the corresponding rise for the rectangular film, for gold, nickel and nichrome, respectively.

As the diameter of the film increases the temperature distribution across the film steadily approaches the one-dimensional distribution derived in Section 2.3.1. When the diameter is 1.0 cm, the distribution across the nickel film is effectively indistinguishable from the curves shown in figure 4, including the region near the boundary. This result follows directly from the theory of Section 2.6.2.

We are able to conclude confidently that the temperature distribution across a thin film infrared absorber is essentially independent of absorber geometry provided the shortest linear dimension of the film is large compared to the thermal spread

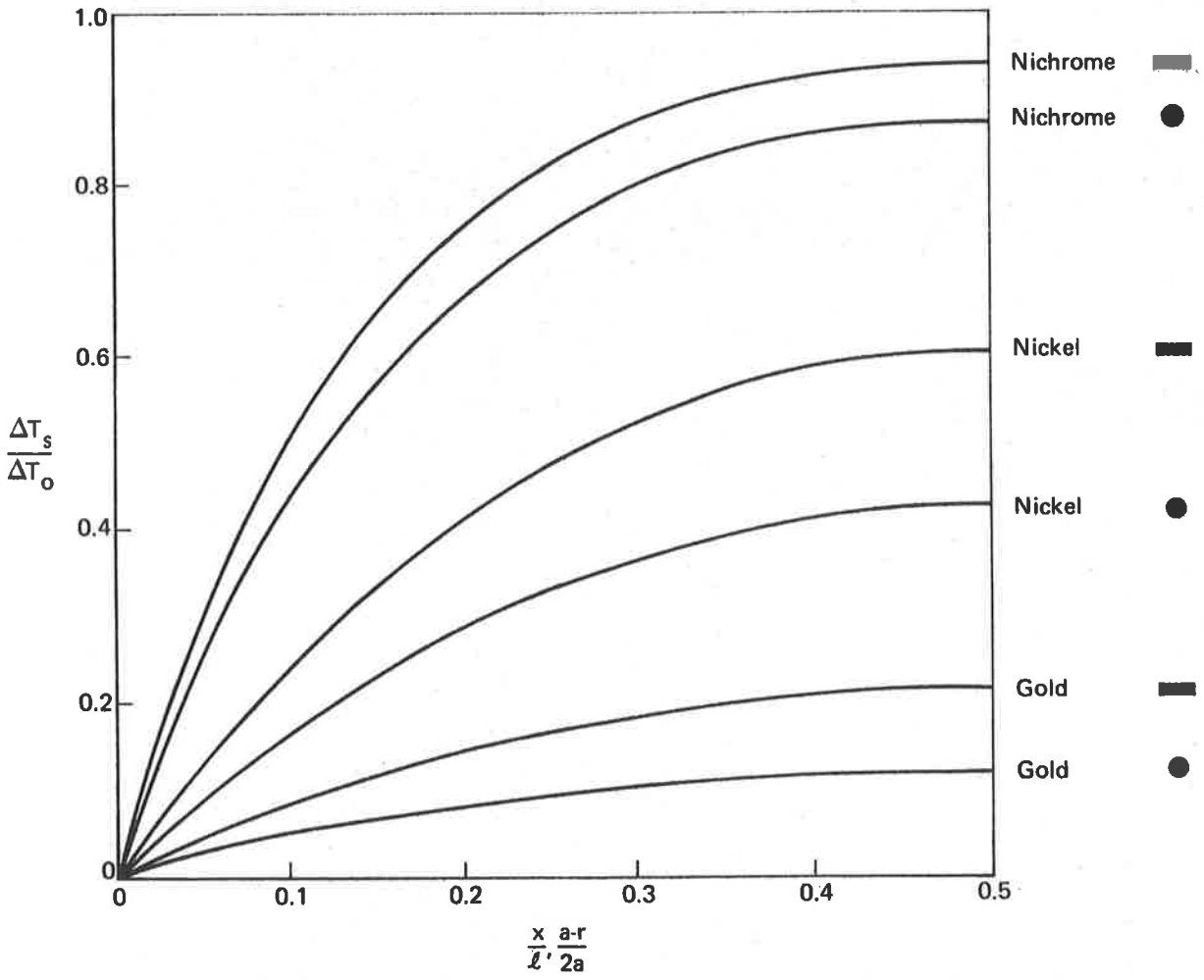

Figure 5. Steady state temperature rise for rectangular and circular absorber elements

constant. Just how large depends on the accuracy required. As a guideline it is readily shown that the error in the application of the one-dimensional theory to the solution of the temperature distribution across a circular absorber of diameter 10χ is less than 2.5%. This guideline is equally applicable to other absorber geometries, such as a rectangular element supported at each edge when the temperature distribution is determined along the centre line between the opposing parallel edges.

3. OPTICAL AND ELECTRICAL PROPERTIES OF THIN METALLIC FILMS

3.1 Introductory note on radiometry

In Section 2 we discussed the heating effects of infrared radiation absorption in metallic films. The efficiency of energy transfer depends on the absorptance of the film, which we have assumed to be equal to the emissivity. This assumption is of fundamental importance in our study of infrared absorption, and is a consequence of the application of Kirchoff's Law (see, e.g., ref. 4). The laws of radiometry require that the sum of the absorptance, α, reflectance, ρ, and transmittance, τ, be unity, thus:

$$\begin{aligned} \alpha &= \varepsilon \\ \alpha+\rho+\tau &= 1 \\ \varepsilon &= 1 - (\rho+\tau) \end{aligned} \qquad (51)$$

where ε is the emissivity. In the strict sense we should call this quantity the "emissance" (see ref. 4), reserving the term "emissivity" for intrinsic material properties. However, it is common practice to use "emissivity" for both intrinsic material properties and measured specimen properties.

The emissivity of a plane surface may be expressed in three different forms :

(a) the hemispherical emissivity, measured over the total hemisphere enclosing the surface;

(b) the directional emissivity, measured at some direction to the surface represented by the angular coordinates (θ,ϕ), or

(c) the normal emissivity, which is the directional emissivity measured normal to the surface.

These may be further divided into spectral emissivity, whereby the emissivity is measured over a small wavelength interval of the emission spectrum and is given a λ subscript; and total emissivity, measured over the total spectral range. The former is just the ratio of the spectral emittance of the surface (radiant power per unit area per unit wavelength interval) to that of a blackbody, and the latter the ratio of the total (integrated) emittance of the surface to that of a blackbody.

In Section 2 we considered only total emissivity. Furthermore, we assumed the absorber film to be a Lambertian surface, i.e. a perfectly diffuse surface with a radiance (radiant power per unit surface area per unit solid angle) independent of viewing angle. For such a surface the hemispherical and directional emissivities are equal. In practice it is found that the difference between the hemispherical emissivity and the normal emissivity is usually small, except for polished metals, where this difference may be as high as 20%; whilst the variation with angle, even for metals, does not become significant until the angle exceeds 45^{o} to the normal.

The hemispherical emissivity is important in the calculation of radiant heat transfer. The normal emissivity, which is the quantity usually measured and quoted, is important in the determination of absorption from distant sources, as in the case of infrared detectors. By definition, the two emissivities are equal for a Lambertian radiator, and in practice the assumption of Lambertian characteristics is sufficient for most applications.

3.2 Electromagnetic theory of the optical properties of absorbing media

The absorption of infrared radiation in thin metallic films can be adequately described by means of classical electromagnetic theory. The interaction of radiation with absorbing media of high electrical conductivity turns out to be much simplified at far-infrared wavelengths, and the absorption mechanism is readily explained from well established theory (see, e.g. ref. 5). The following brief summary outlines the fundamental concepts.

The wave equation for the electric field $\underset{\sim}{E}$ in conducting media is

$$\nabla^2 \underset{\sim}{E} = \sigma\mu\mu_o \frac{\partial \underset{\sim}{E}}{\partial t} + \varepsilon_1\varepsilon_o \mu\mu_o \frac{\partial^2 \underset{\sim}{E}}{\partial t^2} \qquad (52)$$

where σ is the electrical conductivity, μ the permeability, μ_o the permeability of free space, ε_1 the relative permittivity or dielectric constant and ε_o the permittivity of free space. The permittivity is suitably subscripted to avoid confusion with the emissivity.

If we consider propagation parallel to the x-axis we may write a solution to equation (52) in the form

$$\underset{\sim}{E} = \underset{\sim}{E}_o \exp i\omega \left(t - \frac{\underset{\sim}{n}x}{c}\right) \qquad (53)$$

where ω is the angular frequency, c is the wave velocity in free space and $\underset{\sim}{n}$ is the complex refractive index. By convention we define $\underset{\sim}{n}$ as

$$\underset{\sim}{n} = n - ik \qquad (54)$$

where n is the refractive index of the material and k is the absorption index. Substitution of equation (54) into (53) readily yields the observed experimental law for absorption (Lambert's absorption law).

Equation (52) is satisfied, provided

$$\underset{\sim}{n}^2 = n^2 - k^2 - 2ink$$

$$= \varepsilon_1\mu - i\frac{\sigma\mu}{\varepsilon_o\omega} \qquad (55)$$

Thus, for non-magnetic media

$$n^2 - k^2 = \varepsilon_1$$

and

$$2nk = \sigma/\varepsilon_o\omega \tag{56}$$

The classical theory assumes a continuous medium in which the dielectric constant and electrical conductivity both have constant values. This is not so at high frequencies, where both quantities are complex and frequency dependent. Thus, by convention, we write the complex dielectric constant in the form

$$\begin{aligned} \underset{\sim}{\varepsilon} &= \varepsilon_1 - i\varepsilon_2 \\ &= \underset{\sim}{n}^2 \\ &= n^2 - k^2 - 2\,ink \end{aligned} \tag{57}$$

Whence

$$\begin{aligned} \varepsilon_1 &= n^2 - k^2 \\ \varepsilon_2 &= 2nk \end{aligned} \tag{58}$$

and $\varepsilon_1, \varepsilon_2$ are both frequency dependent. A full treatment requires recourse to quantum optics (see, e.g. reference 6 for a useful summary) and is beyond the scope of this study. We need only consider here the broad results for metallic absorption.

3.2.1 Absorption in metals

Optical absorption in metals is concerned with the interaction of incident radiation with free and bound electrons. Ignoring the latter, which is not significant at infrared wavelengths, we find that the Drude-Lorentz theory for free electron absorption in metals gives the following formulae for the dielectric constant (ref. 7).

$$\begin{aligned} \varepsilon_1 = n^2 - k^2 &= 1 - \frac{Ne^2}{m\varepsilon_o}\left(\frac{1}{\omega^2+g^2}\right) \\ \varepsilon_2 = 2nk &= g^2\,\frac{\sigma}{\varepsilon_o\omega}\left(\frac{1}{\omega^2+g^2}\right) \end{aligned} \tag{59}$$

where N is the free electron concentration, m is the electronic mass, e is the electronic charge and g is the collision frequency (the inverse of relaxation time). The low frequency (static) conductivity is given by

$$\sigma = \frac{Ne^2}{mg}, \tag{60}$$

and is the limiting case of the complex conductivity

$$\underset{\sim}{\sigma} = \sigma \frac{1 - i(\omega/g)}{1 + (\omega/g)^2} \tag{61}$$

Thus when $\omega << g$, ε_1 approaches a constant value and equation (59) approximates equation (56).

The value of g can be determined from equation (60). For metals it corresponds to a frequency range in the far infrared. For long wavelengths it is then readily shown that

$$n \simeq k \simeq \sqrt{\frac{\sigma}{2\varepsilon_o \omega}} \tag{62}$$

It would seem that the absorption of thermal infrared radiation in metallic films is a complicated phenomena, not amenable to simple treatment. The situation, however, is not as difficult as it appears. The reflectivity at normal incidence for a metal surface is

$$\rho = \frac{(n-1)^2 + k^2}{(n+1)^2 + k^2} \tag{63}$$

Applying equation (62),

$$\rho = 1 - 2\sqrt{\frac{2\varepsilon_o \omega}{\sigma}} \tag{64}$$

Thus classical theory predicts that a metal, whilst being an excellent absorber, also reflects nearly all radiation incident on its surface. It has been found from experiment that the reflectivity of high conductivity metals is in accord with equation (64) at wavelengths down to about 5 μm. The simple Maxwellian theory is therefore adequate - though perhaps not fully valid - to describe

optical absorption in metals in the infrared at wavelengths greater than 5 μm. It is not adequate in the near infrared, and fails completely in the visible.

3.3 Thermal radiation sources

Reference has already been made to the use of "blackbody" radiation sources in this study. The term "blackbody" is of course a theoretical idealism, but, as noted earlier, such a source can very nearly be realised in practice by means of carefully designed cavities.

This project is concerned with the absorption of thermal blackbody radiation from sources near ambient temperature. The spectral distribution of the emitted radiation is given by Planck's Law and the total energy is determined from the Stefan-Boltzmann Law. Figure 6 shows the spectral emittance for various source temperatures. It will be noted that most of the radiation is emitted in the far-infrared. For a source at $300^{o}K$ the peak of the emission curve lies at 9.6 μm and the curve falls to 0.6% of the peak value at 3 μm. The $400^{o}K$ curve falls to 7.5% of the peak value at 3 μm.

It is well known that when infrared radiation travels any distance through the atmosphere at sea level it is selectively absorbed by atmospheric gases and vapours, primarily carbon dioxide and water. In particular, there exists an opaque region from roughly 5 to 8 μm, and "windows" from 3 to 5μm and 8 to 14 μm, which are of special significance with regard to the detection of thermal radiation.

From the above comments it appears that we will not be far wrong if we make use of the classical theory of electron absorption in metals in order to seek formulae for the absorption of thermal radiation in thin metallic films. This approach leads to a considerable simplification in the theory and yields sufficiently accurate estimates of the infrared absorption.

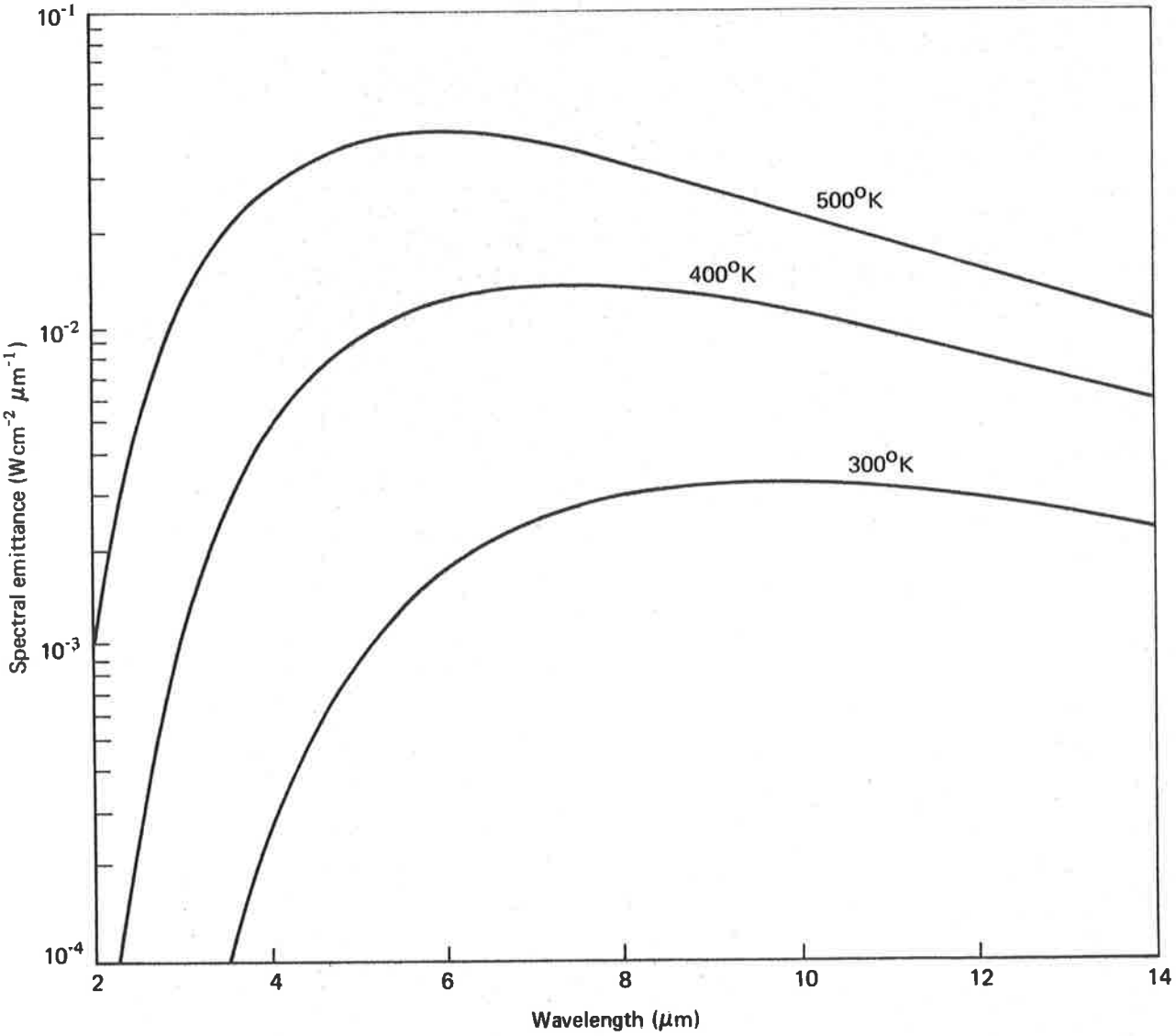

Figure 6. Blackbody radiation for three selected temperatures

3.4 Infrared absorption in thin metallic films

The theory of the optical properties of thin films is well established and excellent treatises on this important topic are given in various texts, e.g., the books by Heavens (ref. 8) and Vasicek (ref. 9). This theory is primarily concerned with non-absorbing dielectric films. We would expect that the results can be extended to thin absorbing films by the introduction of the complex dielectric constant. This derivation has been carried out from basic principles in a laborious but excellent paper by Hadley and Dennison (ref. 10). The results have been checked by the author of this thesis by the more direct method stated above.

The reflectance and transmittance of a thin absorbing film at normal incidence is given by :

$$\rho = \frac{1}{D_o} \cdot \left[(n^2+k^2+1)^2 - 4n^2\right]\left[\cosh\frac{4\pi kt}{\lambda} - \cos\frac{4\pi nt}{\lambda}\right] \tag{66}$$

$$\tau = \frac{8}{D_o} \cdot (n^2+k^2) \tag{67}$$

$$D_o = \left[(n^2+k^2+1)^2 + 4n^2\right]\cosh\frac{4\pi kt}{\lambda} + 4n(n^2+k^2+1)\sinh\frac{4\pi kt}{\lambda} - \left[(n^2+k^2-1)^2 - 4k^2\right]\cos\frac{4\pi kt}{\lambda} + 4k(n^2+k^2-1)\sin\frac{4\pi kt}{\lambda} \tag{68}$$

where t is the thickness of the film and λ is the wavelength of the incident radiation. These equations apply to any absorbing film over the visible and infrared spectrum. For the special case of a metallic film in the far infrared, whose thickness is small compared to the wavelength of the incident radiation, the above equations, with the aid of equation (62), reduce to the simple form

$$\rho = \Phi^2/(\Phi+2)^2$$

$$\tau = 4/(\Phi+2)^2 \tag{69}$$

and, from equation (51), we obtain the absorptance (equal to emissivity)

$$\alpha = 4\Phi/(\Phi+2)^2 \ , \tag{70}$$

where

$$\Phi = \sigma t \sqrt{\frac{\mu_o}{\varepsilon_o}}$$

$$= 120\pi\sigma t \qquad (71)$$

$(\sigma t)^{-1}$ is just the resistance per square (sheet resistance) of the metal film, i.e.,

$$R_S = 120\pi/\Phi \quad \text{ohm per square} \qquad (72)$$

The relationships (69) and (70) are plotted in figure 7. The results show that the maximum absorptance, and hence emissivity, of a thin metallic film is

$$\alpha = 0.5,$$

when

$$\Phi = 2,$$

and

$$R_S = 189 \text{ ohm per square} \qquad (33)$$

The most significant outcome of the Hadley and Dennison theory is that the emissivity of a thin metallic film in the far infrared is uniquely determined by the electrical conductivity of the film. Hence an appreciation of the electrical properties is an essential prerequisite to a study of the infrared properties. This relationship is of particular importance when we come to consider the thermal requirements of the film. In order to achieve a small time constant and minimum thermal spread we must seek electrical continuity and stability in the thinnest possible film. We shall see that this is intimately related to film structure, and hence to nucleation and growth phenomena.

Before discussing electrical properties in more detail we need to consider three further optical aspects, namely the variation of absorption with angle of incidence, the influence of the plastic substrate film, and possible methods of enhancing absorption.

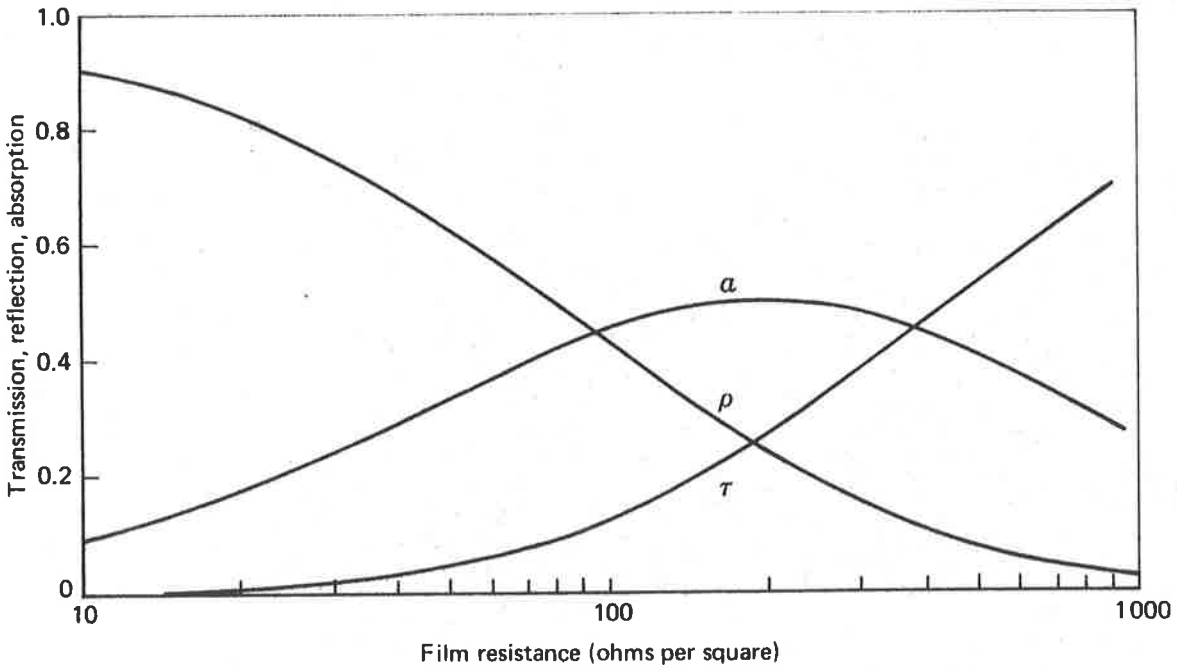

Figure 7. Infrared optical properties of a thin metallic film

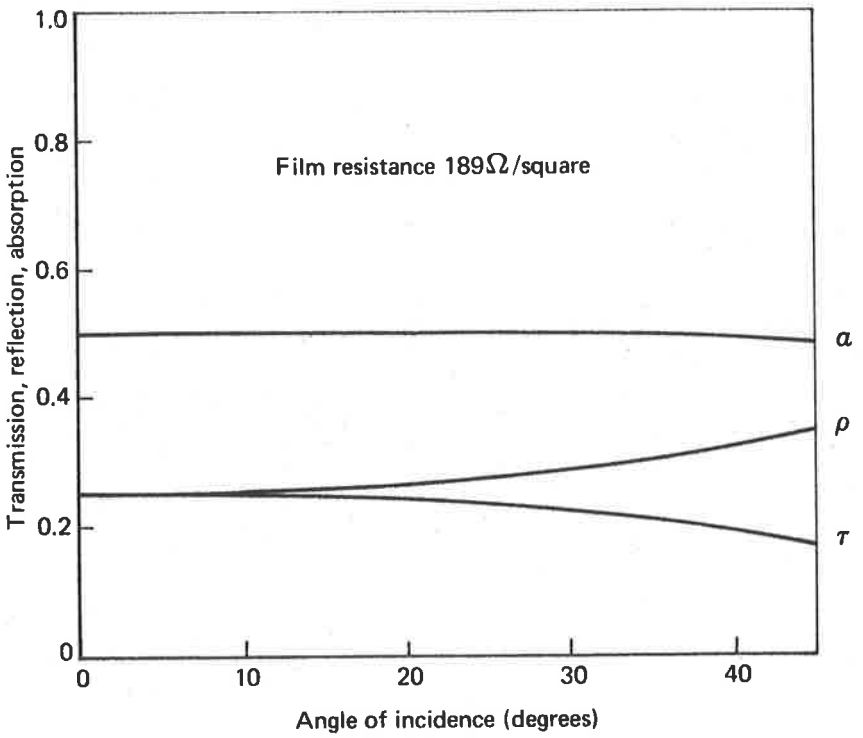

Figure 8. Dependence of infrared optical properties on angle of incidence

3.4.1 Dependence of absorption on angle of incidence

A further derivation of the equations for infrared absorption to include angular dependency leads (ref. 10) to the following modifications to equations (69) and (70)

$$\rho = \frac{\Phi^2}{D_1 \cos^2\theta}$$

$$\tau = \frac{4}{D_1 \cos^2\theta} \qquad (74)$$

$$\alpha = \frac{4\Phi}{D_1 \cos^3\theta}$$

where θ is the angle of incidence and

$$D_1 = \left(\frac{2}{\cos\theta} + \frac{\Phi}{\cos^2\theta} \right)^2 \qquad (75)$$

The graphical results for $\Phi = 2$, i.e., for a film resistance of 189 ohm per square, is given in figure 8. As the angle of incidence increases the reflectance increases, and is compensated by a decrease in transmittance. The absorptance does not vary greatly from that at normal incidence ($\theta=0$) for angles up to at least 45^{o}, so that for all practical purposes the angular dependance can be ignored. This conclusion is in fact substantiated by the optical measurements described in a later section of the thesis.

3.4.2 Influence of the plastic substrate film

The theory of Hadley and Dennison has been extended by Hilsum (ref. 11) in an effort to seek optimum optical properties for infrared absorbers used in the Golay pneumatic detector. He found that the film absorption depended on the direction of incidence of the incoming infrared radiation. When the metallic absorber film was deposited onto a dielectric support film and the radiation was incident on the surface of the absorber, the absorptance was found to be

$$\alpha = \frac{4\Phi}{D_2} \cdot \left(\cos^2 \frac{2\pi n_1 d}{\lambda} + \frac{1}{n_1^2} \sin^2 \frac{2\pi n_1 d}{\lambda} \right) \tag{76}$$

where n_1 is the dielectric constant of the dielectric film and d its thickness, and where

$$D_2 = n_1^2 \left(\frac{\Phi+1}{n_1^2} + 1 \right)^2 \sin^2 \frac{2\pi n_1 d}{\lambda} + (\Phi+2)^2 \cos^2 \frac{2\pi n_1 d}{\lambda} \tag{77}$$

However when the radiation is incident on the dielectric film

$$\alpha = 4\Phi/D_2 \tag{78}$$

When d=0 the equations reduce to the expressions for a self-supported film. As d increases the absorption decreases in the case of equation (76) and increases for equation (78). We will ignore the former and note that in the latter case maximum absorption occurs when

$$\sin^2 \frac{2\pi n_1 d}{\lambda} = 1$$

i.e.

$$\frac{2\pi n_1 d}{\lambda} = \frac{\pi}{2} \tag{79}$$

$$n_1 d = \frac{\lambda}{4}$$

and

$$\alpha = 4\Phi/n_1^2 \cdot \left(\frac{\Phi+1}{n_1^2} + 1 \right)^2 \tag{80}$$

The magnitude of the absorption is clearly greatest for materials of high refractive index. The value of n_1^2 for thermoplastic materials is typically 2.5, and we readily find that this gives a maximum absorption of 0.71 when the film resistance is approximately 125 ohm per square. However, to achieve this absorption the thickness of the substrate must be about $\lambda/6$, i.e., at least 1μ. In this study we are more likely to consider the use of plastic films having a thickness of the order of 1000Å. In this case we have

$$\frac{2\pi n_1 d}{\lambda} \simeq 0.1,$$

and a brief calculation using equation (78) shows that the plastic

substrate provides an almost negligible contribution to absorption.

3.4.3 Double metal film

Interference effects can also be utilised by depositing a thin metallic film on both sides of a dielectric film. Maximum absorption is again obtained in accordance with equation (79). In this case we have

$$\alpha = 4/n_1^2 . \left(1 + \frac{(1+\Phi)^2}{n_1^2}\right) \qquad (81)$$

The highest absorptance is obtained for the lowest refractive index dielectric layer, a maximum of 0.83 being achieved with an air separation. It is again found that the separation distance is unrealistic for the experiments considered later in this study.

It is also quite feasible to increase the absorption by depositing a highly reflecting layer on the reverse side of the plastic film, which again needs to be very thick - in this case approximately $\lambda/4$. In theory, this technique gives almost total absorption. However, none of the above methods of enhancing absorption are of practical value in this study because ultrathin films are required in order to achieve the desired thermal properties.

3.5 Electrical conduction in thin metallic films

It has been shown above that the far-infrared optical properties of thin metallic films can be adequately described in terms of the theory of free electron absorption at low frequencies, the absorption reducing to a simple dependency on the low frequency (static) electrical conductivity. It would therefore seem that, at least in principle, it should be necessary only to determine the desired thickness of the film for the appropriate sheet resistance, in order to optimize the infrared absorption. Unfortunately the film conductivity cannot be readily predicted,

and in fact the mechanism of electrical conduction in thin films is not a well understood phenomenon.

The conductivity of an ultrathin film in the initial stages of formation (see, e.g., ref. 14) is many orders of magnitude lower than the bulk conductivity. At this stage the film is structurally discontinuous and charge transfer between "islands" of evaporant is effected by means of thermionic emission and quantum - mechanical tunnelling. The conductivity is exponentially dependent on the inverse of the temperature and is ohmic only for low applied fields. The film is also characterized by a negative temperature coefficient of resistance.

As the film becomes structurally continuous the conductivity increases dramatically but does not, in general, attain bulk conductivity. This is due to structural and impurity defects, residual mechanical stress in the film, and scattering from the film boundaries. Even in thick films, bulk conductivity is not realised; but it may be closely approached in the case of low-defect epitaxial films. In practice it is found that the conductivity is dependent on evaporation rate, substrate temperature, type of substrate, degree of vacuum, and contamination, to name only some of the more important factors.

A theory of electrical conduction in continuous metal films has been developed by Fuchs (ref. 12) and Sondheimer (ref. 13). It is emphasised that, for the reasons given above, this theory can be used only as a rough guide to film conductivity. A summary is given below. For a more detailed treatment of this subject, see, for example, reference 14.

3.5.1 Theory of conduction in continuous metal films

The Fuchs-Sondheimer theory is applicable to a defect-free metallic strip with parallel surfaces. The fall in conductivity with decreased thickness is considered to be due to scattering

from the film boundary when the thickness, t, becomes comparable with, or less than, the bulk mean free path, λ_o, of conduction electrons in the metal. The scattering is defined in terms of a "specularity parameter", p, which has the extremes of unity for perfectly diffuse scattering at the film surface, and zero for specular reflection at the surface. The ratio of the thin film to bulk conductivity is found to be

$$\frac{\sigma}{\sigma_o} = 1 - \frac{3}{2\kappa}(1-p)\int_1^\infty \left(\frac{1}{a^3} - \frac{1}{a^5}\right) \frac{1 - \exp(-\kappa a)}{1-p\exp(1-\kappa a)}\, da \,, \qquad (82)$$

where

$$\kappa = t/\lambda_o,$$

and a is a dummy variable.

For very thin films, when $\kappa << 1$ and $p < 1$, this equation reduces to

$$\frac{\sigma_o}{\sigma} \simeq \frac{4}{3}\,\frac{1-p}{1+p}\,\frac{1}{\kappa(\ell n(1/\kappa)+0.4228)} \,, \qquad (83)$$

and for thick films, when $\kappa > 1$,

$$\frac{\sigma_o}{\sigma} \simeq 1 + \frac{3}{8\kappa}\cdot(1-p) \,, \qquad (84)$$

where both equations are expressed as the ratio of thin film to bulk resistivity $1/\frac{\sigma}{\sigma_o}$.

The thick film approximation is in fact found to be accurate to a maximum error of 7% when κ is as small as 0.1. The thin film approximation often cannot be applied in any case, as the thickness then corresponds to the region where the film is discontinuous and conduction takes place by means of a different mechanism.

The theory may be extended to include the temperature coefficient of resistance (T.C.R.) of thin metallic films, where

$$\text{T.C.R.} = -\frac{1}{\sigma}\,\frac{d\sigma}{\sigma T} \qquad (85)$$

The full equation (82) has been evaluated by Soffa (15), with the

results shown in figure 9. We may use this data to obtain a rough approximation of the film thickness required for maximum infrared absorption.

The bulk conductivity of a metal is given by equation (60). The mean free path is related to the collision frequency by

$$\lambda_o = v_f/g \text{ cm} \tag{86}$$

where v_f is the electron velocity, or, more correctly, the velocity at the surface of the Fermi distribution. It can be expressed in the form

$$v_f = \left(\frac{3N}{8\pi}\right)^{\frac{1}{3}} \cdot \frac{h}{m} \text{ cm.s}^{-1}, \tag{87}$$

where h is Planck's constant. Inserting the constants, we obtain

$$\lambda_o = 1.27 \frac{\sigma_o}{N^{2/3}} \times 10^4 \text{ cm}, \tag{88}$$

σ_o being given in $\Omega^{-1}\text{cm}^{-1}$. The electron concentration can be approximated by using Avogadro's number, N_A (6.025×10^{23} g. mol^{-1}), thus:

$$N = N_A \rho_f/M \tag{89}$$

Here ρ_f is the density (g.cm^{-3}) and M is the molar mass (g.mol^{-1}) and it is assumed that there is one conduction electron per atom. We find that for gold

$$\sigma_o = 4.2 \times 10^5 \ \Omega^{-1} \text{ cm}^{-1}$$

$$\lambda_o \simeq 350\text{Å}$$

and for nickel

$$\sigma_o = 1.1 \times 10^5 \ \Omega^{-1} \text{ cm}^{-1}$$

$$\lambda_o \simeq 65\text{Å}$$

The Fuchs-Sondheimer theory predicts that the absorber film should be less than 50 Å thick. However, it is well known that the theory fails at this order of thickness, more particularly for gold than for nickel.

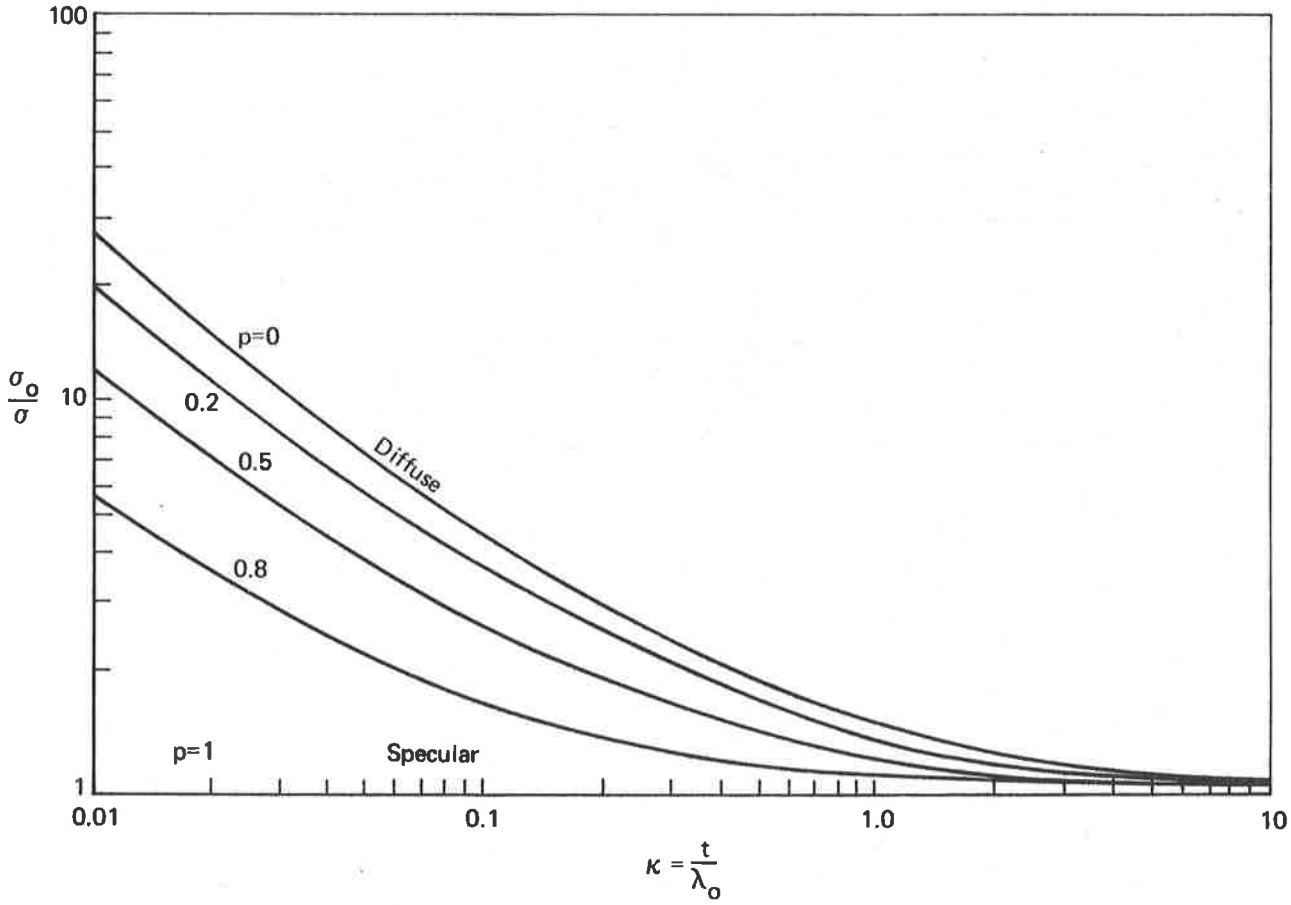

Figure 9. Conductivity of thin films according to Fuchs-Sondhiemer theory

Nevertheless in the absence of more detailed information we would expect that the onset of gross defects and boundary effects is unlikely to be significant until κ falls below unity. Thus it would not be far wrong to seek a thickness of 100 to 200Å for gold and 100Å or less for nickel. This is the most accurate estimate that can be made at this stage.

We can proceed no further without a more detailed study of the nucleation and growth process.

4. NUCLEATION AND GROWTH PROCESSES AND THE STRUCTURE OF THIN METALLIC FILMS

4.1 Introductory concepts

The physical structure of thin metallic films is of fundamental importance in this study. It has been shown in earlier Sections that a requirement for low thermal capacitance and minimum thermal spread demands that the metal absorber film be as thin as possible. This ultra-thin film must then be electrically continuous, and have suitable conductivity in order to attain optimum infrared absorption. It must also be electrically stable and thermally uniform. In the ideal situation which we would eventually hope to achieve, the film would need to be entirely self-supporting and this, in addition, demands the preparation of defect-free, structurally continuous films.

The structural characteristics of a thin film are dependent on the mechanisms of nucleation and growth during the initial stages of formation. We will see that an appreciation of the physics of these phenomena not only provides us with a guide to film deposition parameters, but enables us to predict with reasonable confidence the metals which are most likely to meet the present requirements.

4.1.1 Adsorption of vapour atoms

Metal atoms thermally vaporized in vacuo impinge upon the sub-

strate surface on which condensation is desired with an average kinetic energy:

$$E_{av} = \frac{3}{2} kT \qquad (90)$$

where k is the Boltzmann constant and T is the absolute temperature. For vaporization temperatures of $1600^{o}K$ and $1800^{o}K$ (corresponding to a vapour pressure of 0.01 torr for gold and nickel) the average kinetic energy is 0.2ev and 0.23ev respectively.

On reaching the substrate there are three main alternatives available to the incident vapour atoms (for the following treatment see also ref. 14):

(a) reflection

(b) physical adsorption

(c) chemical adsorption

(d) penetration

Let us assume for simplicity that only physical adsorption takes place - this is reasonable if the substrate is chemically stable and the kinetic energy of the atoms is not too high. The impinging atom is attracted by the instantaneous dipole and quadrupole moments of the surface atoms. This physically adsorbed atom, called an adatom, diffuses across the surface, hopping from one potential well to another, and remains on the surface for a mean stay time:

$$\tau_s = \frac{1}{\nu_o} \exp \frac{E_a}{kT_s} \qquad (91)$$

where E_a is the absorption energy, T_s is the substrate temperature, and ν_o is the adatom surface vibrational frequency (typically 10^{12} to 10^{13} s^{-1}). If the adatom does not combine with other adatoms during its stay time it is desorbed into the vapour phase.

Depending on the conditions of deposition the adatom may or may not attain thermal equilibrium. It has been estimated (ref. 14) that the adatom will lose most of its initial kinetic energy within 2 to 3 lattice oscillations. The relaxation time required to equilibrate is then given approximately by

$$\tau_r = 2\tau_s \exp \frac{-E_a}{kT_s} \tag{92}$$

An equilibrated adatom diffuses over a distance

$$D = 2^{\frac{1}{2}} d \exp \frac{E_a - E_d}{2kT_s} \tag{93}$$

determined from the Einstein relation for Brownian motion. d is the jump distance between adsorption sites and E_d is the activation energy for surface diffusion.

The value of kT_s for substrate temperatures up to several hundred degrees K is typically less than 0.1 ev. The adsorption energy is usually much higher, and when this is so we might expect a short relaxation time. It is found, in general, that $E_a \simeq 4E_d$.

It should be noted that in some cases the average kinetic energy of the incident atoms is larger than the adsorption energy and all impinging atoms may not be physically adsorbed. Furthermore thermal equilibrium may not apply, e.g., when the impingement rate exceeds the adatom diffusion rate.

4.1.2 Initial nucleation

It is well known that the final structure of a thin film is strongly dependent on the characteristics of deposition during initial nucleation. This is a complex process, markedly influenced by a number of deposition parameters, and therefore not readily amenable to analytical treatment. Several theories have been proposed (see, e.g., references 14, 16, 17, 18, 19). None of these are entirely satisfactory, but are in broad agreement with observed

phenomena.

The first adatoms appearing at the substrate execute a random walk as they diffuse across the surface. If, during the lifetime τ_s, given by equation (91), they encounter other adatoms, mutual capture may occur with the subsequent formation of an atomic cluster or nucleus. This nucleus will not be stable, unless the size of the 'critical nucleus' - usually composed of only a few atoms - is exceeded. Eventually a saturation density of stable nuclei is reached; newly arrived adatoms are then captured by stable nuclei, and a three-dimensional 'island structure' begins to form.

Let us assume that the substrate is a smooth, inert surface, having N_o adsorption sites per unit area. If the arrival rate of single atoms is R (atom cm^{-2} s^{-1}) then we might suppose that in time τ_s the equilibrium population of single adatoms would be

$$N = R\tau_s \tag{94}$$

However when capture occurs the lifetime is less than τ_s, and we are likely to have

$$N = R\tau_c \tag{95}$$

where τ_c is the mean lifetime before capture.

It can be shown (ref.18) that above a transition temperature T_o, given by

$$T_o = \frac{2E_a - E_d}{k\ell n(N_o \nu_o / R)} \ , \tag{96}$$

condensation is initially incomplete, i.e., some adatoms are desorbed. In this case the saturation density of stable nuclei is

$$N_s = N_o \exp . \left[-(E_a - E_d)/kT_s\right] \tag{97}$$

Below T_o condensation is more complete, i.e., all adatoms are captured, and hence all incident atoms will form stable pairs, with a saturation density

$$N_s = \left(\frac{N_o R}{\nu_o}\right)^{\frac{1}{2}} \cdot \exp\left(\frac{E_d}{2kT_s}\right). \qquad (98)$$

It is of interest here to evaluate T_o. Let us assume

$$2E_a - E_d = 1.25 \text{ ev},$$

corresponding to an adsorption energy in the range 0.5 to 1.0 ev. For a deposition rate of $1\text{Å}\ s^{-1}$ and an adsorption site density of $10^{15}\ cm^{-2}$, and for a typical value of ν_o of $10^{12}\ s^{-1}$,

$$T_o \simeq 515^oK$$

It will be noted that T_o is strongly dependent on the adsorption energy and hence on the type and physical condition of the substrate surface. It is less sensitive to change in deposition rate.

This simplified outline of the initial nucleation process represents an idealised situation. It does not take into consideration some important deposition parameters, e.g. kinetic energy of the vapour atoms, and cannot be expected to account fully for the observed phenomena. A notable deficiency in the above treatment is the tendency towards "agglomeration" (see Section 4.2.1) as the substrate temperature increases, with the result that the saturation density represented by equation (97) is not realised. In general, therefore, we should not expect to find a sharp transition temperature.

In summary, we might expect that growth takes place on an island structure of density decreasing with increasing substrate temperature but relatively insensitive to deposition rate. At very high deposition rates the island density will increase due to the strong interaction between incident vapour atoms and hence short

lifetime before capture. This is indeed what is observed in practice.

Progressive nucleation presupposes a certain degree of supersaturation. Nucleation theory (refs. 14, 20) predicts that with increasing supersaturation (higher melting point materials, lower substrate temperatures) a large number of smaller sized stable nuclei are formed.

4.2 Observed nucleation and growth phenomena

4.2.1 Adatom surface mobility and film agglomeration

A useful qualitative description of nucleation and growth may be given in terms of the migration or "mobility" of adatoms on the substrate surface. Adatom surface mobility is found to increase

(a) with increasing substrate temperature,

(b) with films of low-melting point materials,

(c) for smooth, inert substrates, and

(d) with an oblique angle of incidence of the vapour stream

A high surface mobility is observed to give rise to increased film "agglomeration". Agglomeration is a descriptive term for the tendency to form larger islands. High agglomeration implies large grain size and low island density. The film becomes continuous at a higher average thickness and will have less frozen-in structural defects. As we might expect, agglomeration increases with decreasing nucleation density.

Under conditions of thermal equilibrium we would expect the adatom mobility to increase with increasing deposition rate and kinetic energy of the arriving atoms. However at high deposition rates, when the arrival rate is larger than the rate of surface diffusion, adatoms react strongly with each other, resulting in low

surface migration. An increase in the initial nucleation density may also be brought about by the presence of electrostatic charges on the incident atoms, by the penetration of energetic atoms into the substrate surface, by the influence of adsorbed impurities, and by the use of a non-inert physically non-uniform substrate. All of these factors lead to lower agglomeration.

4.2.2 The growth sequence

Initial nucleation cannot be readily observed because the size of the nuclei is beyond the resolution capability of electron microscopy. Subsequent growth has however been carefully observed and recorded in a number of laboratories, the best known published work being that by Pashley et al (refs. 21, 22) who observed growth phenomena within the electron microscope. The generally accepted growth sequence may be summarized as follows :

(a) Initial nuclei formation, as discussed previously

(b) After attaining a saturation density, newly arrived atoms contribute to an increase in size of the islands, without any significant increase in numbers

(c) A further increase in size accompanied by a considerable decrease in island density as the islands coalesce. This gives rise to

(d) a connected network, usually developing into a channeled structure, and finally

(e) a continuous, hole-free film

The coalescence stage has been described by Pashley as "liquid like" - although the deposit is certainly not liquid - and it is observed that the later stage of coalescence is dependent mainly on the arrival of freshly evaporated atoms. This implies that

with a high deposition rate there is a rapid termination in the coalescence process.

The dependence of film growth on deposition rate is not always clear. Thus Chopra (ref.23) has observed that during the initial growth of gold and silver films agglomeration increased with deposition rate, for rates in the range 0.3 to 10 $\text{Å}s^{-1}$. This is contrary to common belief, for it is usually accepted that grain size during growth is not strongly influenced by deposition rate except when the deposition rate is very high.

Chopra also noted that for a fixed deposition rate agglomeration increased with higher evaporation rates, i.e., kinetic energy of the vapour atoms. Whilst this may be so for a given metal, the size of stable nuclei is small for high melting point metals and hence the island density should be high for these metals. It is well established that fine-grain deposits are indeed obtained for such metals as platinum, nickel, chromium, tungsten and molybdenum.

4.2.3 Film structure

It has been noted above that fine grain deposits are to be expected with high melting point materials and for high deposition rates and low substrate temperatures. Films deposited under these conditions are more likely to attain structural continuity at a lower average thickness than highly agglomerated films prepared at low deposition rates and high substrate temperatures. However the films would probably have a greater number of frozen-in defects.

Films deposited onto amorphous substrates are generally polycrystalline, regardless of substrate temperature. Epitaxial growth usually requires a single crystal substrate (cleaved mica, NaCl, MoS_2, etc.) with deposition at an elevated substrate tempera-

ture. The higher substrate temperature also reduces defects and assists in removing substrate contamination; factors which, together with a contamination-free vacuum environment, are essential to high grade epitaxy.

An interesting growth pattern may be observed when the substrate surface has a rough, granular or porous texture. Alumina substrates fall into this category. A surface of this type should give rise to a fine-grain deposit due to low adatom migration. However a heavier deposit is needed to obtain structural continuity due to the greater effective surface area and the penetration of vapour atoms into the porous structure. We may well expect a similar situation with plastic substrates, as the physical structure of these materials would tend to suggest extensive penetration, especially for high melting point evaporants. This penetration has been observed by the author and is described in a later section of the thesis.

Many authors have noted that the structure of films deposited on to different amorphous substrates (e.g. glass and plastic), and under the same deposition conditions, is of similar texture.

4.2.4 Substrate transition temperatures

It is clear that the temperature of the substrate has a marked influence on the growth process. How general this influence should be is not readily obvious, as growth is also strongly dependent on other parameters; although we do know that a higher substrate temperature increases adatom mobility and encourages agglomeration, and is essential for epitaxy.

Russian investigators have observed a relationship between substrate temperature, crystalline structure, and the bulk melting

point of the metal. Their observations appear to apply to a wide range of metallic evaporants.

The Russian research is summarized in references 24 and 25. The essential results of this work are that three broad regions can be identified which are directly related to crystalline structure as a function of both substrate temperature, $T_s(^oK)$, and the melting point of the evaporant, $T_m(^oK)$. These are as follows :

(a) $T_s \geq \frac{2}{3} T_m$: In this region film condensation occurs via a vapour → liquid → solid transformation. During initial formation the deposit consists of large, spherical crystallites which are sometimes faceted. The region extends to the so called "critical" temperature, above which condensation cannot be observed.

(b) $\frac{1}{3} T_m \leq T_s \leq \frac{2}{3} T_m$: Condensation occurs via a vapour → solid transformation. For amphorous substrates the crystallites are large and flat, with smooth or faceted outlines. This is the region favoured for epitaxial growth. The use of single crystal substrates affects the results, in particular by extending the region to higher temperatures.

(c) $T_s \leq \frac{1}{3} T_m$: Condensation is via a vapour → solid transformation, and there is evidence in some cases of the transformation vapour → liquid → solid. Crystallites are minute 'droplets', sometimes too small to be resolved by electron microscopy.

The above suppositions are in general agreement with published descriptions of film formation. Perhaps the best corroborative example is the extensive work reported by Pashley et al (refs. 21, 22) on epitaxial films of silver and gold, which were deposited on-

to single crystal substrates at a temperature of 350°C.

Further evidence of temperature transition regions is to be found in early papers by Levinstein (ref. 26) and Sennett and Scott (ref. 27), in both cases relating to room temperature amorphous substrates. In general, it was found that fine-grained structureless deposits were obtained with high melting point metals, the crystallite size progressively increasing for lower melting point metals, in broad agreement with the above predictions. Rapid evaporation also accentuated the formation of "aggregated" deposits.

4.3 Electrical conduction

The preceding discussion on the formation and structure of thin films can leave no doubt as to the fundamental significance of the nucleation and growth process to electrical conduction in this metallic films. During the early stages of formation conduction takes place by means of thermionic emission and tunnelling between islands, the former being favoured for larger inter-island spacing. The substrate has an additional influence as it is now widely believed that electron transfer for the barrier mechanisms takes place via the substrate.

4.3.1 Final film resistance

The bridging of islands during coalescence is accompanied by a dramatic increase in conductivity. As we have seen, the average thickness at which this occurs - called the "critical thickness" - is strongly dependent on deposition parameters. It follows that the final resistance of a thick continuous film also depends on the conditions of deposition.

Films deposited on to room temperature substrates are observed to have a higher resistance than films deposited (on to the same

substrate) at a higher substrate temperature; although in the latter case the decreased resistivity is achieved at a greater final thickness (see e.g. Chopra et al, reference 28). An increase in substrate temperature above a certain value typical of the material will be accompanied by a sharp rise in resistance. This effect is discussed in Section 4.3.2.

The texture and condition of the substrate surface also has a marked influence on final resistance. The resistance of a film deposited on to an alumina substrate is typically twice as high as that for a glass substrate under identical evaporation conditions. The author has also observed a higher resistance for films deposited on to polymer substrates.

Chopra and co-workers (ref. 28) have found that the resistance of sputtered gold films is lower than that of thermally evaporated films, and in each case epitaxially grown films prepared on heated (mica) substrates had a lower resistance than polycrystalline films deposited on to cold substrates - substantially in agreement with the abovementioned tendency. The critical thickness was much sharper for the epitaxial films. These results are in accord with the observations of other authors; however the method of evaporation is evidently important as the resistance of films has been elsewhere reported to be lower for thermally evaporated films than for sputtered films.

4.3.2 Aging effects

The resistance of continuous metallic films deposited on to room temperature substrates usually decreases with time, becoming stable after several hours. This aging effect can be accelerated by baking the film, and subsequent cycling below the aging temperature

generally induces no resistance instability (i.e. the film resistance is reversible). A decrease in resistance after deposition may not occur with unstable or chemically reactive materials. The author has noted an increase in resistance with aging for nickel and nichrome films, evidently due to oxidation. The aging of nichrome films can again be accelerated by heating, and aged films are remarkable stable. In other cases an increase in resistance can be traced to substrate heating during deposition.

Belser (ref. 29) has described the effect of thermal aging on a number of metallic films, which were deposited on to glass substrates at room temperature by means of both thermal evaporation and sputtering. Belser postulates that there is a preferred aging temperature for each material, which is dependent on film thickness but closely associated with the recrystallization temperature of the metal. The aging process assists in the removal of strains induced in the film during deposition, removes adsorbed and occluded gas and promotes growth in the size of crystallites. Aging at the preferred temperature can reduce film resistance to between 25 and 50% of the "as-deposited" resistance. The change can be even higher for ultrathin films. However heating to higher temperatures causes a sudden rise in resistance due to film aggregation. Aging is more pronounced with sputtered films, but the preferred temperature is higher than that required for thermally evaporated films.

Belser's results are essentially in agreement with the observations of most investigators and help to explain anomalies reported in the literature. The preferred temperatures and resultant crystalline structures are also much as we would expect from our know-

ledge of the growth process. However it is emphasised that the growth process during post-deposition annealing is different from that which occurs at the same temperature during initial formation.

Aging of metal films can also be accomplished by passing an electric current through the film. This method has been used extensively in the author's laboratory, particularly for gold films deposited onto plastic substrates, where thermal aging is impractical.

4.3.3 Electrostatic charge effects

It was noted earlier that the presence of electrostatic charges on incident atoms contribute to an increase in the initial nuclei saturation density, with a subsequent reduction in agglomeration. Electron irradiation has a similar effect. Several authors have also noted that the use of measurement voltages during deposition, e.g., for monitoring film resistance, influence the growth process and in some instances the field in the vicinity of crystal-controlled thickness monitors has been known to disturb the vapour stream.

The influence of electrostatic fields applied during the deposition of silver and gold has been extensively studied by Chopra (ref. 30). He applied a d.c. field of up to $150 V.cm^{-1}$ in the plane of the film and observed a marked influence on the growth process. This field was detrimental to sputtered films due to modification of the glow discharge. However for thermally evaporated films the field induced coalescence of the island structure at an earlier stage of growth than is normally observed. The effect was more marked at higher substrate temperatures, although, as we would expect, the film resistance for a given thickness was higher. Continuous films deposited under an applied field were lower in

resistance than those obtained without a field, a consequence of recrystallization and reorientation of nuclei during the coalescence phase. The field is only effective before and during coalescence.

For gold and silver it appears that the electrostatic field effect is not very significant for room temperature substrates. This may not be so for lower melting point metals. On the other hand, high melting point metals such as nickel, chromium and platinum might not be influenced by applied fields up to quite high substrate temperatures.

Aging and electrostatic effects clearly merit further consideration in the attempt to prepare ultrathin, stable infrared absorbing films.

4.4 Selection of suitable metals for thin film infrared absorbers

The foregoing description of nucleation and growth in metallic films, and the dependence of these processes on various deposition parameters, is substantiated by the vast majority of published work. Considerable thought has been given by the author to these factors in the search for suitable materials and appropriate methods of preparation of ultrathin infrared absorber films. Considerations leading to the final selections are discussed below.

The essential specifications for the desired metallic film are :

(a) Physical continuity in the thinnest possible film achieving maximum absorption; defect free

(b) Electrical surface resistance of approximately 200 Ω per square in the thinnest possible film

(c) Electrical stability and thermal uniformity

(d) Chemical stability

(e) Ease of preparation, and repeatibility

(f) Low thermal conductivity

(g) Preparation on thermoplastic substrates

Plastic substrates are particularly useful for research purposes as they facilitate ease of measurement of thin film parameters. They are also of some interest as support films for infrared detectors. The use of thermoplastic substrates does,however, place a restriction on the range of substrate temperatures which can be employed. We therefore have the additional specification :

(h) Maximum substrate temperature generally less than 150^{o}C.

Evidently we must seek a metal which forms a stable, low resistance, microcrystalline film on substrates near room temperature. The film would probably be formed at high deposition rates to induce rapid coalescence and reduce contamination. Room temperature deposition may lead to excessive film defects, so that an aging cycle would appear to be essential. Consideration might also be given to the possibility of inducing early coalescence with the aid of electrostatic fields.

In the first instance it would seem reasonable to reject all metals for which the value Tm/3 (see Section 4.2.4) is less than, say, 450 to 475^{o}K. We thus exclude metals with a melting point of less than about 1350^{o}K. These metals are usually agglomerated to a greater or lesser degree and are often electrically or chemically unstable. In the 'transition' region we have such metals as silver, copper and gold. These have been rejected on the basis of known structural characteristics, high thermal conductivity and (except gold) chemical or electrical instability in thin film form. In the high melting point range we need to consider such metals as nickel, titanium, palladium, platinum, iron, chromium, etc., and the refractory metals tungsten and molybdenum. Many of these were discarded because of their high thermal conductivity or tendency to oxidize and, in some cases,

known difficulty of preparation. Of the remainder, nickel was chosen for detailed study. Less extensive experiments with gold and a nickel-chromium alloy are also reported in later sections of the thesis. An initial evaluation of chromium and platinum films was carried out.

It is of interest to note that germanium and silicon form amorphous films on room temperature substrates. These metals can,however, be immediately rejected because of high electrical resistivity and hence low infrared absorption. They are in fact used as window materials in the infrared.

4.4.1 Gold films

Gold would appear to be eminently suitable because of ease of preparation and chemical inertness. Gold films have in fact been used extensively in the author's laboratory as infrared absorbers. However, there is abundant evidence of structural non-uniformity in films of thickness suitable for infrared absorption (see e.g., ref. 22), and a careful aging cycle is required to reduce electrical instability. The thermal conductivity of gold is also high. To some extent the aim of the present research project is to replace gold with a superior absorbing metal. It was therefore considered desirable to prepare gold absorber films for comparison with films of higher melting point metals.

4.4.2 Platinum films

There is ample evidence in the literature (refs. 25, 26, 29, 31, 32) of the ultra-fine grain, uniform texture of platinum thin films, regardless of substrate type and for substrate temperatures in the range $77^{o}K$ to $600^{o}K$. Platinum is also chemically inert and therefore, like gold, not susceptible to reactive contamination during or after deposition. Its thermal conductivity is also much

lower than gold. Platinum can be deposited using electron beam evaporation apparatus.

Our assessment would suggest that platinum is perhaps the most promising metal for investigation as a thin film infrared absorber. Palladium is an alternative metal worthy of consideration. Unfortunately, initial experiments with platinum have indicated certain technical limitations in the deposition process, primarily concerned with damage to the fragile polymer substrates. The author has little doubt that these difficulties can be overcome. However, in order to satisfy the broad aims of this project, it seemed expedient to investigate a metal having a lower melting point than platinum but retaining most of the desired characteristics listed in the foregoing specification.

4.4.3 Nickel films

Nickel is also known to form fine grain deposits (refs. 26, 27 33, 34). Preparation in high to ultrahigh vacuo is required to avoid oxidation (ref. 34). The thermal conductivity of nickel is lower than platinum, favouring decreased lateral thermal spread. Nickel is readily evaporated from a resistance heated tungsten helix or from an electron beam deposition source.

It is worthy of note that both nickel and platinum films are of interest as the sensitive element of infrared bolometer detectors.

4.4.4 Alloy films

Initial work in this project was carried out using nickel-chromium alloy (nichrome) films, primarily for the purpose of testing apparatus and validating measurement techniques. Nichrome is also a useful thin film absorber material. It can be deposited as an extremely thin film and has a very low thermal conductivity.

Nichrome films are stable after aging, and this factor, together with a low temperature coefficient of resistance, favours application as a resistive element in thin film microcircuitry. However, because of its low temperature coefficient of resistance, nichrome is not suitable for use as a bolometer detector.

Experimental studies on nichrome films are also reported in later sections of the thesis.

5. PREPARATION OF METALLIC FILMS

5.1 Vacuum coating unit

The high vacuum coating unit used in this project is illustrated in figure 10. It is a research orientated system constructed in the author's laboratory specifically for the preparation and systematic study of thin metallic films. The pumping unit consists of an Edwards type 403 4-inch (10cm) oil diffusion pump, backed by a 200 $\ell.min^{-1}$ two-stage Gaede rotary pump. The diffusion pump is charged with Dow-Corning type 705 silicone oil. The chamber pressure achieved during deposition cycles is 2×10^{-6} torr, measured with a calibrated Penning gauge. A dual Pirani gauge, with heads fitted to both the foreline and vacuum chamber, is used for the measurement of high pressure. A water-cooled "cold cap" is fitted to the diffusion pump to reduce backstreaming.

The vacuum chamber is supported on a 12in (30cm) diameter stainless steel service ring fitted with 10 standard 1in (2.5cm) diameter vacuum ports. The vacuum ports provide chamber entry for electrical leads and external mechanical controls. All baffle plates, supports and shutters within the vacuum chamber are prefabricated from stainless steel. Chamber components are chemically cleaned and degreased at regular intervals to reduce contamination. Viton elastomer vacuum seals are used throughout.

The vacuum coating unit is located in a clean air environment and the

Neg. No. N73/633

Figure 10. Vacuum coating unit

backing pump exhaust is vented to the external atmosphere.

Several safety features were incorporated in the coating unit to provide protection during prolonged and unattended pumping cycles. A flow switch fitted to the diffusion pump water cooling line actuates a solenoid valve when the flow rate falls below a preset level, cutting off water flow to the pump. The flow switch also isolates the diffusion pump circuit. Protection against a drop in chamber pressure is effected by a vacuum switch, which is actuated at 5 torr. This switch controls both the diffusion pump circuit and the high voltage supply used for gas discharge cleaning and electron beam evaporation. A "manual" bypass circuit is incorporated to allow the diffusion pump to remain operative during vacuum recycling.

5.1.1 Ancillary coating unit

A general purpose coating unit was used for the preparation of thin film electrical contacts and mirror coatings, and for the deposition of silver layers required in multiple beam interferometry. This unit was also used for pilot experiments on nickel, chromium and gold absorber films. The attainable vacuum is better than 1×10^{-5} torr.

5.2 Deposition control techniques

The conditions of vacuum deposition may be expected to have a marked influence on the optical and thermal properties of thin metallic films. This conclusion was reached in Section 4 from a study of nucleation and growth phenomena. It is thus desirable to maintain an accurate and effective control of the deposition process. In this project electrical film resistance, film thickness, deposition rate and chamber pressure were continuously monitored. The experimental procedure is described below. Control instrumentation is shown in figure 11. The monitor

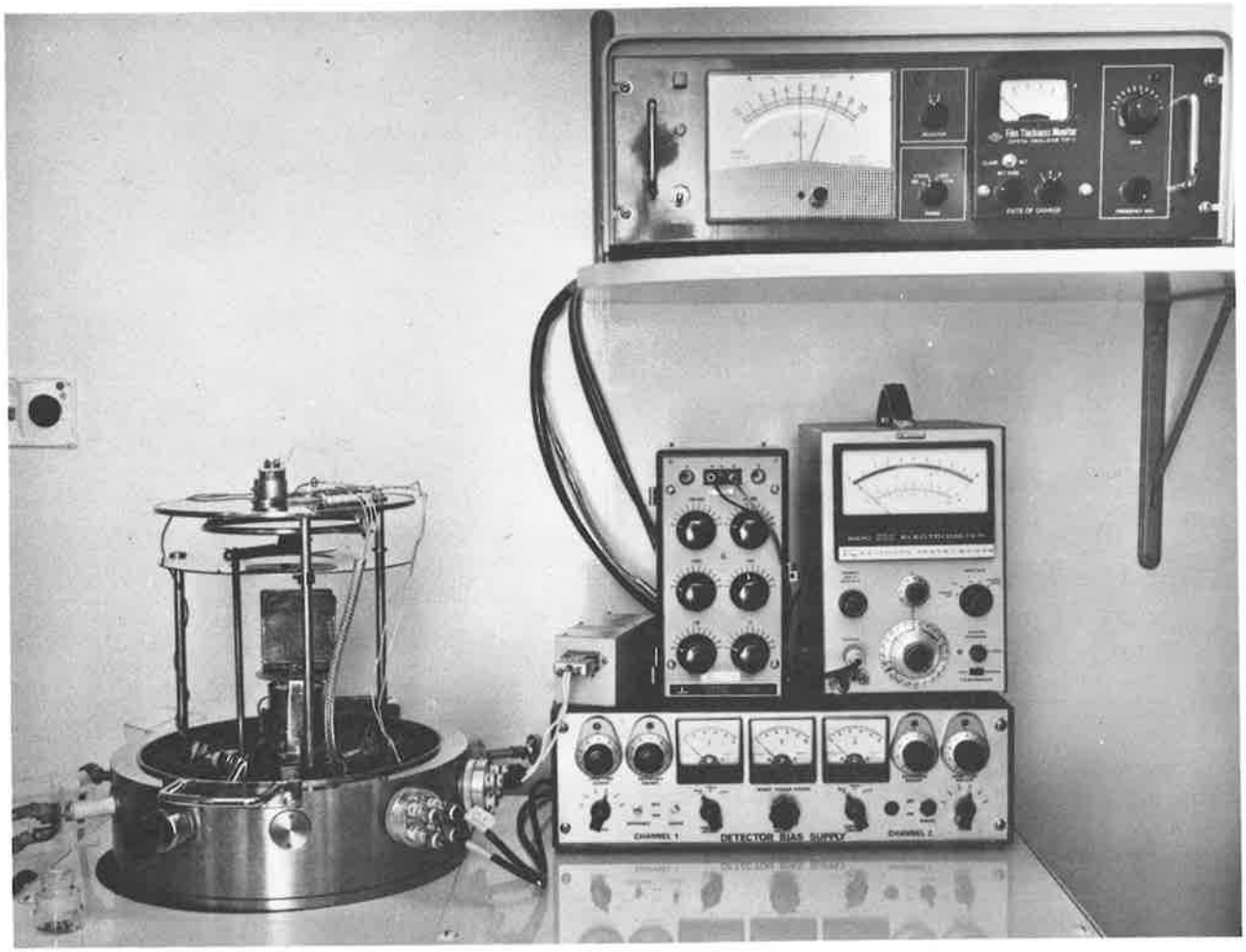

Neg. No. N73/632

Figure 11. Deposition control instrumentation

circuit is illustrated schematically in figure 12.

5.2.1 Film resistance

Electrical resistance was monitored during deposition using a simple two-probe measurement technique. The substrate was coated with suitably shaped evaporated gold contacts. Electrical connection was made to the gold electrodes by means of 1mm x 0.025mm nickel strip sealed to the gold with conducting epoxy cement. After testing a number of silver-loaded epoxy resins, Epo-tek type 410LV was finally selected for this application. The nickel strips were connected to tinned copper leads using Canon gold-plated pin connectors. These leads were insulated with woven fibre glass sleeving to reduce outgassing. A high vacuum leadthrough in one of the chamber ports provided access to the external measurement circuitry.

Two methods were employed for the measurement of film resistance. In the first of these methods resistance was measured directly on the Ohmmeter ranges of a Keithley Model 610C electrometer. The electrometer recorder output was connected to a Rikadenki Model B-34 three-channel potentiometric pen recorder. A precision decade shunt, connected to the electrometer via a terminal box, was used as a resistance reference.

The above direct method was replaced during the latter stages of the research program by a more sophisticated measurement technique. A test current was supplied to the monitor substrate from a constant current voltage source and the resistance determined by measurement of the voltage drop across the specimen. In this arrangement, illustrated in figure 12, the electrometer was used as a voltmeter and deposition monitor. A calibrated resistance reference was

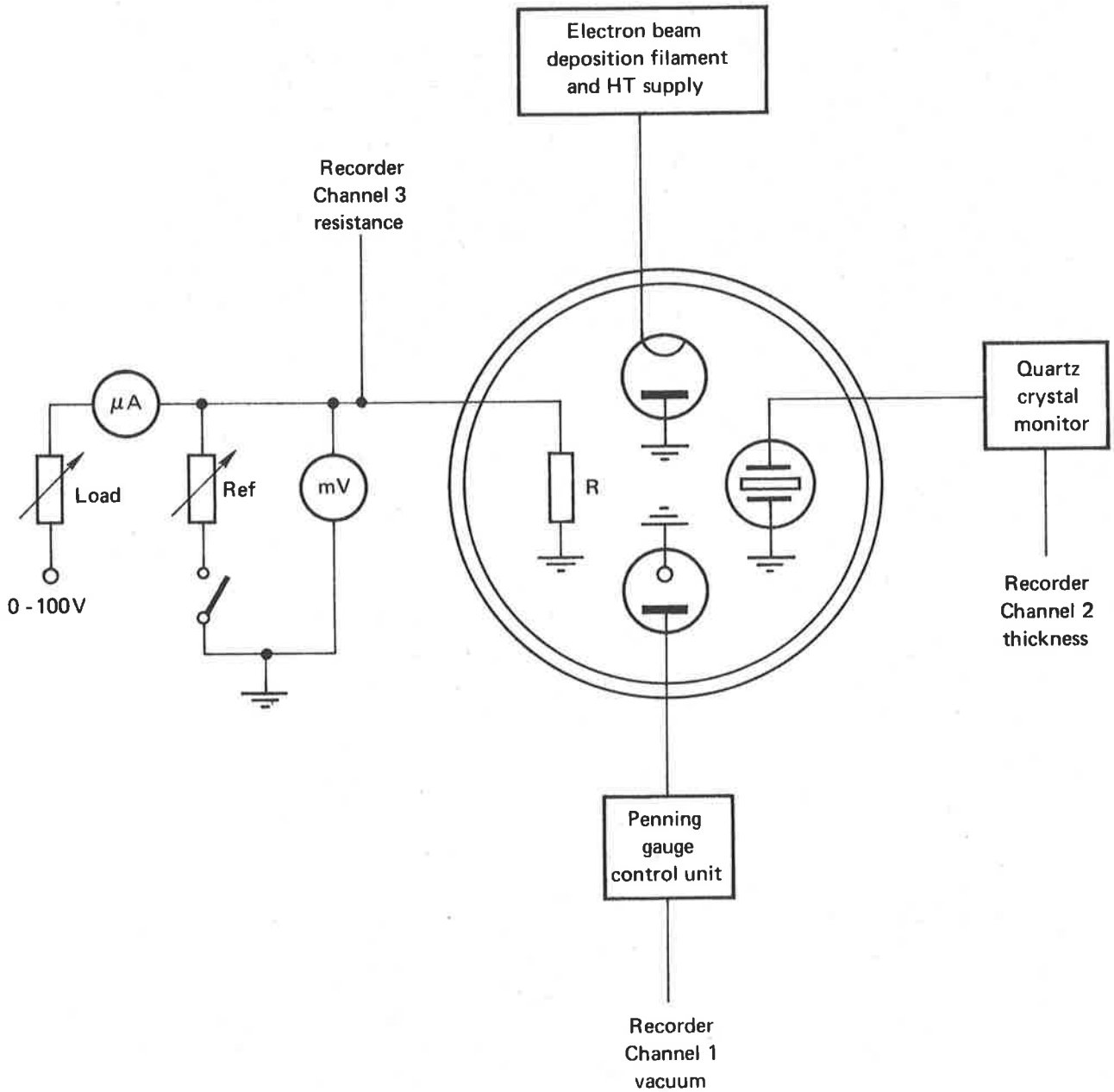

Figure 12. Monitor circuit schematic

incorporated within the voltage supply unit and was adjustable in 10 Ω graduated steps from 0 to 10kΩ. Two test channels are available enabling a second specimen to be monitored during the same deposition. This facility was used to compare the resistance of films formed on different substrate materials.

The standard test current was 10 μA. This value was selected as a suitable compromise between measured voltage and permissible Joule heating of the substrate. Prior to deposition the electrometer and pen recorder were calibrated and the voltage source set to LOAD, with the reference adjusted to give a suitable full scale meter reading, usually 1kΩ corresponding to a voltage drop of 10mV. In this position the resistance monitor slide was wired in parallel with the reference. During deposition, when the meter reading dropped to mid scale, the voltage source was switched to READ, thereby removing the reference resistance from the circuit. The electrometer and recorder then indicated a linear measurement of film resistance. This technique also provided a permanent record of the resistance calibration.

5.2.2 Deposition rate and film thickness

Deposition rate and film thickness were measured with a quartz crystal thickness monitor. An Edwards Model 1 monitor was used for the deposition of nichrome, nickel, chromium and gold. This unit was replaced by a Toyocom Model TVF-1 monitor for a series of precision-controlled nickel evaporations. The Toyocom monitor is more suitable for research applications because of its higher stability and extended range capability. Both units make use of the shift in resonant frequency of an AT-cut quartz crystal to measure mass and hence thickness of the deposited film. It can be

shown (ref. 35) that the film thickness, t, is related to frequency shift, Δf, by the formula

$$t = \left(\frac{\Delta f}{f_o}\right)\left(\frac{\rho_q}{\rho}\right) \cdot d_q \times 10^8 \quad \text{Å} \qquad (99)$$

where f_o is the resonant frequency (Hz), ρ_q is the density of the quartz crystal (2.65 $g.cm^{-3}$), ρ is the density of the evaporant ($g.cm^{-3}$) and d_q is the crystal thickness (cm). It is assumed that the electroded area of the crystal is uniformly coated with the evaporant material. For the Edwards monitor

f_o = 6MHz,

and d_q = 0.279mm,

$\therefore$ t = 1.23 $\Delta f/\rho$ Å. (99A)

For the Toyocom monitor

f_o = 5MHz,

and d_q = 0.334mm,

$\therefore$ t = 1.77 $\Delta f/\rho$ Å. (99B)

In practice, the value of ρ is uncertain, and the monitor is usually calibrated for each evaporant using an absolute thickness measurement technique. Multiple beam interferometry was used in this work.

During deposition the frequency shift was continuously displayed on the Rikadenki recorder. A deposition rate recorder-output was also available from the Toyocom monitor. However, rate was usually observed directly from the monitor's rate meter and checked by computation from the frequency shift traces.

5.2.3 Chamber pressure

The Penning gauge ouptut was connected to the third channel of the Rikadenki recorder, providing a continuous record of chamber

pressure during deposition. Recorder outputs were also available from the Pirani gauge units; these were occasionally used to monitor outgassing cycles.

In some instances, when it was desirable to monitor an additional deposition parameter, e.g., rate of deposition or a second resistance measurement, the chamber pressure was recorded on a Goerz Minegor Type RE501 potentiometric recorder.

5.2.4 Deposition time

An event marker is fitted to the Rikadenki recorder. This was actuated at the commencement and conclusion of deposition, coincident with the opening and closing of a mechanical shutter interposed between the evaporant and substrate.

5.3 Substrates

It is obviously desirable to prepare all of the film samples required for a particular series of measurements during a single deposition. To do so ensures that there is a unique relationship between film thickness, structure, resistance and the measured optical and thermal properties. This requirement was achieved as follows.

Substrates were mounted on a 9in (33cm) diameter 16-gauge stainless steel support plate. The substrates were arranged within a 7.5cm diameter circle at the centre of the support plate, immediately above the evaporation source. It can be shown (ref. 36) that the thickness, t, at a distance, r, from the centre of the plate is

$$t = t_o\left[1+(r/h)^2\right]^{-\frac{3}{2}} \qquad (100)$$

where h is the vertical distance from the vapour source to the centre of the plate and t_o is the thickness at the centre of the plate. This equation applies for a point evaporation source, and represents the worst practical case. Greater uniformity is achieved with an extended source,

such as a resistance heated tungsten filament. Inserting r (3.75cm) and the evaporation distance, h (20cm), we obtain

$t \simeq 0.95\ t_o$

Thus the maximum thickness variation is 5%. In practice the variation is much less, both for the individual substrates and from substrate to substrate. The maximum substrate size was 2.5cm diameter and substrates were arranged on a circle about the source, thereby ensuring uniformity between specimens.

The substrate arrangement for a typical nickel evaporation is illustrated in figure13. The substrates are mounted in holders fitted to the support plate. The holders can be removed to facilitate substrate preparation and assembly in a laminar flow work station. The function of the various substrates is described below.

5.3.1 Resistance measurement

Two types of substrates were employed for resistance measurements.

(a) Glass substrates :

25mm long x 12.5mm wide glass substrates, having a standardized electrode geometry, were prepared in large batches and used extensively throughout the research program. One of these substrates was included as a reference in most depositions. Soda-lime glass was used for routine measurements; borosilicate glass was preferred for accurate measurements because of its superior chemical stability. The substrate was masked to expose a 6.25mm wide strip to the evaporant, oriented at right angles to the gap between the gold contacts, and the resistance element was a 6.25mm square, defined by the gold contacts. The resistance was thus measured directly in ohms per square. The substrate was spring loaded in the substrate holder (see figure

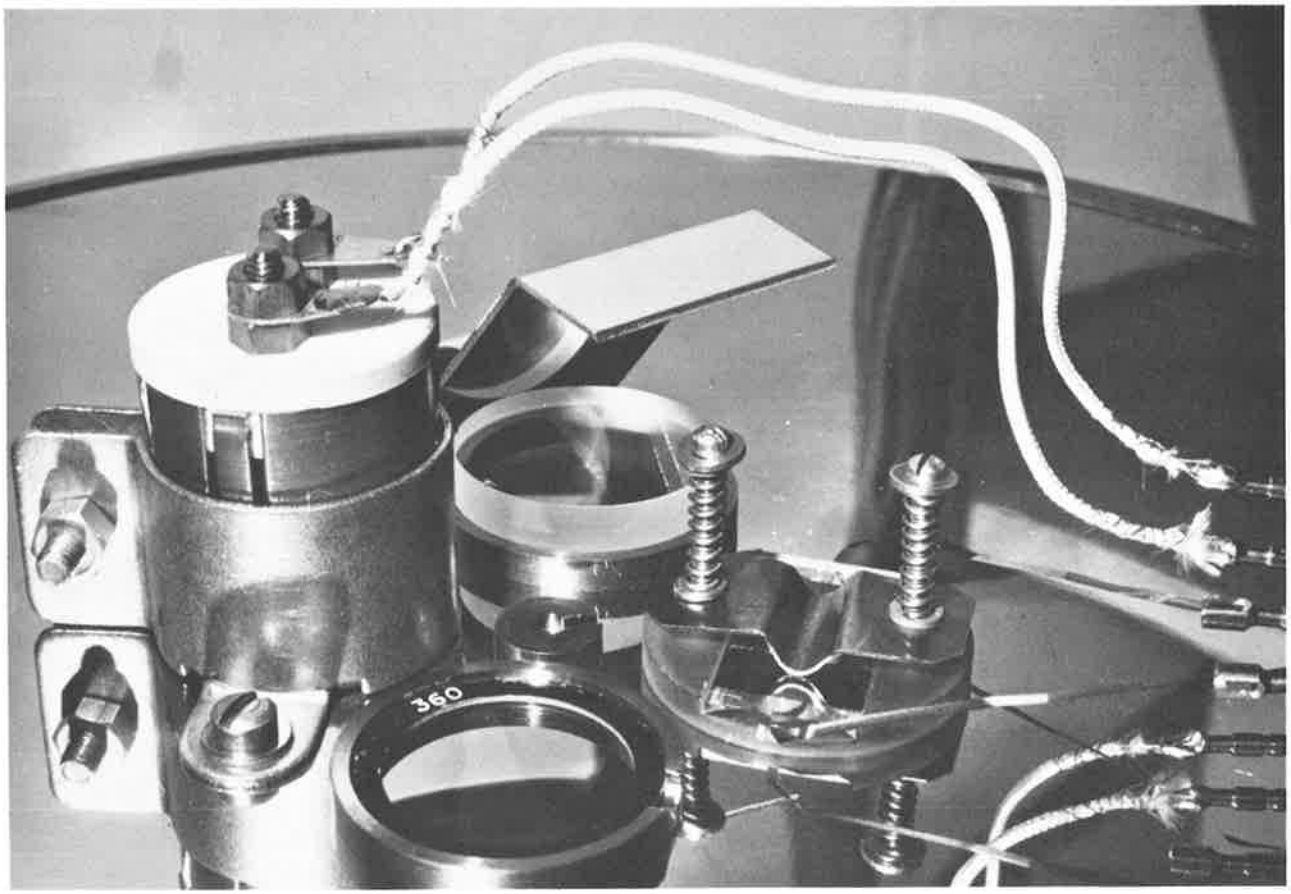

Neg. No. 18A

Figure 13. Substrate arrangement

13). The holder was machined from cast epoxy resin.

(b) Polymer film substrates

Substrates were prepared with various electrode geometries, depending on requirements for thermal measurements (Section 5.3.6). It is important that measurements of resistance be carried out on films deposited on to plastic substrates because these substrates were used for the measurement of optical and thermal properties, and there is reason to suspect that the resistance may differ for various surface structures.

5.3.2 Thickness monitor sensing head

The sensing head was clamped to the support plate with the quartz crystal element exposed to the vapour stream and positioned at the same evaporation distance as the other substrates (see figure 13).

5.3.3 Thickness measurement

A 25mm diameter x 6.25mm thick glass disc, ground and polished to one fringe on the face exposed to the evaporant, was mounted in a precision-machined brass substrate holder, as shown in figure 13. This holder was shaped to expose only one half of the disc to the vapour stream.

After deposition the disc was coated with an opaque silver layer and the film thickness was determined by multiple beam interferometry. This measurement was also used to calibrate the thickness monitor.

5.3.4 Infrared measurements

The substrate consisted of a thin self-supporting plastic film mounted on a 25mm o.d., 20mm i.d. aluminium annulus. This mounting ring was of a standardized design to match the work

holders of various infrared instrumentation. The holder for the mounting ring was precision-machined brass. The entire substrate surface was exposed to the evaporant. One such substrate is illustrated in figure 13.

The preparation of the plastic films is described in Section 5.4. The films have a high infrared transmission and low emissivity and are therefore particularly suited to measurement of the infrared optical properties of the deposited metallic film.

5.3.5 Electron microscopy

A 3mm diameter electron microscope grid carrier was mounted in a brass substrate holder at the centre of the support plate. A 500 line per cm copper grid was used in the earlier research on nichrome films. This was replaced for the study of nickel films with a 250 line per cm London Finder grid. The substrate was a thin self-supporting plastic film.

After deposition the grid carrier was transferred to a grid storage unit for subsequent examination of film structure by transmission electron microscopy. The plastic film transmits the electron beam. However, the choice of plastics is important; lower melting point plastics tend to rupture due to beam heating.

5.3.6 Measurement of thermal properties

Polymer substrates used for resistance measurements were specifically designed for the study of thermal properties. Self-supporting plastic films were mounted on 25mm diameter x 1.5mm thick epoxy annuli or slotted discs. The substrates were masked to generate the appropriate film patterns. The most common element sizes were a 12.5mm x 2.5mm strip and a 2.5mm square.

5.3.7 Measurement of film resistance on plastic substrates

Discrete measurements of film resistance were carried out on absorber films deposited on to the standard 25mm diameter plastic substrates. The measurement jig consists of two concentric gold-plated brass cylinders clamped in an SRBF mount. The film is placed in physical contact with the coplanar end faces of the cylinders. The resistance measured between the cylinders is :

$$R = \frac{1}{2\pi} \cdot \ell n\left(\frac{r}{r_o}\right) \cdot R_s \qquad (101)$$

where r_o is the radius of the inner cylinder, r is the radius of the outer cylinder and R_s is the sheet resistance (ohm per square).

5.4 Preparation of polymer film substrates

A number of polymers were investigated for their suitability as ultra-thin infrared-transmitting substrates. The films were prepared from solutions of the polymers in organic solvents using a technique employed extensively in the author's laboratory. This technique, to be described below (Section 5.4.6), can yield uniform films of thickness 500Å or less. Typical solution concentrations are 1% to 2% weight per volume.

We have found that organic solvents with an evaporation rate of approximately 1/10 to 1/15 relative to ether are the most suitable for the preparation of solvent-cast films. Thus amyl acetate and xylene are useful solvents. It is of course not always possible to achieve this ideal because of the solution properties of the various plastics. Indeed many desirable plastics cannot be used because they have a low solubility in the most suitable common solvents. This difficulty can often be overcome by the use of latent solvents or diluents.

The polymer materials should have a high molecular weight and after casting into thin membranes, should be suitably crosslinked or "tangled"

so that they remain self-supporting whilst retaining flexibility. Unfortunately polymers which appear eminently suitable are often difficult or impossible to prepare because of brittleness or low solubility. Some polymers may be readily cast but fracture either during deposition or when only moderately heated. These same films may, however, be more suitable for use in electron microscopy. The polymers investigated in this research project are discussed in the following subsections. Crosslinking techniques were not studied.

5.4.1 Cellulose nitrate

Cellulose nitrate (collodion) films have been used widely in the author's laboratory. Highly uniform films are cast from amyl acetate solutions. Collodion was used extensively in this study, particularly for the measurement of optical and thermal properties. Collodion films are flexible and strong but are easily damaged in the electron microscope.

5.4.2 Polyvinyl formal

Polyvinyl formal (formvar) films, cast from 1% and 2% W/V chloroform solutions, were investigated as a replacement for collodion for use in electron microscopy. The films are easy to prepare and are more resistant to rupture in the electron microscope. Polymer powder was purchased from Polaron Instruments Limited. The molecular weight is not known.

5.4.3 Polyvinyl chloride

Polyvinyl chloride (PVC) films were prepared from 9:1 methyl ethyl ketone/toluene solutions. The PVC used was Corvic 20-6506-00, a high molecular weight formulation (K-value 65) provided as a high purity sample by Imperial Chemical Industries. 2% solutions were prepared by dissolving the polymer in the solvent

at 40°C using a reflux condenser. The toluene acted as a diluent and dispersent. Good quality films may be cast from this solution.

5.4.4 Chlorinated PVC

This polymer was investigated as a possible alternative to PVC. The plastic is marketed as Genclor-S, manufactured by I.C.I. It has the advantage of solubility in a wide range of organic solvents. Thin films were readily cast from methyl isobutyl ketone solutions. Although suitable for certain specialized applications, this polymer appears to have no particular advantage in the present context over the materials mentioned above.

5.4.5 Polyvinylidene chloride - acrylonitrile copolymer

The polymers polyvinylidene chloride and polyacrylonitrile would appear to be particularly suitable for use as self-supporting substrates, but have only low solubility in common solvents. Their copolymer is, however, soluble in selected solvents, and would be expected to retain at least some of the desirable properties of the parent polymers.

The polymer investigated was Saran F-300, a high molecular weight formulation provided by the Dow Chemical Company. Thin films were readily cast from 1% and 2% W/V solutions in 80:20 methyl ethyl ketone/methyl isobutyl ketone. Methyl ethyl ketone is the active solvent; methyl isobutyl ketone is a latent solvent. Other solvents, e.g., amyl acetate, may be added as diluents.

5.4.6 Preparation of self-supporting films

The film casting technique described here has been used extensively for many years in the author's laboratory. The experimental apparatus is illustrated in figure 14. The films are prepared

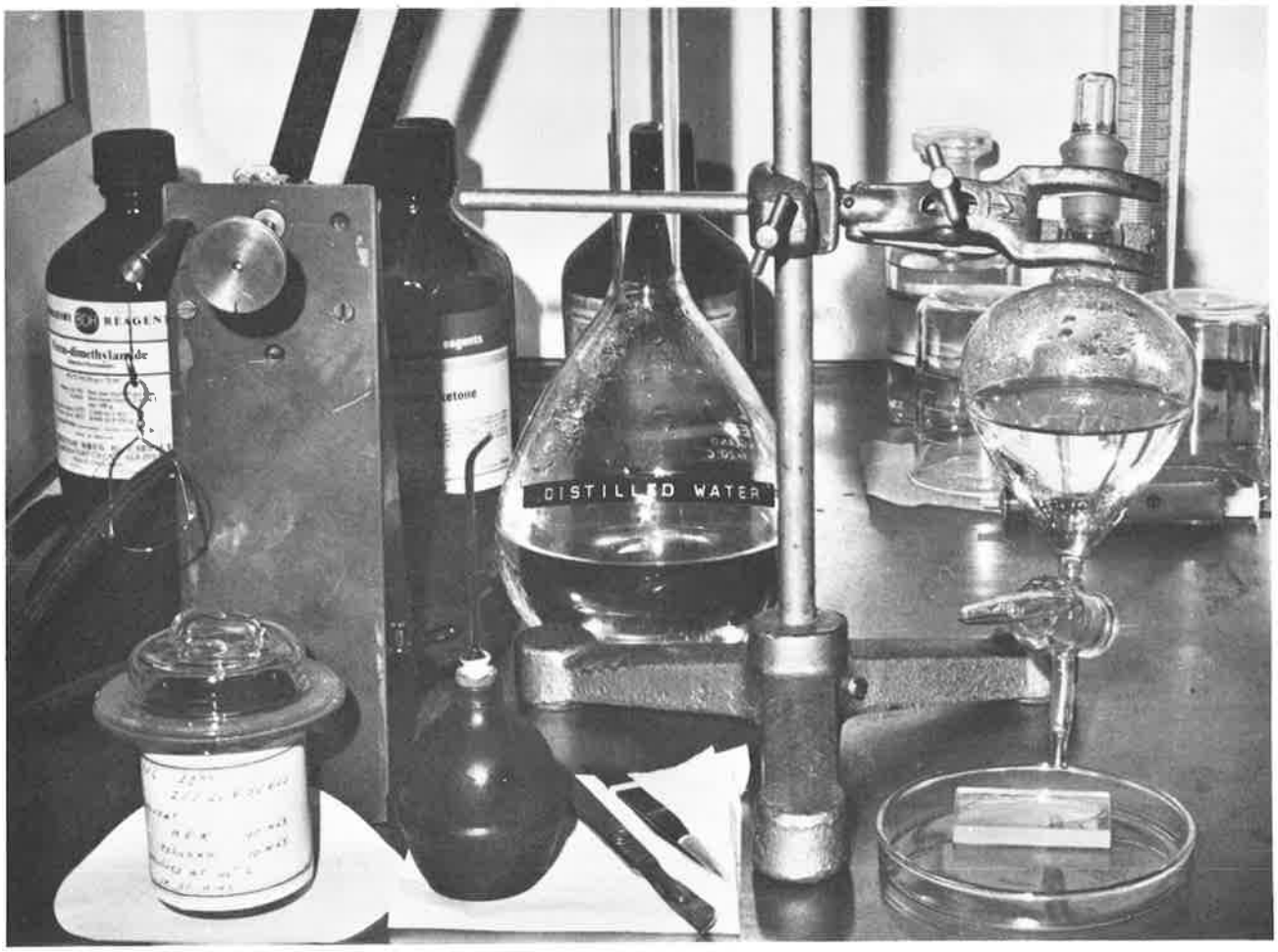

Neg No. 23A

Figure 14. Apparatus for the preparation of polymer films

by lowering a glass disc into the polymer solution and withdrawing at a constant rate, using a small synchronous motor. The withdrawal rate in this work was 8 $cm.min^{-1}$. After coating, the disc is scribed at the edge with a scalpel then placed in a Petri dish, where it rests against a support at an angle of about 20^{o} to the horizontal. Distilled water is slowly added to the Petri dish and the film separates from the disc and floats to the water surface. It is then collected on a 25mm diameter aluminium annulus. Films of uniform thickness are readily prepared by this method from 2% W/V solutions. When thinner films are required the glass disc is precoated with an evaporated potassium bromide separating layer. The technique is not suitable for the preparation of thick films because of variation in thickness; however, a slower withdrawal rate may overcome this problem.

All polymers were filtered using Millipore micro-syringe apparatus with MF Mipor or Mitex final filters.

Polymer substrates for electron microscopy were prepared by the above method and transferred to grid carriers using a precision punch. Each 25mm diameter film yielded 6 or more grid carrier substrates.

5.4.7 Selected polymer films

The polymer materials discussed above are all easily cast into thin films and have useful applications as substrates or as protective layers in vacuum and optical technology. Many other polymers were investigated; however, these were either difficult to cast or were inferior to the materials previously described. The author is continuing a study of certain promising high-working-temperature polymers. Polyacrylonitrile (PAN) in particular, has

very considerable potential. PAN films have been successfully prepared by spin coating techniques, but a routine high-yield process schedule has not, as yet, been perfected for our infrared absorber studies.

In this project collodian and PVC were used for infrared and thermal studies; collodion, PVC and formvar for electron microscopy. Saran films have so far proved disappointing; they appear to rupture easily during deposition and cannot withstand heating above 70°C. Some relevant properties of the selected polymers are listed in Table 3.

TABLE 3

SELECTED POLYMER FILMS

Film Type	Concentration (% Weight Per volume)	Solvent	Rupture Temperature (°C)
Collodion	2	Amyl acetate	160
Formvar	2	Chloroform	120
PVC	3	MEK/toluene	140
Genclor-S	2	MIBK	110
Saran F-300	2	MEK/MIBK	70

The rupture temperature cited in the table refers to 25mm diameter films.

It is clearly difficult to predict with certainty the suitability of the various polymers as thin film substrates. Thus we have the surprising result that collodion films will withstand heat treatment up to 150°C, whereas the other plastics, notably Saran, rupture at a lower temperature. The situation is further complicated by the tendency of large-diameter films to rupture during deposition. Here

again, collodion proved to be superior to the other materials tested. On the other hand, collodion is more easily damaged in the electron microscope.

The thickness of collodion and formvar films used in this project was 500 to 1200Å. PVC was selected when thicker films were required. These PVC films were more uniform in thickness than collodion (because of the lower vapour pressure of the solvent) and were free of strong absorption peaks in the infrared.

5.5 Cleaning and handling of substrates

The need for substrate cleanliness in thin film technology cannot be over-emphasised. In this project direct handling of substrates was avoided if possible, and where unavoidable, polythene or terylene gloves were used. In general,however, substrates were cleaned and transported in glass holders and were manipulated with suitably shaped tweezers. They were stored in dust free containers (in some instances vacuum desiccators), and preparation for deposition was carried out in a laminar flow work station.

The cleaning schedule used for glass substrates is as follows :

(a) ultrasonic agitation in trichloroethane (Dowclene WR)

(b) clean in hot R.B.S.25 solution

(c) rinse in hot distilled water

(d) rinse in ethanol

(e) rinse in distilled de-ionized water

(f) water removal with blast of filtered dry nitrogen

(g) dry in oven at 60 to 80°C in covered container

It will be noted that the schedule does not include a final solvent degreasing, e.g., vapour degreasing in isopropyl alcohol. The solvent must be extremely clean, otherwise a residue will remain on the glass

surface. The above schedule avoids this difficulty and yields contamination free substrates.

Dowclene WR solvent was preferred for the final stage of large scale cleaning operations.

5.6 Deposition of gold films

All gold films were prepared in the ancilliary coating unit. Gold was evaporated from a 0.25mm thick molybdenum dimpled-strip vapour source. The evaporant was 0.5mm diameter high purity gold wire.

The substrate arrangement used in the ancilliary coating unit was similar to that described in Section 5.3. A simplified resistance measurement technique was adopted, in which the substrate was inserted in a simple voltage divider circuit and the voltage drop monitored with a d.c. null voltmeter. During some depositions film resistance and thickness monitor frequency shift were recorded on a Honeywell ultraviolet spot-galvanometer recorder.

5.7 Deposition of chromium films

A brief study was made of chromium films for comparison with nickel and nichrome films. Chromium was evaporated from a resistance heated molybdenum source similar to that used for gold. The evaporant was 325 mesh 99.9% pure chromium powder. Chromium sublimes direct from the solid and does not alloy with the source material. It adheres strongly to glass substrates, and for this reason is often used as a "keying" layer for poorly adherent evaporants such as gold.

Chromium films of resistance 200 ohm per square were found to be very much thicker than nickel, gold and nichrome films of similar resistance. This phenomenon is probably the result of superficial oxidation during deposition at a pressure of 10^{-5} torr. Chromium films did not show any marked instability in air; however, the results of this limited study

are inconclusive, the value of the chromium depositions lying mainly in the interpretation of film structure (Section 10).

5.8 Deposition of nichrome films

The nickel-chromium alloy used in this project was Nichrome-V, manufactured by British Driver-Harris Co. Ltd. The composition of the alloy is 80 parts nickel and 20 parts chromium. The nichrome was evaporated from a 3-strand (3 x 1mm diameter) resistance-heated tungsten wire helix filament vapour source. The evaporant comprised short lengths of 1mm diameter nichrome wire crimped to the filament. A filament current of about 60A at 8.5V was required for deposition.

The filament was "flash" cleaned prior to melting the evaporant. The evaporant readily wets the tungsten. However, rapid alloying occurs; hence to avoid filament failure a new filament was used for each deposition. This procedure also helps to ensure a uniform film composition, as successive evaporations from the same filament yield a varying nickel-chromium alloy ratio. The evaporant charge was approximately 0.75g.

Films were prepared in the vacuum coating unit described in Section 5.1 and deposition was monitored with the apparatus described in Section 5.2.

5.9 Deposition of nickel films

Nickel films were studied extensively during this project. Because of the large number of specimens required for optical, structure and thermal analysis, two vacuum coating units were used for film preparations. Systematic research studies were carried out using the coating unit described in Section 5.1. The ancillary unit was used for pilot depositions and certain specialised experiments. This duplication afforded information on the influence of different methods of deposition on film properties.

5.9.1 Filament vapour source deposition

A resistance heated tungsten wire helix vapour source was used for nickel depositions in the ancilliary vacuum coating unit. A heavy 3-strand (3 x 1mm diameter) helix was employed to avoid rapid filament burnout due to alloying action, and the weight of evaporant was kept below 1/6 of that of the tungsten source.

The evaporant was Johnson-Matthey Grade A (99.5%) nickel wire, commonly called Nickel 200. A filament current of 80A at 3.0V was required for deposition.

5.9.2 Electron beam deposition

Electron beam deposition was chosen for detailed research studies on nickel infrared absorber films. This method of deposition offers many advantages in thin film research, notably the ability to prepare high purity films of a wide range of 'difficult' evaporants. Nickel is one such difficult material. With the exception of aluminium oxide, it alloys or reacts with all common source materials. This problem can be avoided with electron beam deposition. When the evaporant is vaporized from a water-cooled hearth or crucible, interaction with the source does not take place. Furthermore, during initial outgassing cycles many contaminants are either removed from the evaporant by vaporization, or are "leached out" to the cold area adjacent to the hearth. There is no contamination from the source material and evaporation takes place from an intense heat zone defined by the focussed electron beam. The deposited films, using high purity evaporant, are therefore of high purity. In addition, a number of depositions can be carried out from the same evaporant charge.

A Planer type EBS1 electron beam evaporation source was used for

the deposition of nickel films. This unit is a commercial version of the Unvala deposition source (ref. 37). It is an electrostatically-focussed diode electron gun of the "work-focussed" type. The principle of operation may be understood upon reference to figure 15. Electrons emitted from the circular filament are repelled by the negatively charged filament shield and focussing cage, and are constrained to move in a curved path to impinge on the evaporant, which rests on a water-cooled copper hearth held at earth potential. Electron focussing is achieved by raising or lowering the focussing cage. The specified minimum spot size is less than 1mm; in practice the observed spot size for metal evaporants was about 2mm.

Grade A nickel (Nickel 200) was used for the preparation of infra-red absorber films. This material has a minimum nickel content of 99.5%.

Work-focussed sources of the Planer type are space charge limited. This sets a limit to the deposition rate, depending on the type of evaporant. The source is particularly prone to field effects, and a pseudo-triode action has been observed (ref. 38). A disturbing characteristic, which is observed with metallic evaporants, is high voltage discharge caused by ionization of the vapour cloud surrounding the evaporant. To cope with this discharge the electron gun power supply must have ample surge protection and must continue to function without interrupting the deposition. The discharge may damage fragile substrates, and may either damage or induce transients in monitoring circuitry.

The Planer source was found to be markedly prone to high voltage discharge effects, including cold emission between the filament shield

Neg. No. 6A

(a) Planer source with electron deflector plates

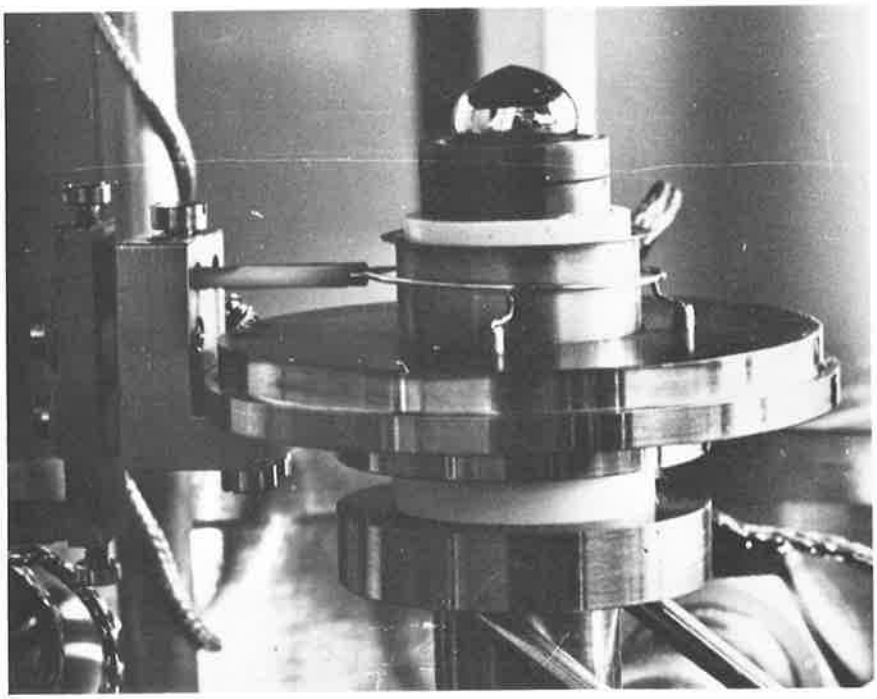

Neg. No. 17A

(b) Showing focussing cage removed

Figure 15. Electron beam deposition source

and hearth pedestal. It was found necessary to make extensive modifications to the commercial power supply, primarily the provision of a new RLC filter for surge limitation, and improved overload protection devices. A matched Planer power supply was not available.

A marked improvement in the operation of the Planer source was achieved by inserting an insulator sleeve between the hearth pedestal and filament shield of the electron gun. This eliminated cold emission and reduced discharges during deposition. The exposed surface of the insulator (see figure 15) became coated with metal during deposition - although not in direct line with the evaporant - necessitating cleaning after each process. Failure to remove this coating resulted in an increase in the number of discharges, and excessive current leakage. A silica sleeve was found to be the most effective; however, the metal coating was difficult to remove. Boron nitride was subsequently used in the Planer source. This material is readily machined and the metal contaminant easily removed with a scalpel blade.

Another serious characteristic was the high electron density in the undisturbed vapour beam. This phenomena is common to all types of high voltage electron beam deposition sources, and is probably caused by specular reflection of some of the electrons in the primary beam. With the Planer source, operated at a voltage of 4kV and emission current of 100mA, an electron current of 250 μA was measured at a 25mm diameter collector plate situated in the substrate plane. This resulted in total destruction of polymer membrane substrates (approximately 50% of electrons of 4kV energy are absorbed by a 1000Å thick polymer film), and it became

impracticable to monitor film resistance during deposition. This difficulty was largely eliminated by placing parallel electrostatic deflector plates above the source, with one deflector held at filament potential. A circular metal plate with a 2cm diameter aperture was inserted immediately above the focussing cage, and was also held at filament potential. This arrangement is illustrated in figure 15. The measured electron current at the substrate was reduced to less than 1 μA.

We should note, finally, a further consequence of the use of a water-cooled hearth. Nickel depositions carried out from a graphite hearth placed in physical contact with the water cooled hearth pedestal, were accompanied by excessive spitting of the evaporant. No spitting was observed when nickel was evaporated from the copper hearth, which was soldered to the pedestal to achieve maximum heat sinking.

Nickel depositions from the copper hearth were carried out at a voltage of 4 to 5kV and an emission current of 100mA. The filament current was 18 to 20A. Sufficient specimens were obtained to satisfy the requirements of this project.

6. OPTICAL MEASUREMENT TECHNIQUES

6.1 Measurement of film thickness

The thickness of metal absorber films and polymer substrates was measured with a Tolansky multiple beam interferometer. This instrument, illustrated in figure 16, was designed and constructed in the author's laboratory. The initial design study was carried out by a co-worker and is described in an internal report (ref. 39). The interferometer was assembled, aligned and tested by the author and his technical staff. The author is also responsible for the provision of reference optical flats

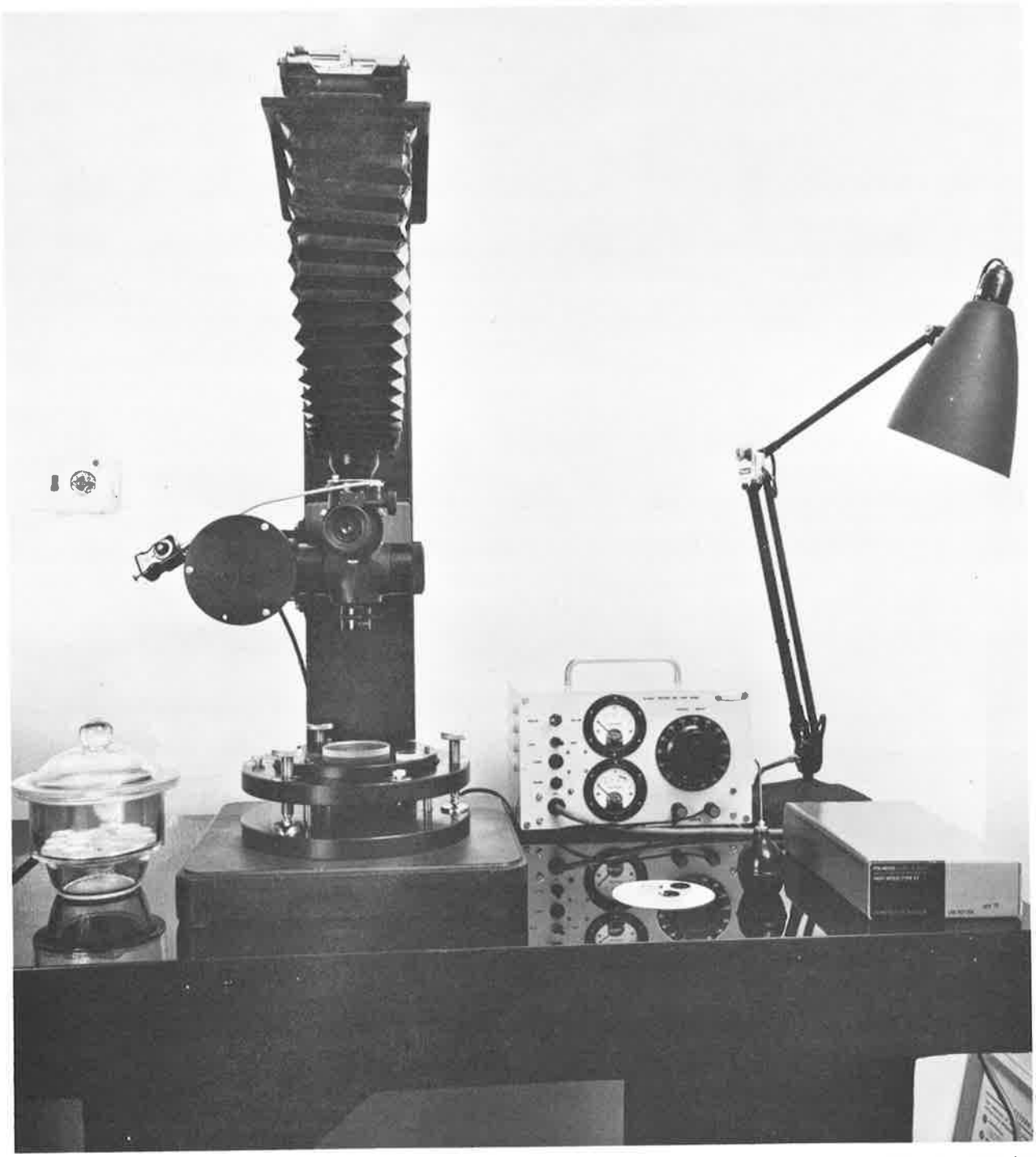

Neg. No. N73/631

Figure 16. Tolansky multiple beam interferometer

and validation of the interferometer for the accurate measurement of film thickness.

6.1.1 Tolansky interferometer

Multiple beam interferometry was developed as a thickness measurement technique by Tolansky (ref. 40) and is now well established in thin film technology (refs. 35, 36). An excellent review is given in reference 41. When operated in the reflection mode, the technique requires that the thin film to be measured be coated with an opaque, highly reflecting surface layer. This layer is brought into close proximity to a master optical flat, forming a narrow wedge between the two surfaces. The master flat is coated with a highly reflecting, partially transmitting surface film. This arrangement is illuminated with monochromatic radiation and the resultant intense fringe pattern is viewed in reflected light. If a ledge is formed in the specimen prior to deposition of the reflecting layer, then the fringe pattern is displaced along the ledge. The displacement is a measure of film thickness, according to the equation

$$t = (n+a/b)\,\frac{\lambda}{2} \qquad (102)$$

where n is the fringe order, a is the fringe displacement (measured as a fraction of one fringe width), b is the fringe separation and λ is the wavelength of the radiation source.

The preparation of the specimen film for thickness measurement is a simple procedure. The specimen is coated with an opaque silver layer by vacuum deposition. This layer should be evaporated at room temperature using a high deposition rate to achieve a fine grain film. Scrupulous cleanliness is essential. The ledge is formed on the specimen film (prior to silvering) by etching, or by

masking during the deposition. In this project the 25mm diameter glass substrates described in Section 5.3.3 were used, and the silvered specimens were stored in a vacuum desiccator to avoid tarnishing.

The master flat must satisfy certain optical requirements if sharp, high contrast fringes are to be obtained. The fringe intensity at normal incidence is given by the Airy formula

$$I = \frac{I_0}{1+F\sin^2(2\pi d/\lambda)} \quad , \tag{103}$$

where d is the wedge spacing and λ the wavelength of incident radiation.

F is the Fabry coefficient of fineness, and is determined from

$$F = \frac{4R}{(1-R)^2} \tag{104}$$

where R is the reflectance of the coated surface of the master optical flat. Clearly R should be as large as possible. Of more direct practical value is the fringe half width, W, which, when $I = I_0/2$, is given by

$$W = \frac{1-R}{\pi R^{\frac{1}{2}}} \quad , \tag{105}$$

expressed as a fraction of the fringe spacing. For maximum resolution we seek a high reflectance.

If the master flat coating is absorbing, the fringe shape remains the same but the contrast is reduced. In the ideal case (no absorption)

$$C_o = \frac{(1+R)^2}{(1-R)^2} \quad , \tag{106}$$

however, for non-zero absorption the actual contrast is

$$C_a = C_o/(1+\frac{A}{T})^2 \tag{107}$$

Thus a second requirement is that the ratio of the absorption to transmission, A/T, must be as small as possible. The film must,

of course, be partially transmitting to enable the fringes to be seen.

The best metallic reflector is silver. However, the highest attainable reflectivity for silver films is about 0.95 and the absorptivity is then approximately 0.04. Multilayer dielectric coatings can be prepared with an absorption of less than 0.005. These coatings are mechanically durable and do not tarnish, and hence are an obvious choice for interferometry. The author employed two master optical flats in this project. The reflecting surfaces were Jacka mirror coatings, one having a reflectance of 0.92 for routine measurements, the other 0.95 for high resolution measurements. Assuming A = 0.005, the above theory provides :

MASTER 1 $R = 0.92$ $A/T = 0.067$ $C_a/C_o = 0.88$ $W = 72.5$ Å

MASTER 2 $R = 0.95$ $A/T = 0.11$ $C_a/C_o = 0.81$ $W = 44.5$ Å

The line half width is given for a wavelength of 5461Å (mercury green). The reflectances of the mirror coatings were peaked at this wavelength.

The surface of the optical flat should be very smooth; in fact this is more important than flatness. The thickness of the flat should be no less than 1/6 the diameter to avoid flexure and consequent fringe bending. Finally, it should be thermally stable. The flats used in this work were manufactured from Homosil (silica) in the Weapons Research Establishment optical laboratories. They were polished to 1/10 fringes and specified scratch and sleek free. The dimensions of the flats are 7.5cm diameter, 1.25cm thick.

The incident radiation is collimated mercury green light (wavelength 5461Å). The source is a medium pressure mercury arc lamp.

6.1.2 Thickness measurements

The best fringes are obtained at the smallest wedge angle and minimum wedge spacing. The wedge angle is limited in practice by localized pressure effects, which cause fringe bending. The technique used in this study was to set visually the interferometer for the sharpest, undisturbed fringe pattern, then photograph the pattern with the Polaroid camera attachment shown in figure 16. The fringe separation and step displacement were then measured with a travelling microscope and the thickness calculated from equation (102). The final thickness was deduced from the statistical average of a minimum of 6 sample measurements.

A typical fringe pattern is illustrated in figure 17. The measured instrument accuracy using the statistical sampling technique was $\pm$ 5Å for films of thickness greater than 100Å. It was found that approximately 4 fringes/cm gave the highest accuracy. The attainable fringe half width was less than 50Å, using a master flat with 0.92 reflectance. The line width set a lower limit to routine thickness measurement of 50Å with an accuracy of $\pm$ 10Å. With care, greater accuracy is possible.

6.2 Measurement of spectral absorptance

6.2.1 Infrared spectrophotometer

The transmittance and reflectance of thin metallic absorber films were measured over the spectral range 1 to 16 μm with a Beckman Model IR4 double-beam infrared spectrophotometer. The film absorptance was deduced from equation (51). Specimens were prepared by deposition of the metal on to thin polymer substrates mounted on standard 25mm o.d., 20mm i.d. aluminium annuli, as described in Section 5.3.4. The thickness and sheet resistance

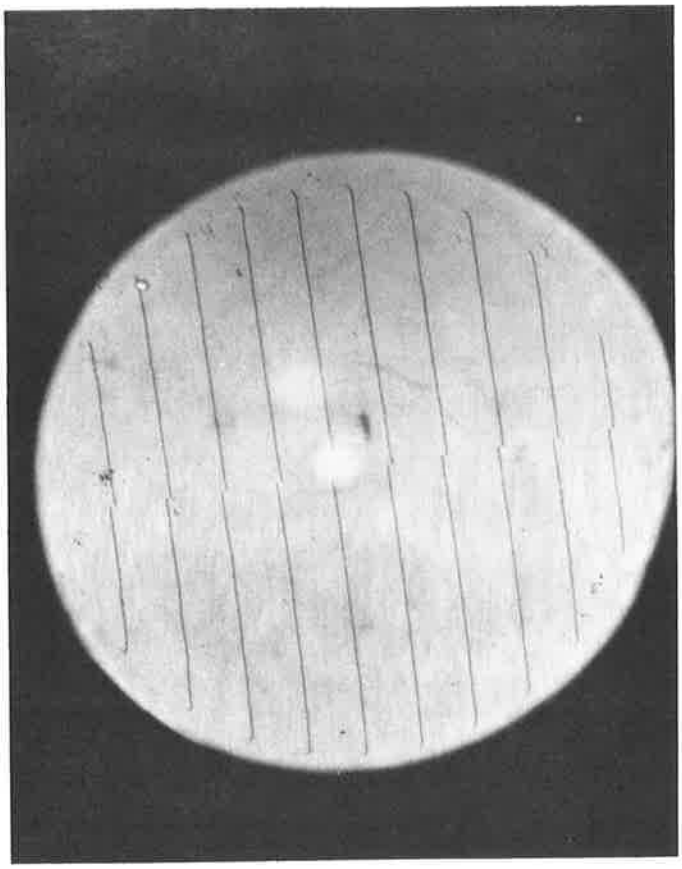

Wavelength	5461 Å
Master reflectance	0.95
Film thickness	238 Å

Figure 17. Tolansky fringe pattern

of the films were determined prior to optical measurement.

The infrared spectrophotometer is illustrated in figure 18.

The Model IR4 spectrophotometer is essentially a transmission measuring instrument. Precision work holders have been manufactured specifically for use with the 25mm annuli. Spectral transmission scans are executed automatically over the range 1 to 16 μm with a routine resolution of better than 0.03 μm. The transmission measurement accuracy is typically 1% or less.

Spectral reflectance is measured with a "reflectance attachment", which is provided as an instrument accessory. This device comprises an aluminized 120^{o} icosceles prism, and a specimen holder. When placed in the transmission path, radiation is reflected at a 60^{o} angle of incidence from the first prism surface to the specimen which is orientated parallel to the transmission path, thence to the second prism surface where it is reflected back along the original path. The radiation path is thus arranged symmetrically, so that the incident angle at the specimen is 30^{o}. Great care must be taken with alignment.

The first step in the reflectance measurement is to insert a freshly aluminized mirror in the specimen holder and execute a spectral scan. This provides a 100% reflectance reference. The mirror is then replaced with the specimen and a second scan is carried out. During this entire operation a second reflectance attachment, with an aluminized mirror inserted in its sample holder, is positioned in the reference path of the spectrophotometer to compensate for instrument spectral non-linearity. If, at any given wavelength, the reflectance measurement for the mirror reference scan is ρ_r, and for the specimen scan is ρ_s, then

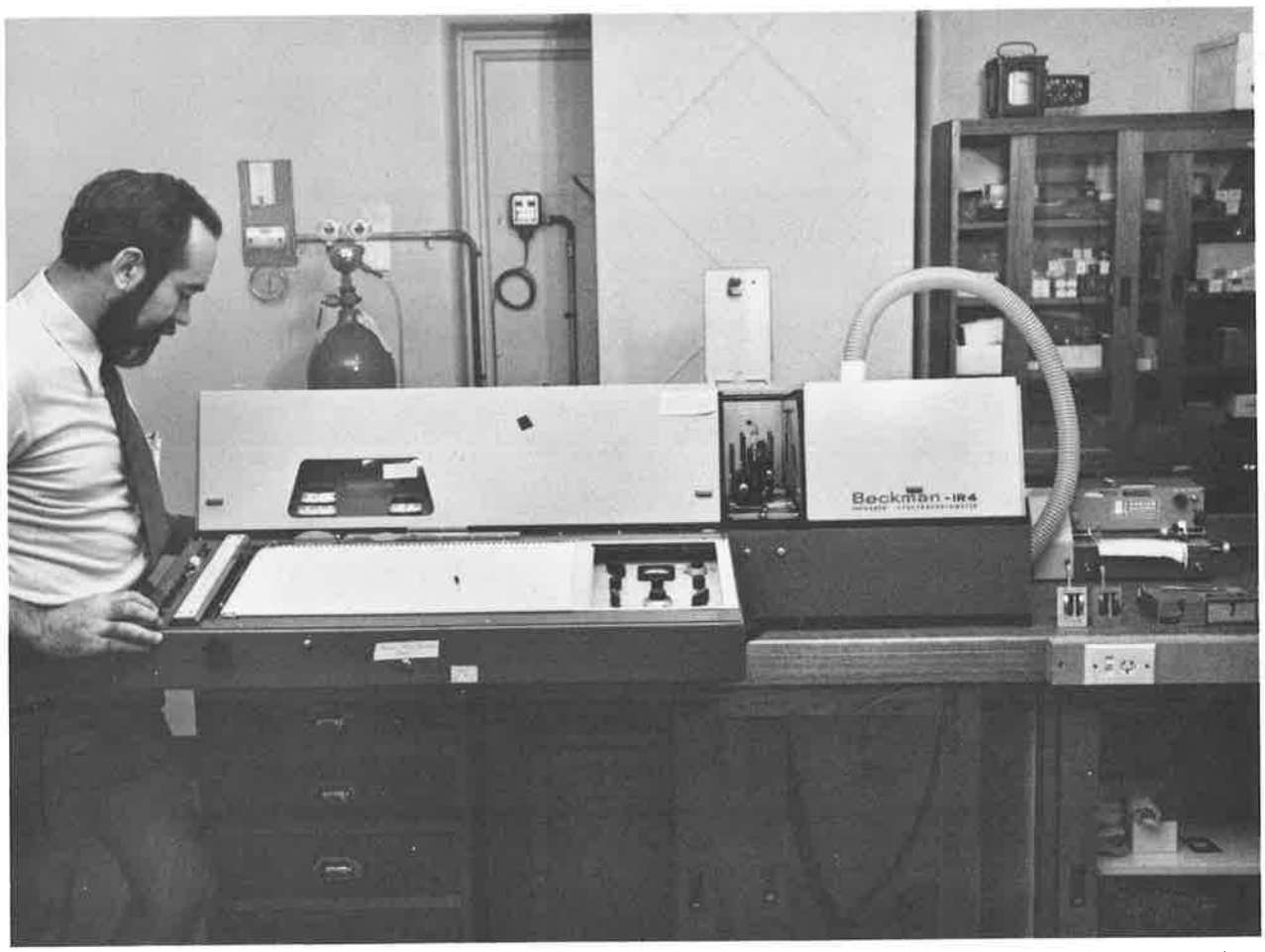

Neg. No. N73/629

Figure 18. Infrared spectrophotometer

$$\rho_r = \rho_p^2 \, \rho_m$$

and

$$\rho_s = \rho_p^2 \, \rho_f \quad , \tag{108}$$

where ρ_p, ρ_m and ρ_f are the reflectance of the prism, reference mirror and specimen film, respectively. Hence

$$\rho_f = \frac{\rho_s}{\rho_r} \, \rho_m \tag{109}$$

Thus the measurement of specimen reflectance is independent of the prism reflectance but assumes a knowledge of the reflectance of the aluminized reference mirror. Fortunately, this information is well known (see, e.g., ref. 42). Furthermore, the reflectance of vacuum deposited aluminium in the infrared is relatively insensitive to the conditions of preparation. A small drop in reflectance is observed with aging. Consequently, reference mirrors used in this project were stored in a vacuum desiccator.

6.2.2 Polymer substrates

In Section 5.4.7 a brief summary was given of research on polymer membrane substrates. It was found that of the many polymers successfully cast as thin self-supporting films, none proved to be superior to cellulose nitrate (collodion) for use as an infrared absorber substrate. Only one polymer studied, polyacrylonitrile, shows more promise; however, we have not yet established a high-yield preparation technique for ultra-thin films of this material. Accordingly, collodion substrate films were used for routine infrared measurements. PVC films were employed when a thicker substrate was required, e.g., when the fragile collodion films were damaged during deposition, and then only because the PVC substrates have no strong absorption peaks.

The measured spectral absorptance of a 850Å thick collodion film, at normal incidence, is shown in figure 19. This spectrum is typical of the substrates used for infrared measurements. There are four distinct absorption peaks, at 6 μm, 7.8 μm, 9.3 μm and 11.9 μm. The spectral reflectance is almost constant at approximately 2%; and the observed transmission spectrum is of similar (but inverted) shape to that shown in the figure. The absorption peaks, whilst of minor annoyance in absorber measurements, are used to advantage as a film reference. We have calibrated the 7.8 μm peak for the measurement of collodion thickness.

The collodion substrate is seen to have relatively little effect on the optical properties of metallic absorber films, particularly for wide-band applications. The integrated absorption over 2 to 16 μm of the 850Å thick film is 0.009, and over the 8 to 14 μm atmospheric window 0.014.

6.2.3 Spectral measurements

There are two important factors which must be taken into consideration in the measurement of spectral adsorptance of metal films on polymer film substrates, using the instrumentation described in Section 6.2.1 above :

(a) The influence of the polymer substrate

(b) The effect of measurement at non-normal incidence

These factors have relevance in both the measurement technique adopted and the interpretation of the final spectral scans.

Firstly we note that the metal film and polymer substrate are not independent of each other, but in fact together constitute a composite thin film interference filter (see Section 3.4.2). Thus the commonly applied technique of inserting an identical substrate

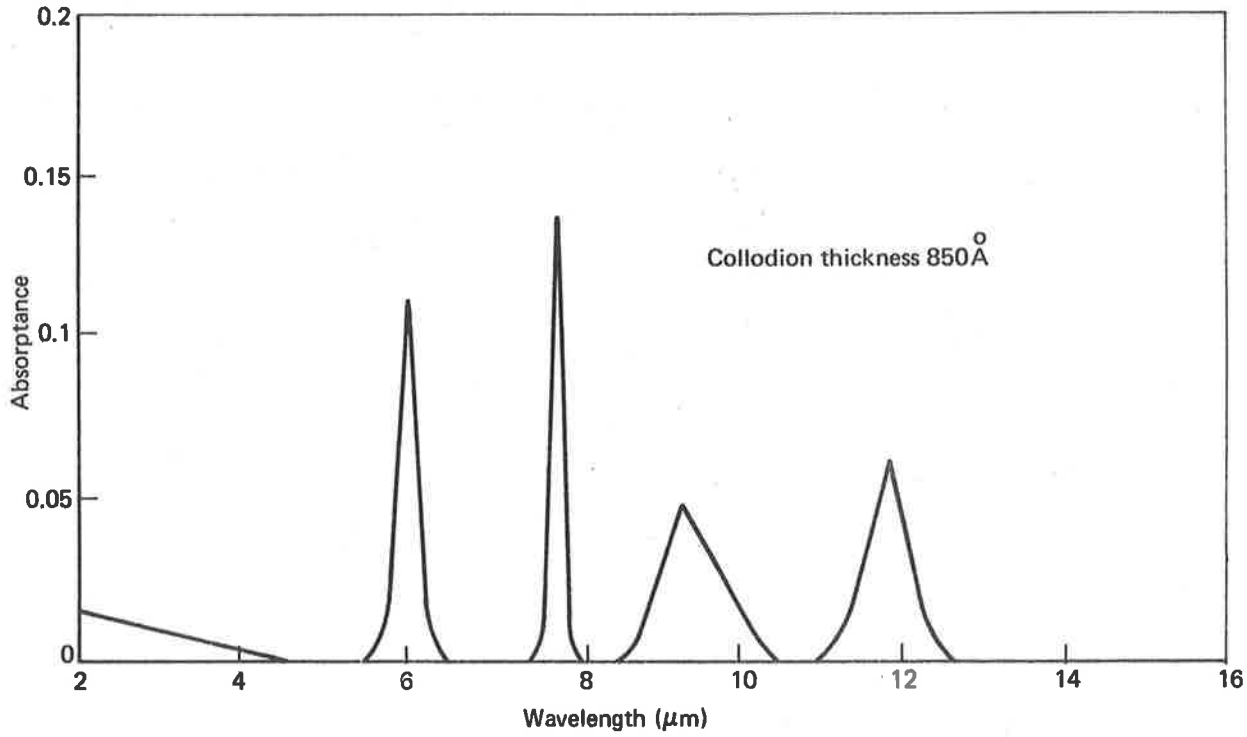

Figure 19. Spectral absorption of collodion substrates

in the reference path of the spectrophotometer, to compensate for the specimen substrate, is strictly invalid. The author has observed that when this approach is used the spectral characteristics of the substrate are still reproduced on the spectrophotometer trace. It is therefore more desirable to work with an air reference and determine, on analytical grounds, the contribution of the substrate to the measured reflectance. The simplest approach, noting that the polymer film does not greatly influence the final result, is to ingore the substrate altogether. In practice it is usually the substrate-absorber combination which is of interest. In this project results are quoted for the composite film and substrate thickness is recorded as a parameter.

The second factor concerns the angle of incidence used in the spectrophotometer measurements. We have regularly observed in absorber studies that the measured reflectance of the composite film varies by up to 5%, depending on whether the metal absorber (which we call side α) or the polymer substrate (side β) faces the incident beam. The reflectance of side α is always higher. The explanation lies in the theory stated in Section 3.4. The difference in reflectance cannot be explained in terms of the theory for normal incidence. This theory states that the transmittance should be the same for sides α and β, and this is in fact observed. Equations (76) and (78) predict that the reflectance for side α is higher than that for side β, but for a 1000Å thick polymer substrate the difference is insignificant. However, for a 30^{o} angle of incidence, the reflectance of the absorber alone is expected (equation (74)) to be 3.7% higher than at normal incidence, for a 189 ohm per square film. We therefore

deduce that the observed difference in reflectances for sides α and β is associated with the large angle of incidence.

The solution to this problem is elucidated in figure 8. The transmittance is similarly influenced by angle of incidence, but the resultant of absorptance is almost independent of measurement angle. Hence it is important that the reflectance and transmittance are both measured for the same side of the composite absorber film and at the same angle of incidence. Whichever side is measured, the resultant absorptance - determined from equation (51) - should be the same, and very nearly equal to the value at normal incidence. This is indeed what is observed in practice.

6.3 Measurement of total emissivity

6.3.1 Emissivity apparatus

An alternative method of determining the absorptance of a thin infrared absorber film is to measure the radiant emittance (radiant power per unit area), W, of the specimen film, and then compare this value with the radiant emittance, W_{bb}, of a blackbody at the same absolute temperature. From the Stefan-Boltzmann Law

$$\varepsilon = W/W_{bb} \qquad (110)$$

where ε is the emissivity (strictly, emissance) of the specimen, and is equal to the absorptance (see Section 3.1). This value of ε is the total emissivity, i.e., integrated over the blackbody spectrum for the given temperature. However, if, as theory predicts, the absorptance spectrum is flat above 2 μm wavelength, then the total greybody absorptance should compare favourably with the spectral absorptance measured as described in the preceding subsection.

The emissivity of absorber films was measured with an Emissivity Test Apparatus, which was designed and assembled by one of the author's associates. The author is responsible for recent modifications, introduced to improve instrument sensitivity. The apparatus consists of an isothermal enclosure and a broad-band infrared radiometer. The specimen to be measured, usually in the form of the standard 25mm diameter annulus, is placed in the enclosure adjacent to a blackbody reference of roughly the same dimensions. The specimen and blackbody are mounted on a rotatable disc (the "specimen wheel"), which is machined to accommodate a number of additional specimens for analysis during the same measurement cycle. The wall of the enclosure is water cooled and the chamber itself is heated with a controlled warm air draught. A potassium bromide window is fitted to the wall of the enclosure for specimen observation.

The specimen and window are situated on the optical axis of the infrared radiometer. The radiometer comprises an f/0.8, 25mm focal length monocentric reflecting optical system, and a germanium-immersed thermister flake bolometer detector. The radiation is mechanically chopped at a frequency of 72Hz. An optical modulation reference signal is provided by a pea-lamp-photodiode combination fitted to the chopper wheel assembly.

A new low noise amplifier, with phase sensitive rectification, is being developed for the Emissivity Apparatus. In this project, as a temporary arrangement, the author used a P.A.R. Model HR-8 precision lock-in amplifier to process the detector output. The amplifier was phase-locked on to the chopper reference and the amplified output signal was monitored on a Minigor Type RE501

potentiometric chart recorder.

The Emissivity Test Apparatus is illustrated in figure 20. The radiometer cover was removed for the photograph to display the optical system, and the lid of the enclosure is shown raised to illustrate the specimen holder arrangement.

During operation, one of the specimen holders is left blank, exposing a clear aperture on the specimen wheel. When the disc is rotated the detector field of view images, in turn, the specimen, the blackbody reference, and the wall of the enclosure. It is essential that the wall of the enclosure be at constant temperature; otherwise the measured absorptance will be in error, the error being a maximum for 100% reflecting films. For this reason an aluminized mirror was included in one of the specimen holders, to act as a zero absorptance reference. The specimen wheel is slightly rotated from the normal to avoid back reflection to the detector. This procedure leads to a remarkably simple computation of specimen emissivity, as derived in the following analysis.

If the temperature of the specimen and the blackbody is T (^{o}K) and the temperature of the enclosure wall is T_o (^{o}K), then the radiant emittance, as measured at the detector, is :

for the blackbody,

$$W_{bb} = \sigma T^4 \tag{111}$$

for the enclosure wall,

$$W_o = \sigma T_o^4 \tag{112}$$

and for the sample,

$$W = \varepsilon\sigma T^4 + \rho\sigma T_o^4 + \tau\sigma T_o^4 \tag{113}$$

where ε, ρ and τ are the emissivity, reflectance and transmittance of the sample. Noting that

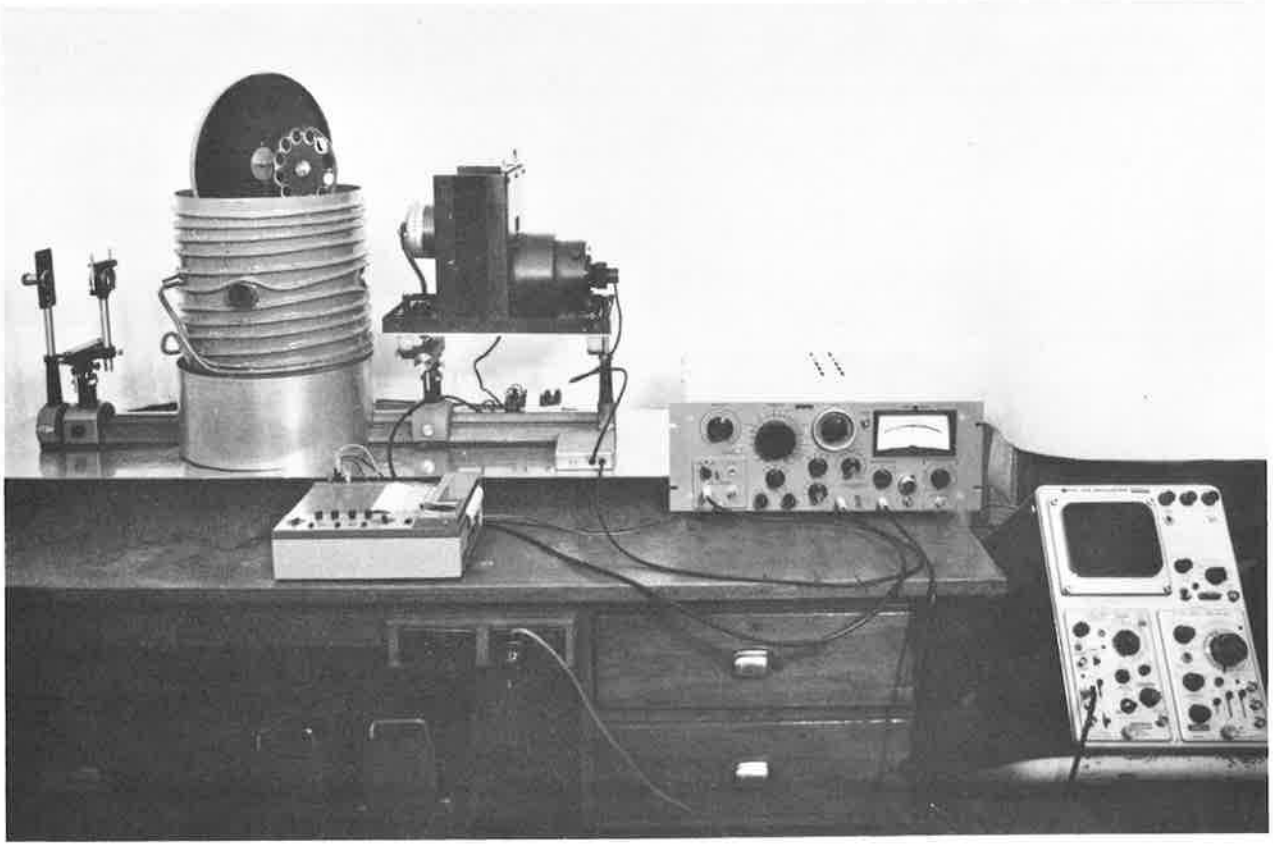

Neg. No. N73/630

Figure 20. Emissivity test apparatus

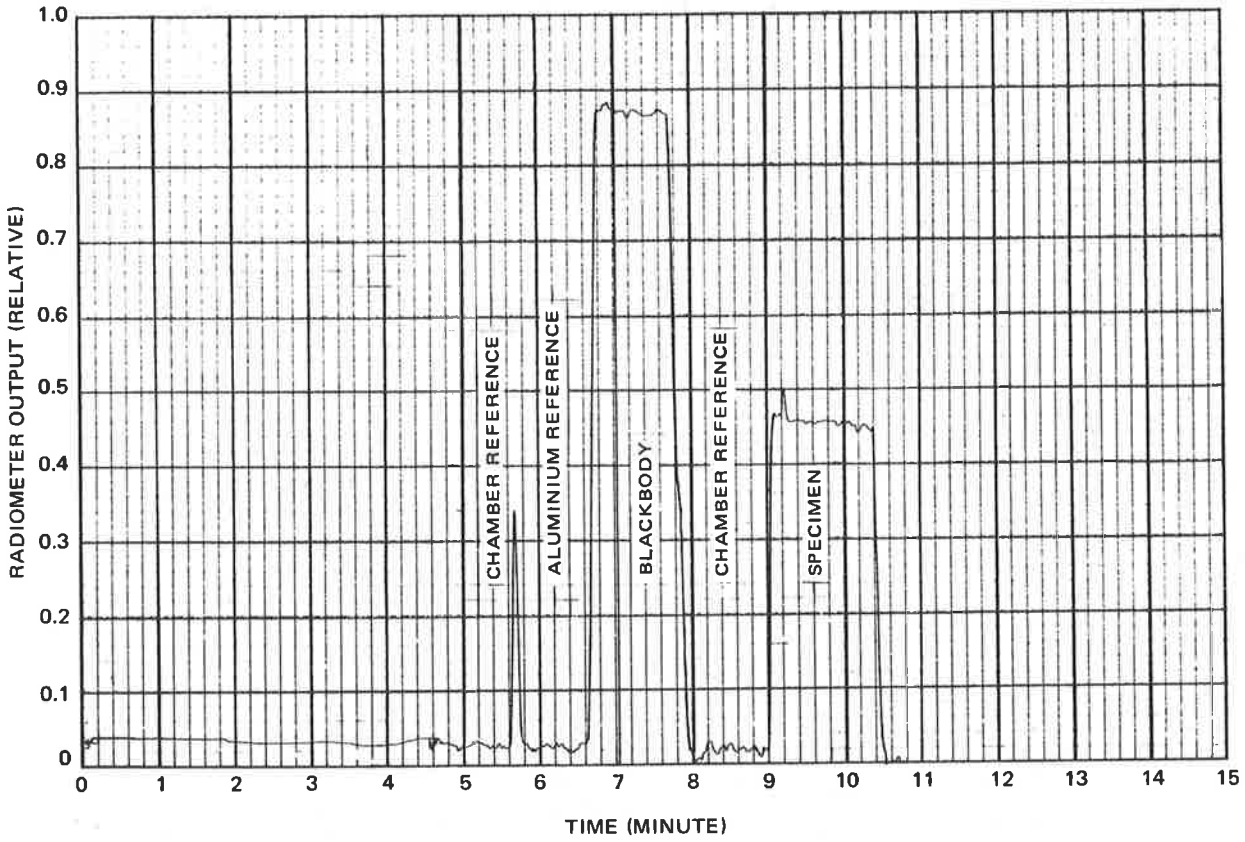

Figure 21. Chart recording of emissivity measurement

$$\varepsilon+\rho+\tau = 1,$$

a simple reduction gives

$$\varepsilon = \frac{W-W_o}{W_{bb}-W_o} \qquad (114)$$

Thus if the detector amplifier is linear, then the film emissivity can be calculated from

$$\varepsilon = \frac{V-V_o}{V_{bb}-V_o} \qquad (115)$$

where V, Vo and V_{bb} are the corresponding signal voltages. The technique therefore requires measurement only of relative signal voltages.

The procedure described above was followed in this project. A typical output trace is shown in figure 21.

7. GOLD FILMS

Gold film infrared absorbers and bolometer detectors have been used extensively in the author's laboratory. Experimental techniques for the preparation of gold absorber films have been established for many years, and numerous measurements have been made of infrared absorptance. Nevertheless, gold was studied in this project for two reasons :

(a) Gold is known to form coarsely crystalline, aggregated deposits. It is desirable to study a material of this type in order to test, and hopefully validate, the theory and predictions enunciated in earlier sections of the thesis.

(b) We have not fully understood many of the observed physical properties of of gold absorber films. The present study, with its broad research basis, should help to clarify previous areas of doubt.

7.1 Film deposition

A total of 25 gold films were prepared in the ancilliary vacuum coating unit. The deposition rate, with one exception, was 1.0 to 2.0Å.s^{-1}. The

exception was a single deposition at $0.1\text{Å}.s^{-1}$, carried out to assess the influence of a slow rate on physical properties.

Thickness was measured for eight specimens. The quartz crystal monitor calibration is shown in figure 22. Also plotted is the theoretical prediction determined from equation (99A), which is based on the bulk density of $19.3g.cm^{-3}$. The measured thicknesses suggest an apparent film density of $13.7g.cm^{-3}$. An evident error of 20 to 30Å for two of the specimens has been traced to contamination of the optical flats due to poor cleaning. The actual thickness measurements are accurate to $\pm$ 5Å.

7.2 Electrical properties of gold films

The most noticeable electrical characteristic of gold films deposited on to glass substrates is that it is difficult to prepare a film of precisely determined resistance. When deposition is stopped the film continues to "form", with a consequent resistance overshoot; and the resistance may continue to fall through many orders of magnitude. The greatest change takes place within a few minutes of deposition. A film deposited to 200 Ω per square will typically stabilize at 50 Ω per square or less. Much the same final result is obtained if deposition is stopped at 500 Ω per square. The resistance overshoot is less marked for polymer substrates. A 200 Ω per square film was observed to stabilize at 120 Ω per square.

The final resistance was found to be sensitive to deposition rate, the type and condition of the substrate, and the substrate temperature. Thus the onset of conduction for a film deposited at $0.1\text{Å}.s^{-1}$ was noted to occur at roughly twice the thickness of films deposited at 1 to $2\text{Å}.s^{-1}$. Conversely, conduction commenced at a lesser thickness for films deposited at a high deposition rate.

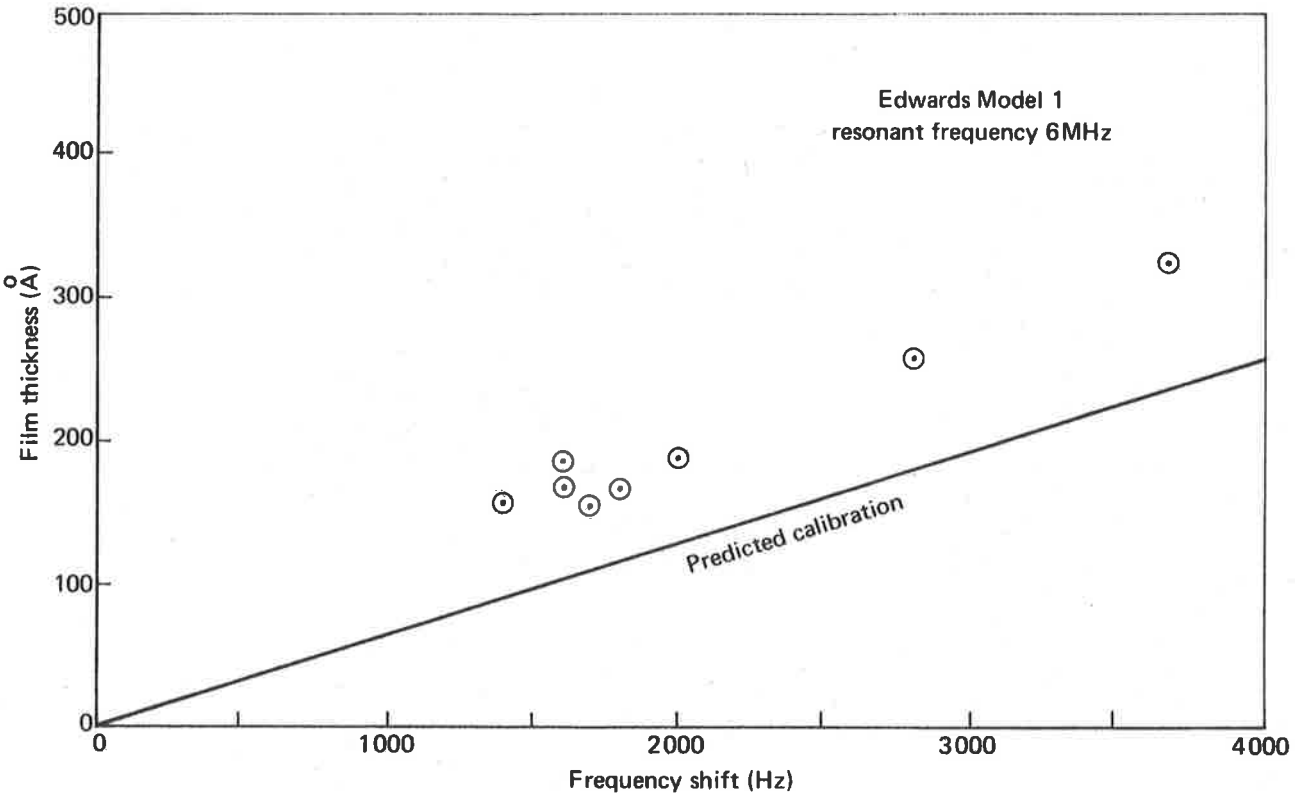

Figure 22. Quartz crystal monitor calibration for gold films

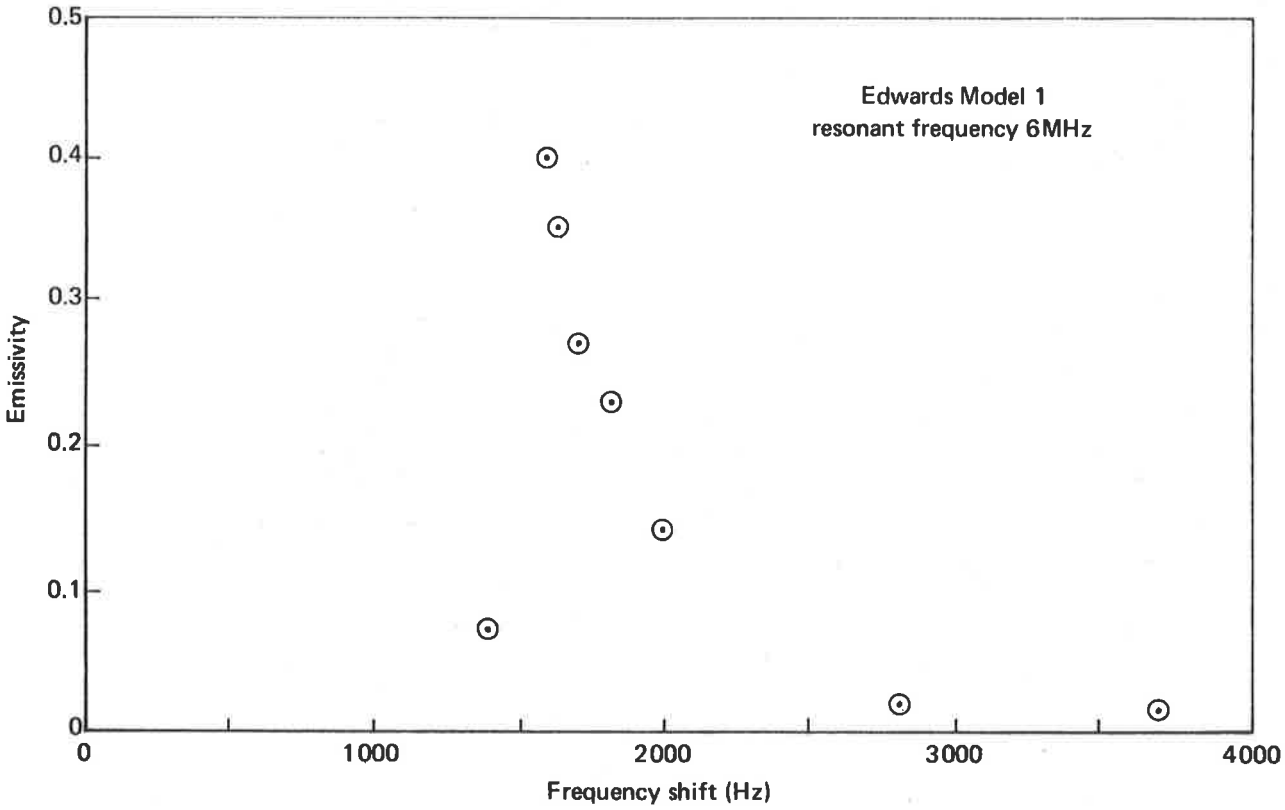

Figure 23. Emissivity of gold films

Contrary to expectation, conduction was observed to commence at an earlier stage during deposition for films deposited on to collodion substrates, than for films prepared on glass substrates; and the final resistance was lower for the collodion substrates. This is probably a consequence of both the higher mobility on the glass surface and the coarsely crystalline structure of the gold films. The latter probably favours coalescence at an earlier stage of growth on the uneven polymer substrates.

The technique employed by the author's associates for the preparation of gold bolometer elements on collodion substrates provides for the application of a d.c. "forming current" during deposition, generated from a constant current power supply. This is followed after deposition by a "current aging", in which the applied current is higher than the normal operating bias current. The optimum forming conditions are determined by experiment. For example, the short circuit "forming current" for a 0.2mm long x 0.05mm wide bolometer element was 100 μA, and the applied voltage was 12V. The maximum power transfer would occur when the bolometer resistance is equal to the source resistance, which in this case was 120kΩ. Thus during coalescence 300μW power ($3Wcm^{-2}$ for this detector size) at a voltage of $600Vcm^{-1}$ was applied to the element. Presumably Joule heating would cause a rise in temperature as islands coalesce; however, the average temperature rise would be insufficient to damage the polymer film.

In this project we have confirmed by experiment that the above technique induces conduction in gold films which would otherwise be highly resistive or insulating. If the postulate of a temperature rise on a microscopic scale is indeed correct, then the phenomenon is in agreement with Chopra's work on field-induced coalescence in gold films (Section 4.3.3, ref. 30).

Finally, electrical aging effects, including the resistance overshoot

observed on the completion of deposition, is considered to be caused by recrystallisation. This is borne out by structural studies reported in Section 10.3.

7.3 Infrared optical properties of gold films

The author has found no simple relationship between the sheet resistance and infrared absorptance of gold films deposited on to collodion substrates. However, there is a unique relationship between absorptance and thickness, which is evidently independent of deposition rate and electrical aging. Thus the theory of Section 3.4 does not apply to gold films prepared on amorphous substrates at room temperature. This is not to say that the theory is incorrect, simply that it is probably applicable only on a microscopic scale. Structural studies (Section 10.3) show the films to be irregular and coarsely granulated and, in the region of maximum absorptance, structurally discontinuous. In agreement with theory, maximum absorptance is 0.5.

Infrared emissivity for several gold specimens, measured with the Emissivity Test Apparatus, is plotted as a function of film thickness in figure 23. Thickness is recorded as frequency shift for the quartz crystal monitor, because of an anomalous thickness measurement for two specimens. Reference to figure 22 shows that the maximum emissivity is attained at a thickness of 160Å. The thickness is seen to be critical. To achieve an emissivity, and hence absorptance, greater than 0.4, a frequency shift of 1500Hz to 1600Hz is required, corresponding to a thickness variation of at most 20Å. In this study the largest measured emissivity (absorptance) was 0.41. There is ample evidence, from the work of the writers associates, that an absorptance approaching 0.5 is possible, and that the maximum is achieved at a frequency shift of approximately 1600Hz with the Edwards monitor. The results shown in figure 23 are, however, the first showing

a precise thickness dependence.

Numerous measurements of the spectral transmission and reflectance of gold films carried out in the author's laboratory have shown that the absorptance is not spectrally flat in the region 1 to 16 μm. The deviation from spectral linearity is least in the region of maximum absorptance, but the absorption increases at the shorter wavelengths for both thicker and thinner films. The spectral absorptance at 10 μm was found to be typically 3 to 5% lower than measurements made with the Emissivity Test Apparatus. However, when integrated over 8 to 14 μm, the two methods of measurement were in good agreement.

Upon consideration of the results of the previous subsection it is not surprising that the sheet resistance of two specimens of identical absorptance can vary from 50Ω per square to at least 10MΩ per square. This result has a particular bearing on the preparation of gold film bolometer detectors. For these detectors we usually seek a stable resistance of 50 to 100Ω per square. It appears from this study that the deposition rate of $13 Hz.s^{-1}$ ($1.2 \mathring{A}.s^{-1}$) normally selected in the preparation process, is in fact an optimum value. Deposition at this rate will achieve, in conjunction with the electrical forming technique, a film of both the desired resistance and optimum absorptance. A faster rate will give films which are too thin, and the converse applies to slower rates. It follows that detectors which do not have the correct thickness should be rejected, albeit that they have the desired electrical characteristics, because the detector responsivity (i.e., volt per watt, see ref. 43), is dependent on infrared absorptance.

8. NICHROME FILMS

8.1 Some reported properties of nichrome films

Nickel-chromium alloys have been extensively investigated as resistance

elements in thin film microcircuits. The preparation and electrical properties of these films are widely reported (see references 44 to 48). Some relevant characteristics of thermally vaporised 80/20 nickel-chromium films are as follows :

(a) Because of the higher evaporation rate of the chromium component it is necessary to use a source temperature in excess of 1600°C to retain stoichiometry in the deposited film. At lower temperatures the films are chromium rich.

(b) Nickel-chromium films oxidise on exposure to the atmosphere and the film resistance rises slowly after deposition. The percentage change in resistance depends on composition and thickness. Films used in micro-circuitry are usually stabilized by heating the substrates to at least 250°C during deposition, followed by post bake cycles. This accelerates the aging process. Films of resistance greater than about 400Ω per square are unstable and cannot be effectively aged.

(c) The thickness of a 200Ω per square film on a glass substrate is reported to be 75 to 100Å. The thickness of a film of the same resistance on a plastic substrate is found to be 250 to 300Å, and on an alumina substrate approximately 500Å.

The reported structure of nichrome films is discussed in Section 10.4.

Published reports on the preparation of nickel-chromium films have been a valuable guide in this project. However, the author is not aware of any reference in the literature to the infrared and thermal properties of these films, the only known work being that carried out in the author's laboratory.

8.2 Film deposition

The deposition technique for nichrome films is described in Section 5.8. 15 specimens were prepared, this being considered a sufficient number

to establish the basic absorber properties of films of this material.

The Edwards thickness monitor was calibrated over the range 80 to 150Å. It was found that the calibration curve changed slope at a thickness of approximately 110Å, indicating a change in the density of the evaporant. This is not unexpected in view of the discussion in the previous sub-section, noting that a new filament and alloy charge was used for each deposition. The calibration is shown in figure 24. The apparent density of the nichrome films, determined from equation (99A), is 5.1 $g.cm^{-3}$ for thicknesses less than 125Å. The density approaches the bulk value of 8.41 $g.cm^{-3}$ for thicker films.

Nichrome films were prepared at a deposition rate of 2.5 to 6.0Å.s^{-1}.

8.3 Electrical properties of nichrome films

Most of the electrical data for nichrome films was measured on glass monitor substrates. The dependence of sheet resistance on thickness for freshly deposited nichrome films, prepared on glass substrates at room temperature, is shown in figure 25. The films become electrically conducting between 60 and 70Å.

An experiment was carried out to determine resistance on collodion substrates. Sheet resistance was monitored on both glass and collodion. It was found that the resistance on collodion was 1.2 to 1.4 times higher than on glass over the range 100 to 1000Ω per square. This is in agreement with measurements made on 25mm diameter annuli, using the jig described in Section 5.3.7. The estimated dependence of resistance on film thickness for collodion, deduced from monitor recorder traces, is shown as a broken line in figure 25. These films become conducting at a thickness of approximately 80 to 90Å.

Figure 25 shows that thickness of a 200Ω per square nichrome film is approximately 120Å for glass substrates and 140Å for collodion substrates.

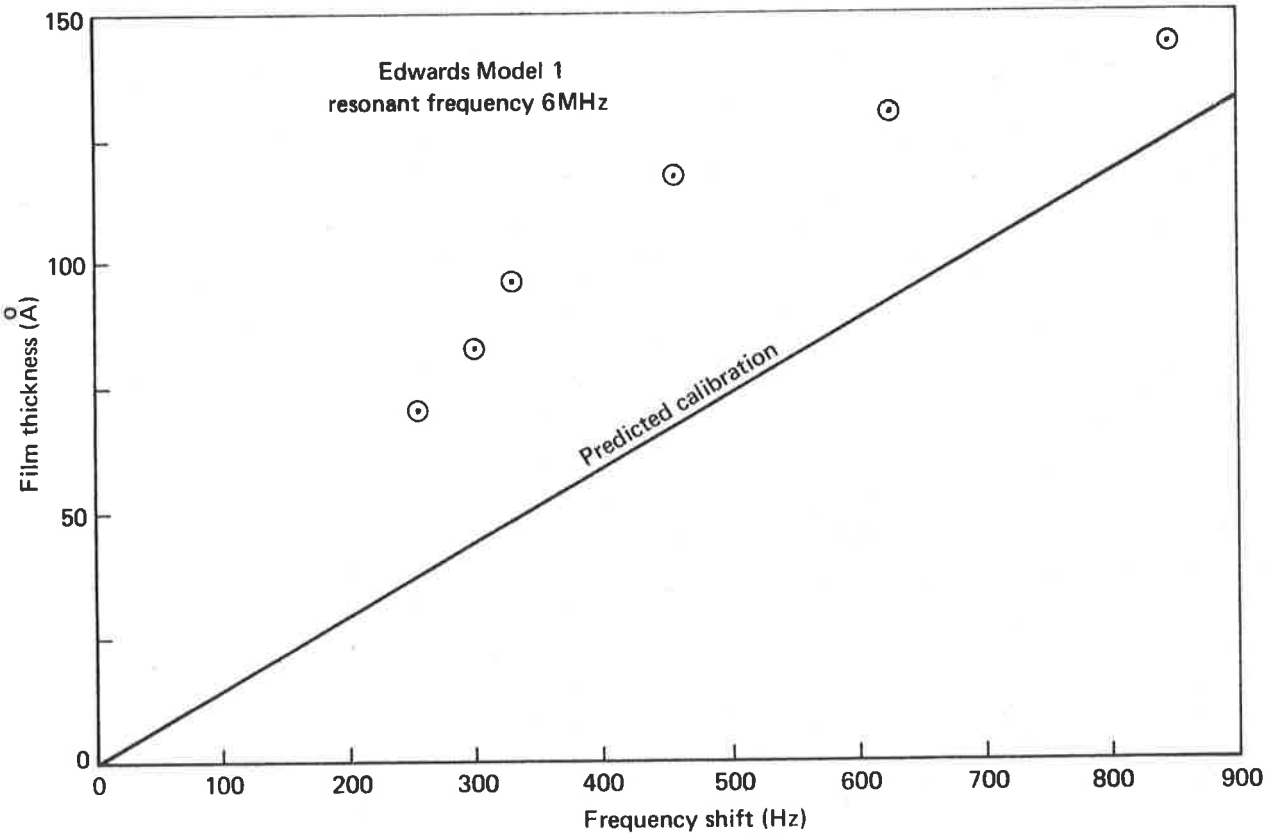

Figure 24. Quartz crystal monitor calibration for nichrome films

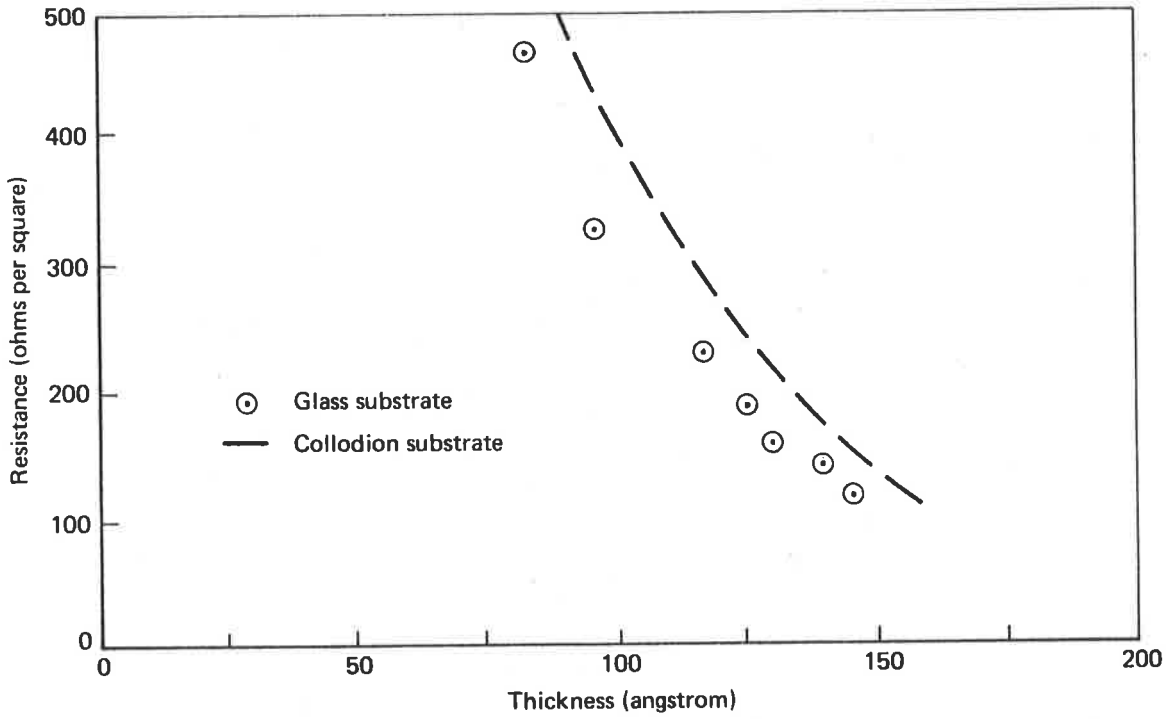

Figure 25. Resistance of nichrome films

The film conductivities are thus $4.2 \times 10^3\ \Omega^{-1}.cm^{-1}$ and $3.7 \times 10^3\ \Omega^{-1}.cm^{-1}$ respectively. The bulk conductivity of Nichrome-V is $9.1 \times 10^3\ \Omega^{-1}.cm^{-1}$. It may be noted that the conductivity for collodion substrates is much lower than reported in the literature (Section 8.1).

Nichrome films can be prepared to an accurately predetermined sheet resistance. Deposition can be stopped at exactly the desired value, in marked contrast to the resistance overshoot observed for more mobile evaporants such as gold. However, the film resistance rises on exposure to air, the percentage change depending of the value of the initial resistance of the freshly evaporated film. The resistance of films of less than 500Ω per square tends to stabilize with time; whereas the resistance of thinner films continues to rise. The typical percentage change measured over a period of 2 years (glass substrates) was found to be as follows :

100Ω per square	5%
200Ω " "	10 to 15%
500Ω " "	25%
1000Ω " "	40%

The rise in resistance is accelerated by thermal aging.

The resistance of nichrome films prepared in a poor vacuum were observed to be much higher, for a given thickness, than the values shown in figure 25. There is little doubt that this is a consequence of oxidation during film formation. The influence of chamber pressure is discussed in Section 9.3.

8.4 Infrared optical properties of nichrome films

A total of 8 films were prepared for infrared absorption measurement. Unfortunately several of these were damaged prior to the completion of spectrophotometer records. Three specimens were selected for detailed analysis.

The most obvious experimental result was the relative ease of preparation of films having near-optimum absorptance. Indeed nearly all of the films had an emissivity (absorptance) in excess of 0.4, covering a resistance range of roughly 100 to 350Ω per square (measured on collodion substrates). The maximum observed absorptance, as measured with both the spectrophotometer and the Emissivity Test Apparatus, was 0.49 to 0.5. The maximum was obtained for films deposited to 175 to 200Ω per square on collodion. At the time of meauurement the film resistance had risen to 225 to 250Ω per square. The spectral absorptance of all specimens was flat to within a few percent over the spectral range 2 to 16 μm.

The above results are in good agreement with the theory of Section 3.4, which predicts maximum absorption at 189Ω per square, with essentially no wavelength dependency. Here again we shall find that there is a close relationship between the observed physical properties and film structure.

9. NICKEL FILMS

Throughout this project major emphasis has been placed on an analysis of the properties of nickel films. A total of 60 nickel depositions were carried out. Of these, more than half were prepared by electron beam deposition. The remainder were deposited from resistance heated tungsten filaments.

The selection of nickel as an appropriate metal for study was based on a systematic theoretical analysis of the thermal, structural and infrared absorption properties of thin metallic films. Nickel is representative of the evaporants which, according to our earlier predictions, should have the preferred absorber characteristics. Its melting point ($1725^{o}K$) is significantly higher than the minimum value of $1350^{o}K$ specified in Section 4.4, and we may therefore be reasonably confident of achieving the desired film structure.

Preliminary experiments with platinum - probably a more suitable absorber material - have indicated that there are several technical problems to overcome before proceeding to higher melting point evaporants. Research on nickel has served to solve many of these problems, and the experimental results have indicated the direction along which future work should proceed.

9.1 Film deposition

Deposition techniques for nickel films have already been discussed (Section 5.9). Both the Toyocom and Edwards thickness monitors were calibrated, the former for electron beam deposition and the latter for tungsten filament sources, from a total of 27 thickness measurements. The measured data for electron beam deposition, together with the predicted monitor calibration (based on equation (99B) and the bulk density of nickel), are shown in figure 26. From the limited measurements for filament vapour sources, we can say little about the thickness relationship for this method of deposition, other than to establish a general trend. The measurements for electron beam deposition are sufficiently comprehensive to exhibit a marked scatter in the thickness data. We may again deduce an apparent density from equation (99B), and find here a range $3.0 g.cm^{-3}$ to $4.5 g.cm^{-3}$, compared to the bulk density of $8.9 g.cm^{-3}$. The thickness measurements are accurate; hence we must presume a variation in the density of the deposits. Some measured points are omitted in the figure. These concern depositions which yielded an excessive thickness for a given frequency shift, and were the first experimental indication of an "anomalous" deposition process, to be discussed in Sections 9.2 and 9.3.

For tungsten filament source deposition, the estimated film density was $5.5 g.cm^{-3}$ to $6.5 g.cm^{-3}$. A very fast deposition yielded a density of $7.2 g.cm^{-3}$.

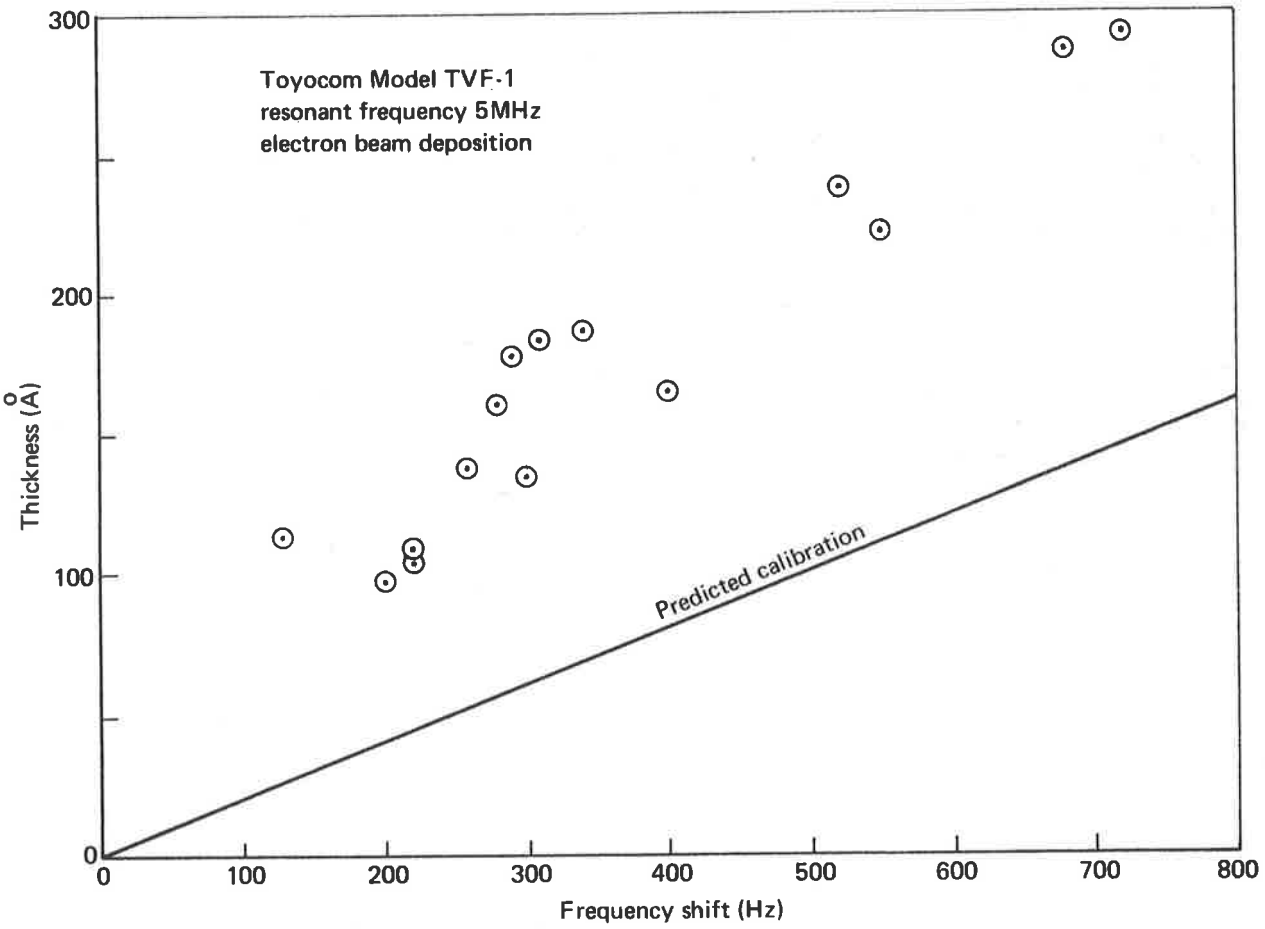

Figure 26. Quartz crystal monitor calibration for nickel films

The deposition rate for electron beam deposition was varied from $1.5\text{Å}.s^{-1}$ to $4.0\text{Å}.s^{-1}$; for filament source deposition the rate was $1.5\text{Å}.s^{-1}$ to $8.5\text{Å}.s^{-1}$.

A further discussion of film density is given in Section 9.3.

9.2 Electrical properties of nickel films

The measured sheet resistance of nickel films on glass and collodion substrates is plotted in figures 27 and 28. At first sight it would appear that the observed resistances are too widely scattered to establish a firm dependence on film thickness. Fortunately there is a plausible explanation for the experimental results. The data shown in the figures are representative of uniform (constant rate) depositions; lower resistance values can, in general, be traced to a fast deposition rate, and occasionally to an improved vacuum. A number of measurements are not recorded. These were cases of excessively high resistance, and without exception all such observations could be traced to either a slow deposition rate or a slowing of rate during the early stages of deposition. For the electron beam deposited films a high resistance was often associated with current leakage across the boron nitride insulating sleeve, causing a sharp drop in deposition rate. Nickel films so prepared were semiconducting.

The resistance of nickel films deposited on to collodion substrates was found to be 1.2 to 1.5 times higher than films of the same thickness on glass substrates.

9.2.1 Electrical conductivity of nickel films

From figures 27 and 28 it is found that the thickness of a 200 Ω per square nickel film is 90 to 100Å on glass substrates, and 130 to 150Å on collodion substrates. These films are slightly thicker than nichrome films of the same resistance. However, the electrical conductivity is approximately $5 \times 10^3\ \Omega^{-1}.\text{cm}^{-1}$ for glass substrates

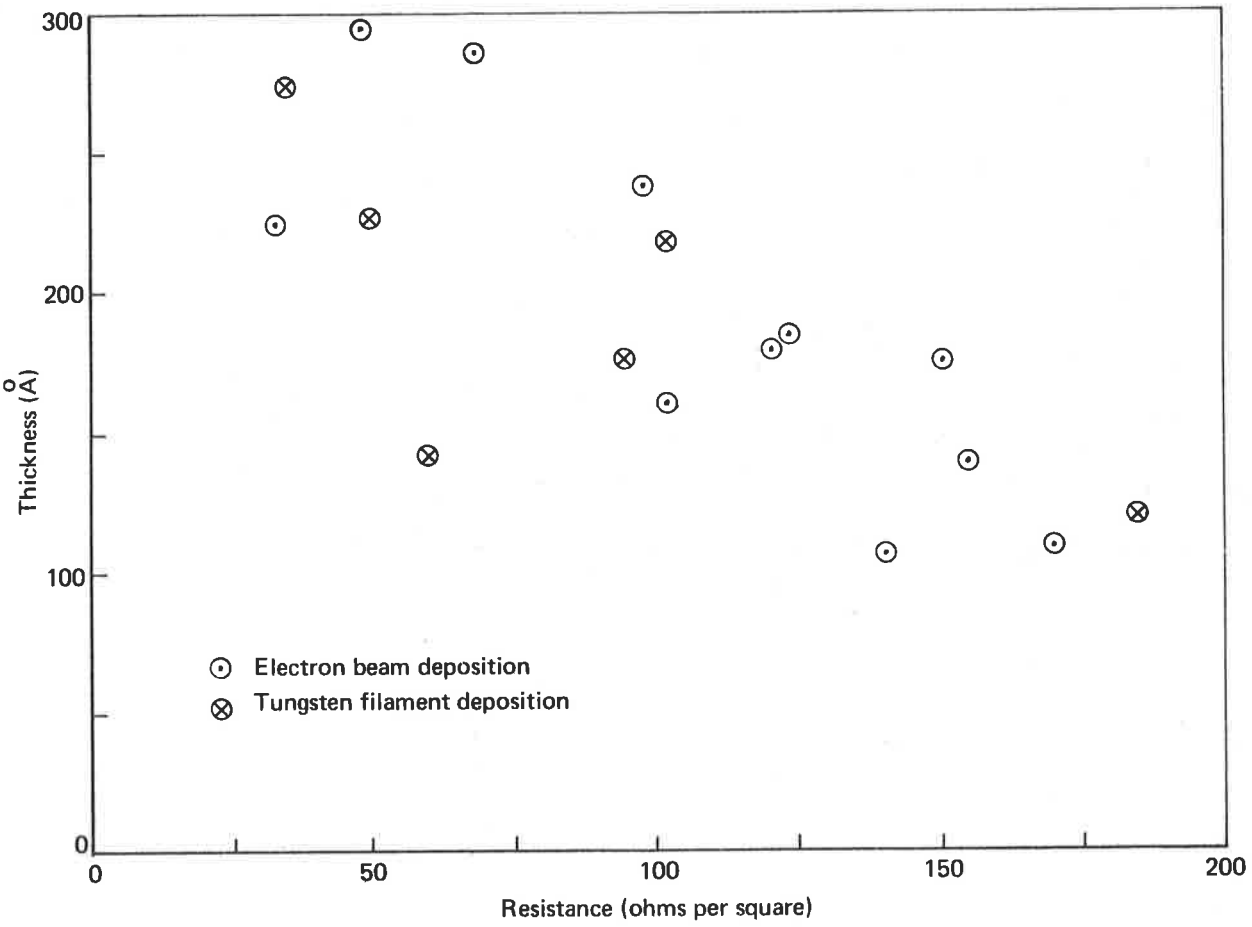

Figure 27. Resistance of nickel films on glass substrates

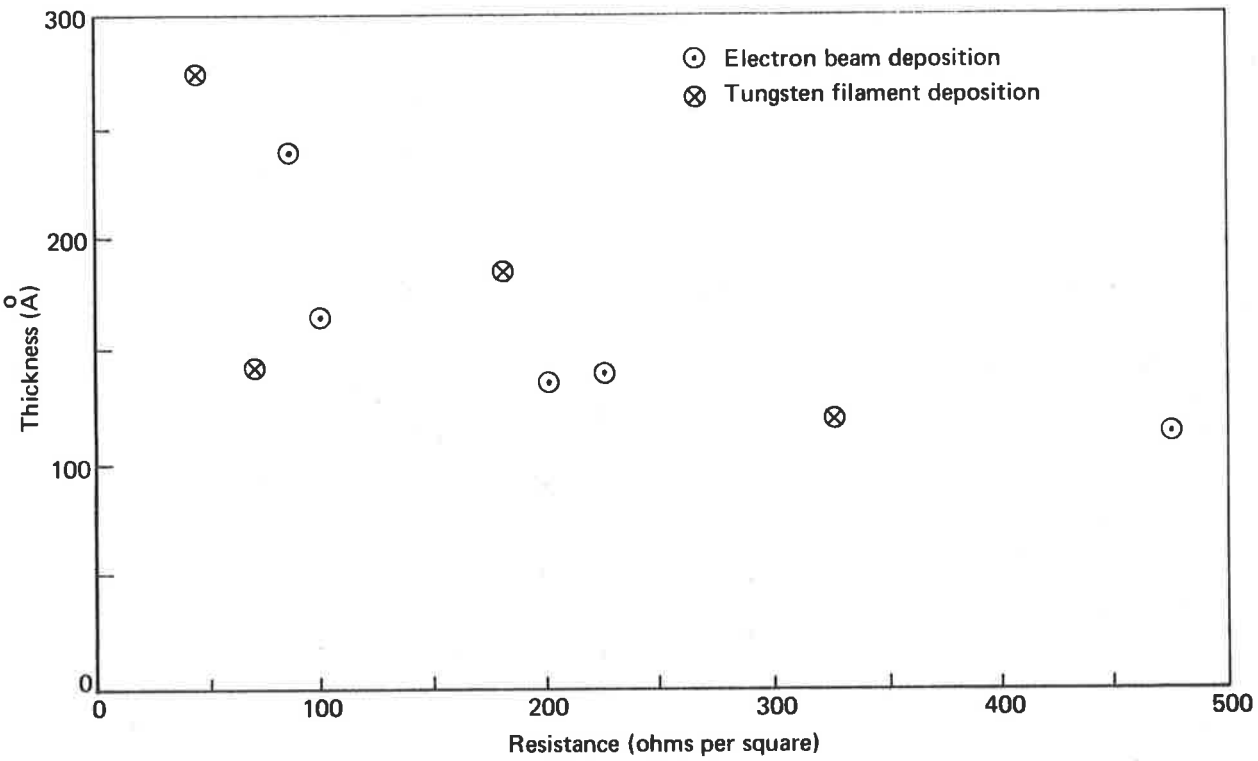

Figure 28. Resistance of nickel films on collodion substrates

and 3.5×10^3 $\Omega^{-1}.cm^{-1}$ for collodion substrates, compared to the bulk conductivity of 1.1×10^5 $\Omega^{-1}.cm^{-1}$. It is of interest to compare this result with theoretical predictions.

In Section 3.5 we deduced a mean free path for conduction electrons, based on one free electron per atom, of 65Å. The assumption of one free electron per atom is questionable, because there is evidence (ref. 49) that only the 4s-band electrons in nickel contribute to conduction, there being approximately 0.6 conduction electrons per atom. Applying this correction to equation (89) we obtain a mean free path of 93Å. The Fuchs-Sondhiemer theory (see figure 9) provides that the ratio of bulk conductivity to film conductivity, σ_o/σ, for a diffuse scattering mechanism is

$\sigma_o/\sigma = 1.45, \quad t = 100Å;$

consequently the resistance should be 14Ω per square. We have seen that this is not the case for the films prepared in this study. For a 100Å thick film,

$\sigma_o/\sigma > 15$ for glass substrates, and

$\sigma_o/\sigma > 20$ for collodion substrates.

Clearly the Fuchs-Sondhiemer theory fails for these films. This can be attributed to :

(a) film density much lower than bulk density,

(b) high concentration of scattering centres, e.g., adsorbed gases,

(c) low film purity

With regard to (a), the apparent film density (Section 9.1) gives a mean free path of 147Å. This only partially explains the low observed film conductivity. In Section 9.3 we will present arguments in support of conclusions (b) and (c).

9.2.2 Electrical aging

The resistance of nickel films always dropped slightly in vacuo following deposition, typically stabilizing at approximately 95 to 98% of the freshly deposited film. There was no marked "overshoot" such as observed with gold films, and it was therefore possible to prepare films of predetermined sheet resistance.

On exposure to air the resistance of nickel films was observed to rise immediately, thence to stabilize within one hour of air admission. Thenceforth the resistance rose slowly, the overall percentage change depending on the value of the freshly deposited film.

The initial rise in resistance was usually no more than 5% for glass substrates, with an overall rise, measured over a period of several months, of 25% maximum for films of 100 to 500Ω per square. The initial rise was higher for collodion substrates, a maximum of 25% being recorded for a 500Ω per square film. Over a period of several months, the resistance of thick films rose by at least 25%, whilst for films of resistance exceeding 500Ω per square, the rise was in excess of 100%.

Absorber films deposited to a sheet resistance exceeding 300Ω per square were too unstable to be of practical value. We shall see (Section 9.5) that aging does not seriously influence the infrared optical properties of thicker nickel films; certainly over the expected working life of infrared detectors incorporating these absorber elements.

9.3 Vacuum and oxidation

We have seen that there are five disturbing factors arising from the experimental results for nickel films, namely :

(a) the apparent film density is much lower than the bulk density;

(b) there is considerable scatter in the observed film resistance, measured as a function of film thickness;

(c) the electrical conductivity is very much lower than the bulk conductivity;

(d) there is a relatively large rise in film resistance on exposure to air; and

(e) we have evidence of "anomalous" depositions, apparently associated with low deposition rates, which yield films of a very high resistance for a given thickness and excessive thickness (low density) for a given crystal monitor frequency shift.

Oxidation cannot fully account for the low apparent film density, because the oxide NiO has a density of $6.67 g.cm^{-3}$. We can,however, expect the structure of the film at least to partially contribute to a reduced film density. This would seem to be the case for gold films (Section 10.3), although nickel films are more continuous and are finely crystalline. On the other hand, we have evidence that a slow deposition rate (less than $1 \mathring{A}.s^{-1}$) gives very low density films, whereas a high deposition rate (greater than $10 \mathring{A}.s^{-1}$) yields almost bulk density. Could occluded gas cause a decrease in density?

Possible contributory factors to (b) through (e) are low film density, excessive electron scattering, occluded gases and low film purity (including oxidation).

It seems likely that the solution to the above problems lies in the impingement rates at the substrate of both the evaporant and residual gases. The evaporant impingement rate is readily deduced from equation 89, thus :

$$N_m = N_A \frac{\rho}{M} R_d \text{ atoms } cm^{-2}.s^{-1}, \qquad (116)$$

where as before N_A is Avogadro's number, ρ is the bulk density ($g.cm^{-3}$), M is the molar mass ($g.mol^{-1}$), and R_d is the deposition rate ($cm.s^{-1}$). It can be shown (see ref. 35, p. 1-81) that the arrival rate for residual gases is

$$Ng = 3.513 \times 10^{22} (MgT)^{-\frac{1}{2}} p \quad \text{molecule } cm^{-2}.s^{-1} \qquad (117)$$

where Mg is the molar mass of the gas ($g.mol^{-1}$), T is the absolute temperature (^{o}K) and p is the partial pressure of the gas (torr).

A recent partial pressure analysis carried out by associates in the author's laboratory has shown that, for vacuum coating units similar to that described in Section 5.1, the major gaseous contaminants are water vapour (mass 18) and a mass-28 constituent (probably carbon monoxide). This is essentially in agreement with the results of other workers in the field. At 10^{-6} torr the water vapour partial pressure was 6×10^{-7} torr, and the mass-28 component 3×10^{-7} torr. When the chamber pressure increases (e.g. during outgassing) the two major components increase in roughly the same proportion, although water vapour appears predominant.

During our nickel depositions we may expect a water vapour partial pressure of 5×10^{-6} to 1×10^{-5} torr. The arrival rate at the substrate is then

$$Ng \simeq 4 \times 10^{15} \text{ molecule } cm^{-2}.s^{-1}$$

This may be compared with the impingement rate for nickel atoms, which, for a deposition rate of $2\text{Å}.s^{-1}$, is

$$N_m \simeq 2 \times 10^{15} \text{ atom } cm^{-2}.s^{-1}$$

This is a far from satisfactory situation. These conditions would favour the trapping of gas molecules during film growth, and deposition takes place in a highly oxidizing atmosphere. Reference to data on the heat of oxide formation for nickel (see, e.g., ref. 35, Ch. 2) would suggest that "reactive evaporation" takes place, so that much of the nickel is oxidized

during deposition. There is now little doubt that the "anomalous" depositions referred to earlier are associated with film oxidation, and that the low apparent film density can be traced, in part, to occluded gas. Adsorbed gas, in addition to the finely crystalline structure of the Ni-NiO film, would be expected to cause excessive electron scattering, further decreasing the film conductivity.

The influence of chamber pressure and deposition rate has been noted by other authors (refs. 34, 46 and 50). In order to minimize oxidation and gas occlusion we need to seek a ratio of nickel atoms to water vapour molecules of at least 10:1. This requires a deposition rate exceeding $10\text{Å}.s^{-1}$ and a chamber pressure of less than 1×10^{-6} torr. It may also be advantageous to deposit a thin dielectric film (e.g., silicon monoxide) on to the nickel absorber to reduce post-evaporative aging effects. A higher substrate temperature is desirable, but unfortunately substrate heating is limited by the polymer membrane substrate.

It is also of interest to note that the ratio of evaporant atoms to water vapour molecules for our chromium depositions (Section 5.7) is about 1:2. In view of the high heat of oxide formation for chromium, it is not surprising that these films were much thicker for a given sheet resistance than either nickel or nichrome films. On the other hand, we must also expect to find an oxide phase in nichrome films.

Finally, we should keep in mind that these considerations would also apply to any other high melting point evaporant which might be considered to be a potential infrared absorber material. On these grounds alone, we can eliminate many materials. On the other hand we may single out certain evaporants, e.g., platinum and palladium, which would appear to show particular promise as absorber materials.

9.4 Stress in nickel films

Mechanical stress in nickel films imposed a serious technical limitation, when the films were deposited on to thin collodion substrates. Stress was observed to cause "bursting" of the film at a substrate temperature well below that of the tested rupture temperature of the collodion. When films survived deposition, the coated substrate sagged on exposure to air. The effect was also evident for nichrome films on collodion substrates, although less marked by comparison. There was no evidence of stress relief in lower melting point evaporants such as gold; however, we have often noted buckling of gold bolometer detector elements.

A summary of the observed stress effects is as follows. These observations refer to plastic substrates mounted on 25mm diameter annuli.

(a) Films which were destroyed during deposition appeared to burst symmetrically, rather than to tear, indicating a circular stress symmetry. Those which survived sagged on exposure to air.

(b) Films often survived in vacuo, then burst after several minutes (sometimes many hours) after deposition.

(c) The problem was most troublesome for electron beam deposition. Collodion films thinner than 1000Å rarely survived deposition. However, thick Saran films (approximately 2000Å), which have a normal rupture temperature of 70°C, always survived.

(d) Films which survived deposition sagged only when air was admitted to atmospheric pressure. They remained taut in vacuo, also when an inert gas was introduced to the vacuum chamber.

(e) The sagged films became taut when placed in an oven at 40°C, and also when re-evacuated. In the latter case total reversal was not always achieved, depending on the elapsed time in the stress-relieved state.

(f) Some substrates, notably PVC, became taut after passing the film

through a solvent vapour, e.g., methyl ethyl ketone. This effect was not permanent.

The author has also found that rectangular absorber elements tend to split during deposition. Those which survive deposition sag or buckle (depending on the dimensions of the element) on exposure to air.

There is little doubt that a stress effect will be present for all high melting point evaporants. The serious consequence of this problem in absorber research prompted a brief study of the nature of stress in thin metal films.

There are three predominant stress functions which influence the formation of the nickel films, namely thermal stress, external stress and intrinsic stress. Thermal stress is given simply by

$$S = (\alpha_f - \alpha_s)\, Y\Delta T \quad , \tag{118}$$

where α_f and α_s are the average coefficients of linear expansion for the film and substrate respectively, Y is Young's modules for the film and ΔT is the temperature difference between deposition and measurement. S is defined to be positive for tensile stress and negative for compressive stress. The coefficient of linear expansion is $1.3 \times 10^{-5}\ ^{o}C^{-1}$ for nickel and typically $1 \times 10^{-4}\ ^{o}C^{-1}$ for polymers, including cellulose nitrate. The thermal stress in the nickel film (after cooling) is therefore compressive. It is not clear what value we should select for Young's modulus. The modulus for bulk nickel is 2×10^{12} dyn.cm^{-2}. However, the modulus for the plastic substrate is approximately 2×10^{10} dyn.cm^{-2}. We may therefore expect that the thermal stress is at most 1×10^{9} dyn.cm^{-2} for a temperature differential of $50^{o}C$.

External stress in the present situation would comprise only the slight tensile stress in the stretched collodion substrate. This would be small in comparison with the other components.

Intrinsic stress is inherent in the film itself. The mechanism of this stress is not well understood, but it should depend to varying degrees on the various deposition parameters - rate, thickness, substrate type and temperature, chamber pressure, etc. It is usually larger than thermal stress, and has a typical range of 1 to 10 x 10^9 dyn.cm^{-2}.

There are many excellent reviews of stress in thin films in the literature (refs. 14, 51,52,53). It is reported that the intrinsic stress for a thin nickel film on a glass substrate at room temperature is 8 x 10^9 dyn.cm^{-2}. The stress is tensile and is probably higher on collodion than on glass. Furthermore, for a temperature differential of 50^oC, thermal stress contributes about 5% to the total stress. This is in broad agreement with the above estimate for thermal stress.

It appears (ref. 51) that the stress in nickel films is very much higher than in gold films. Indeed we may expect this to be the case for all higher melting point evaporants.

Based on the above observations the author proposes the following stress mechanisms for nickel films deposited on to polymer substrates. It is emphasised that this explanation is not, as yet, supported by quantitative measurements.

(a) The deposited films are in a high state of tensile stress.

(b) The polymer substrate creeps (flows) to compensate for the stress in the nickel film.

(c) On air admission the polymer swells due to water vapour adsorption - a known property of these materials. This acts as a stress-relief mechanism, causing the film to sag.

This postulate appears to adequately describe the observed phenomena. The polymer creep (mechanism (b)) is probably strongly temperature dependent, and explains the tendency for films to rupture more easily

during electron beam deposition.

The most obvious solution to this problem is simply to admit air immediately following deposition. This presumes that the collodion will swell before creep has ceased, thereby inducing partial stress relief whilst retaining slight tension. This technique has been successfully applied to films prepared by filament vapour source deposition, but has not been successful for electron beam deposition. In the latter case, failure is probably the result of a slightly higher substrate temperature, caused by an electron component in the vapour stream (see Section 5.9.2).

An alternative approach to this problem is to cool the substrate during deposition (the beneficial effect on the substrate may outweight any increase in intrinsic stress). Alternatively, we should seek a new, more rigid polymer substrate.

The protective dielectric coating discussed in Section 9.3 may afford an added bonus in stress relief. For example, silicon monoxide films prepared by rapid deposition are known to be in compressive stress. This layer would need to be applied immediately following metal deposition.

Whatever may be the best solution, it is clear that the problem must be solved before proceeding to an investigation of higher melting point absorber materials.

9.5 Optical properties of nickel films

A careful analysis was made of the spectral absorptance and total emissivity of 14 nickel specimen films deposited on to collodion substrates. The measurements covered a thickness range of 90Å to 180Å, and the film resistance (as measured on the collodion substrates) varied from 100Ω per square to greater than 1000Ω per square. The study was, unfortunately, hindered by the technical difficulties discussed in the preceding subsections.

Stress effects imposed limitations on optical measurements in two ways. Firstly, it has not been possible at the present stage to prepare large nickel absorber films to a resistance of less than 100Ω per square, because of film rupture. Secondly, films which sagged after deposition could not be used for reflectance measurements. These films were suitable for the measurement of emissivity and spectral transmittance, but gave false values of spectral reflectance. Reflection measurements with the infrared spectrophotometer demand a specularly reflecting surface.

A further cause for concern was the experimental scatter in both the measured crystal monitor frequency shift and sheet resistance as a function of film thickness. As we have seen, these results can be traced to a variation in film composition e.g., adsorbed gas and an oxide phase. Therefore, unlike gold, we should not expect to find a close relationship between optical properties and film thickness. Figure 29 shows that this is indeed the case. The emissivity for electron beam deposition does not appear to be significantly different from that for filament vapour source deposition. All we can say from the measured data is that there appears to be a sharp rise in emissivity at a thickness of approximately 100Å, and that the emissivity is then almost independent of thickness up to at least 200Å.

We find a very different situation when we examine the results for emissivity (absorptance) as a function of sheet resistance. Film absorptance, determined from emissivity measurements, is plotted in figure 30. Also shown is transmittance integrated over 8 to 14 μm. The theoretical curves for the transmittance and absorptance of a self-supporting metal film are included in the figure. The measured values are in good agreement with theory up to at least 300Ω per square. Thinner films had a higher absorptance (and lower transmittance) then predicted. This may be

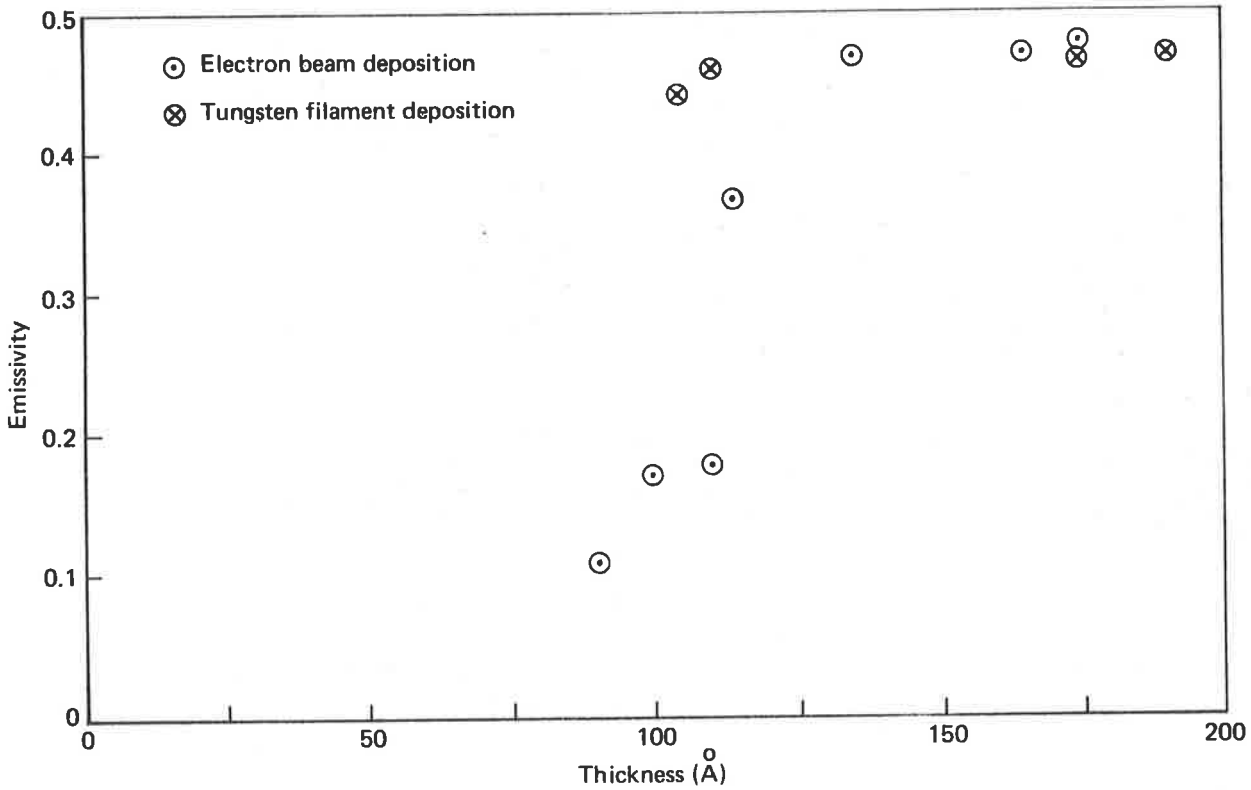

Figure 29. Emissivity of nickel films

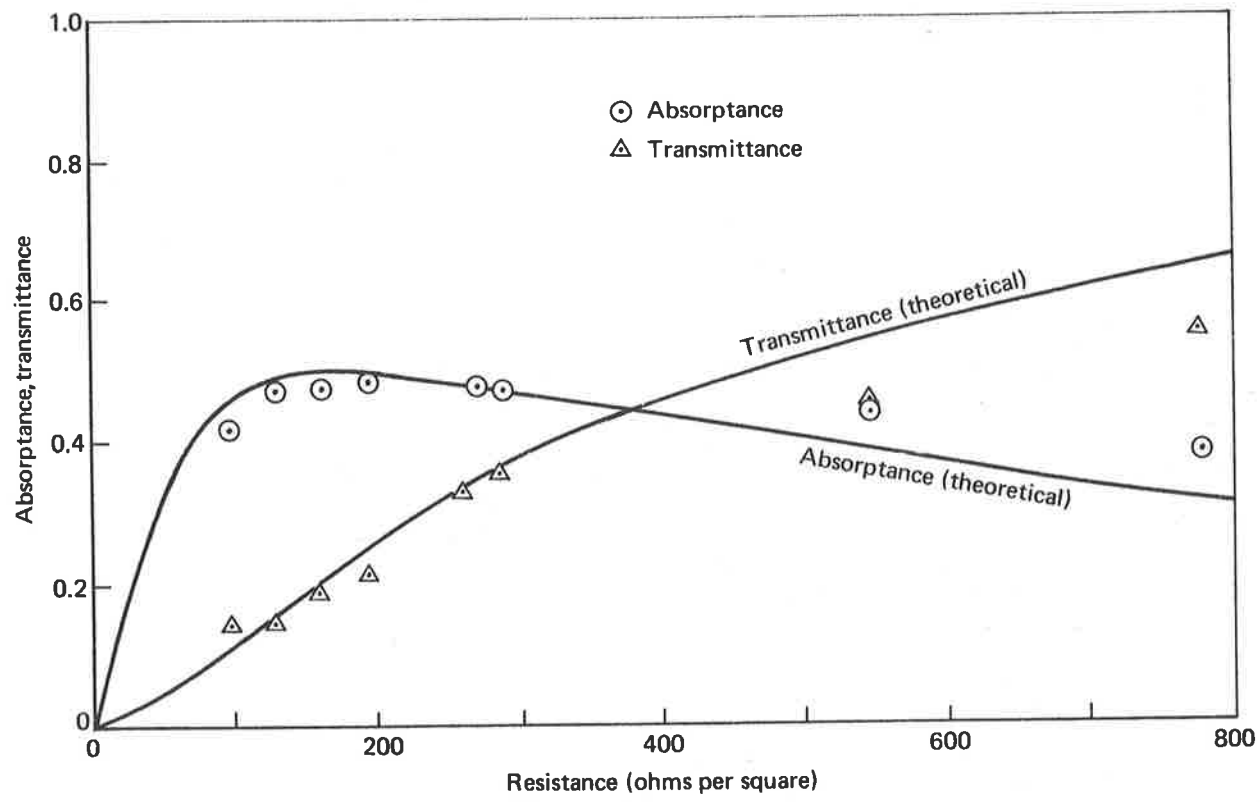

Figure 30. Absorptance and transmittance of nickel films

partly due to the influence of the substrate, but is probably related to film structure. The trend continues for films of much higher resistance.

It was found that the resistance of films which were re-tensioned by swelling in a solvent vapour, rose after becoming taut; however, the optical properties followed the change in resistance. Films of very high resistance still had an absorptance exceeding 0.1.

The spectral absorptance was essentially flat over the region 8 to 14 μm. There was a slight departure from linearity at 2 μm, but this was not usually more than 5%. A spectral plot is therefore unnecessary in this report.

Summarizing, we note that an improvement in deposition technique along the lines described in Sections 9.4 and 9.5 should produce a greater consistency in the optical properties of nickel films. However, it is evident that the preparation of efficient infrared absorbers is not a critical process. Deposition to a resistance of 100Ω per square will yield a film with an absorptance approaching theoretical maximum, and the absorptance will not change significantly with time, even though the resistance may increase to more than 100% of the deposited value.

10. FILM STRUCTURE

10.1 Study of film structure using transmission electron microscopy

A study was made of the structure of metallic absorber films, using conventional bright field transmission electron microscopy. Structural observations were carried out with a Hitachi Type HS-7S 50kV electron microscope. This instrument has an 80000X magnification capability and can be used for electron diffraction studies.

Electron micrographs were prepared for each specimen. There is a practical limit to negative enlargement, determined by negative grain size

and the inherent resolution of the electron microscope. With regard to the latter, there is no point in exceeding a total print magnification of 200000X (500Å per cm), as it was found that practical considerations set a limiting resolution for routine observations of about 25Å.

Ilford NF-40 high resolution plate was used for all observations. Ilford EM-6 plates were also available, but appeared to offer no additional advantages. The grain size of the NF-40 plate contributes to the overall microscope resolution. Plates of finer grain were available, but these required a longer exposure time. It was found necessary to reach a compromise between grain size and exposure time because of specimen movement during observation.

Specimens were prepared by depositing the metal films on thin polymer substrates mounted on 3mm diameter grid carriers, as described in Section 5.3.5. Two nominal microscope magnifications, 10000X and 50000X, were selected for routine observations. In addition to the limitations incurred by negative grain size and specimen movement, the realizable magnification was determined, for many specimens, by low image contrast, making it difficult to achieve an accurate objective lens focus.

A limited and essentially qualitative electron diffraction study was carried out to determine the basic crystallographic characteristics of the specimen films. No attempt was made to compute the camera length, and hence to deduce interplaner spacings. Cubic lattice structure was common to all of the metals studied; thus the lattice type is readily verified by measuring the squares of the radii of the diffraction rings.

All specimens were observed with the metal deposit facing the electron beam. This is a normal precaution, taken to avoid microscope contamination by particulate matter. It was found, however, that reversing the specimen did not influence the observed structure.

10.2 Polymer substrates

Self-supporting polymer film substrates were used for all electron microscope observations. This experimental technique has practical limitations. Most thermoplastic films are fragile, are easily damaged, and tend to move in the electron beam. Film movement was often found to be insignificant for microscope magnifications up to 50000X. However, in some instances the movement was quite rapid, in extreme cases leading to buckling of the entire film.

The most common technique used for specimen examination in modern high resolution microscopy is shadow replication (see, e.g., ref. 53). Unfortunately, the crystallite size of the common shadowing materials is comparable to that of the metal films under investigation, and indeed some of these shadowing materials were actually studied as infrared absorbers. This is not a fortuitous situation, because a small crystal size is considered desirable for both applications. Direct microscopic examination of specimen films supported on polymer substrates is obviously a much simpler technique. In any case we are primarily interested in the properties of this combination.

Two essential requirements of the substrate film are that it must be transparent to the electron beam and must have no observable structure (i.e., low image contrast). The author found that substrates of thickness 800 to 1000Å were suitable. Thinner films were fragile and mobile in the beam; thicker films gave decreased image intensity and were equally prone to damage because of greater electron absorption.

Of the various polymers of suitable thickness which were tested, formar appeared to be the most stable in the electron beam. Collodion substrates were more easily damaged. Polyacrylonitrile (PAN) films appeared to be very robust; however, PAN films prepared to date are too thick

for routine microscopy.

The structure of the polymer substrates was found to be of particular significance. Figure 31 (a) shows an electron micrograph of an uncoated formvar substrate. There is clearly sufficient image contrast to reveal a characteristic structure. Figure 31 (b) shows a thin nichrome film on formvar, illustrating the influence of the formvar substrate. This influence was evident for all finely crystalline deposits. Consequently formvar was rejected as a substrate material, with the exception of the examination of thicker or coarsely crystalline specimens.

The structure of uncoated collodion substrates was difficult to observe because of the low image contrast. By focussing on dust particles, or holes in the film, a vague cellular structure was evident, sometimes with an occasional area of finely crystalline material which is believed to be potassium bromide contamination from the film preparation process. A good example of this structure is illustrated in figure 32 (a).

The observed electron diffraction pattern of an uncoated collodion film is shown in figure 32 (b). The diffuse ring pattern is typical of an amorphous material.

Whilst the structure of collodion would at first appear to be suitable for microscopic examinations, the first electron micrographs of metallic deposits on collodion were extremely difficult to interpret. Many of these deposits appeared as confusing patterns of platelets, mesas and globular structures. The results were both unexpected and inconsistent. In an attempt to solve this problem, collodion substrates were shadowed at 45^{o} with a thin chromium deposit. A micrograph of a shadowed collodion specimen is shown in figure 33 (a), revealing the true structure of the collodion surface. A nichrome film on collodion is illustrated in figure 13 (b). The similarity between the two micrographs is obvious. The

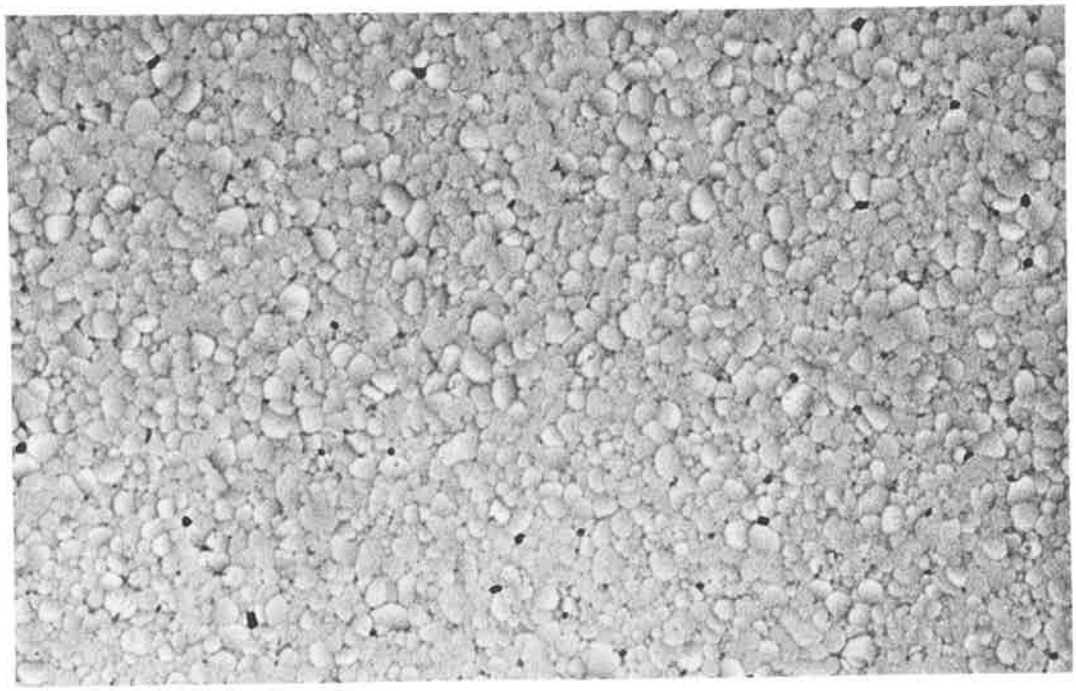

Neg. No. 3011

(a) Formvar substrate. Mag. 20000X

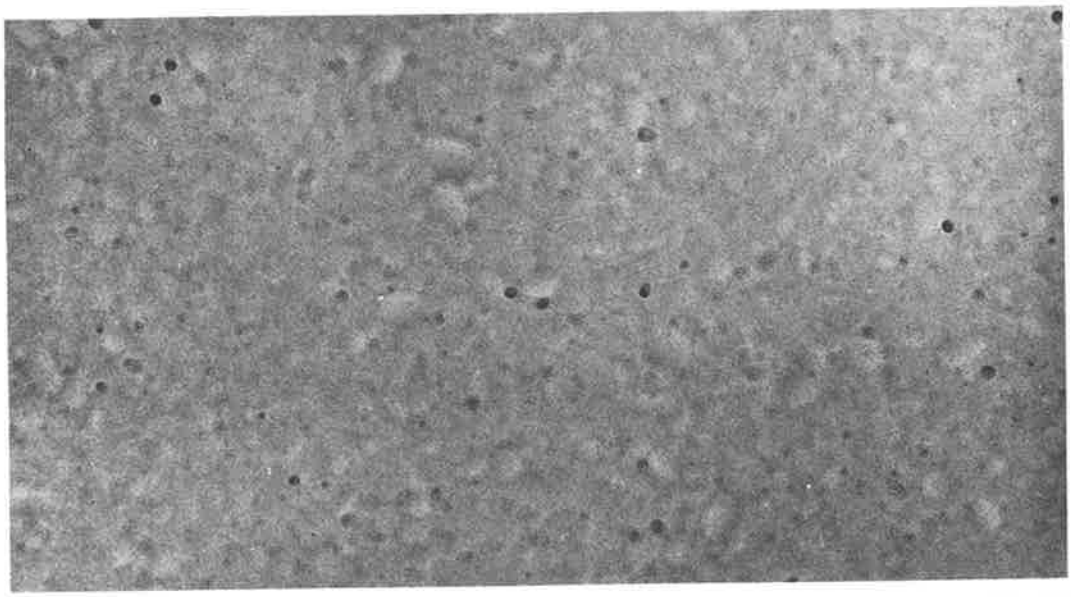

Neg. No. 969

(b) 70 Å nichrome film on formvar. Mag. 20000X

Figure 31. Structure of formvar substrates

Neg. No. 1045

(a) Collodion substrate. Mag. 20000X

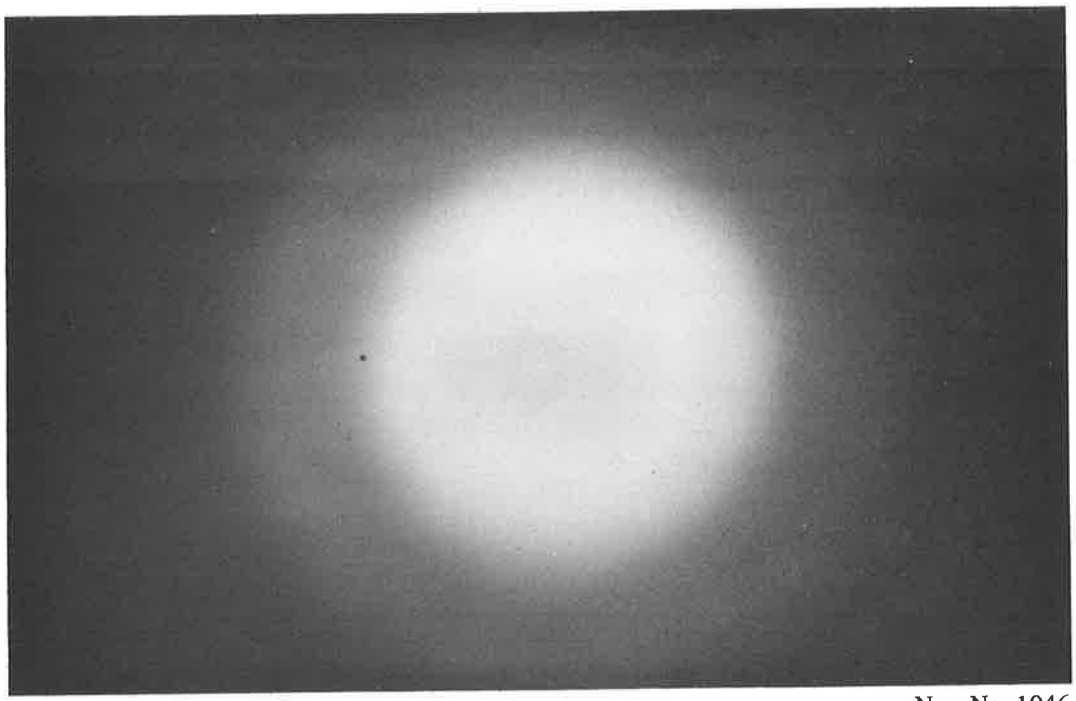

Neg. No. 1046

(b) Collodion electron diffraction pattern

Figure 32. Structure of collodion substrates

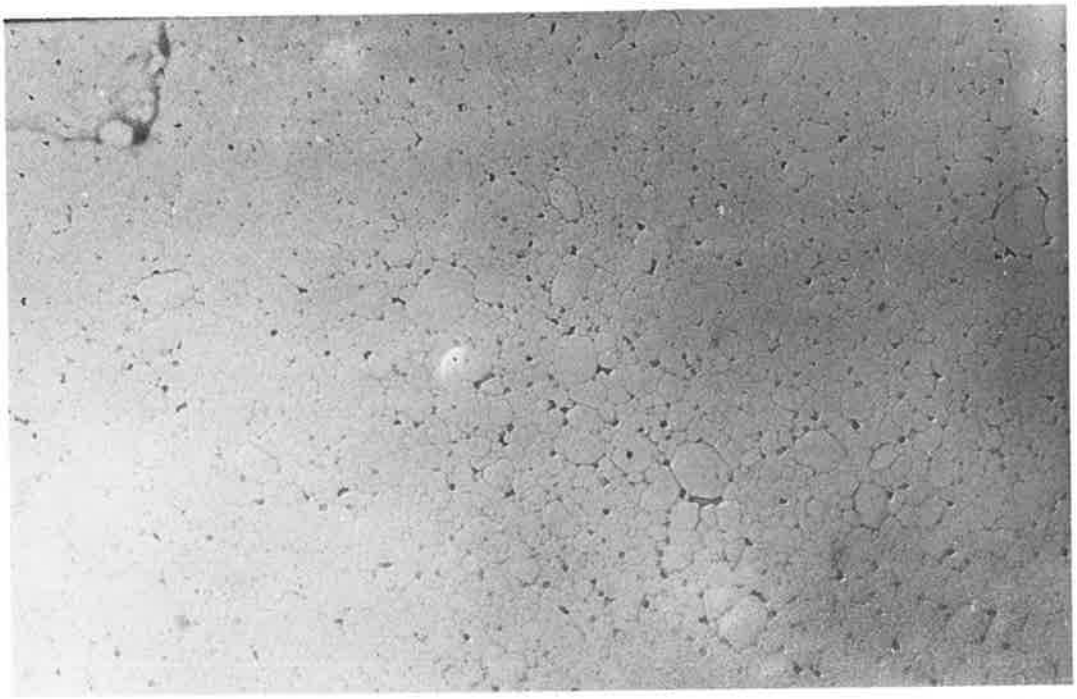

Neg. No. 1053

(a) Collodion substrate shadowed with chromium. Mag. 20000X

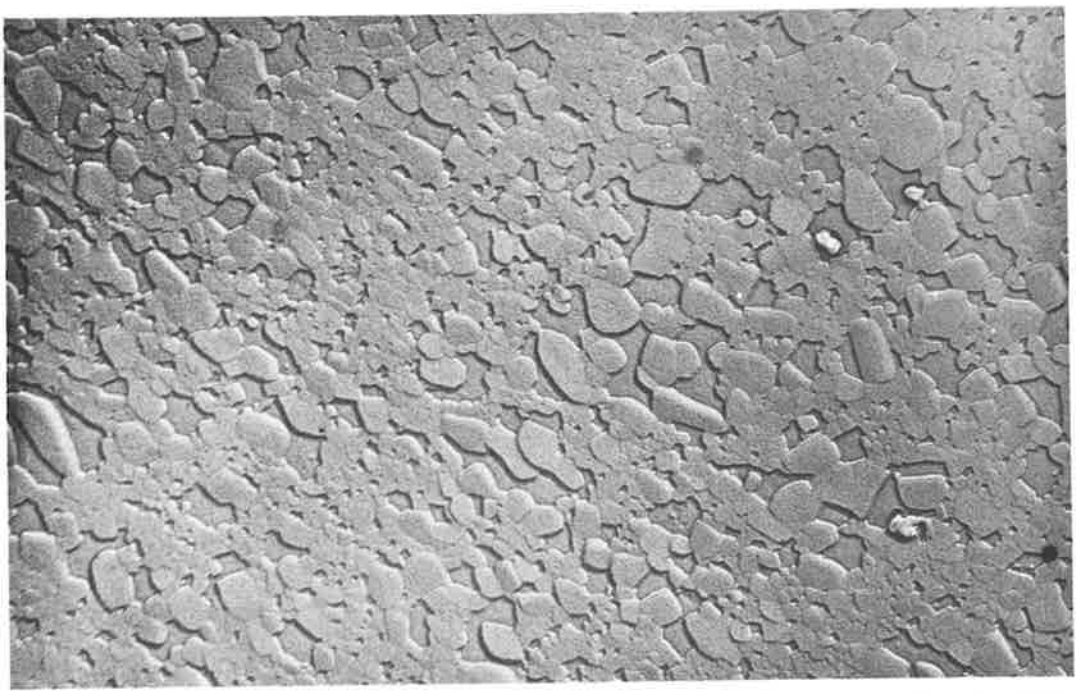

Neg. No. 2913

(b) Thick nichrome film on collodion. Mag. 20000X

Figure 33. Influence of collodion substrates in electron microscopy

large "mesa" structure in both cases is of size 0.1 to 0.5 μm. A careful study also reveals a fine filamentary structure, of diameter approximately 30 to 50Å, which is believed to be molecular chains in the collodion substrate.

The anomalous structural effects described above were observed only with the finely crystalline, higher melting point metals studied in the proejct. This phenomenon is now considered to be the result of substrate heating during deposition, causing substrate distortion with a consequent shadowing (or pseudo-shadowing) action. It is also felt that similar conditions, prevailing in experiments carried out by various authors (see e.g., references 26, 27) may have lead to previous misinterpretations of observed structures.

10.3 Structure of gold films

Gold film infrared absorbers and bolometer detectors have been used extensively in the author's laboratory. Electron microscope examinations have added considerably to our understanding of the physical properties of these films. Figure 34 shows electron micrographs of two gold films of thickness (a) 165Å and (b) 250Å. The films are seen to be coarsely crystalline aggregates. Thinner films are agglomerates which grow into the structure illustrated in micrograph (a), a typical structure observed for the maximum measured infrared absorption. The characteristic "fissures" are gaps in the gold film (not the substrate). The fissures are gradually filled as deposition continues, to give the structure shown in micrograph (b). Figure 35 (a) is a high magnification reproduction of a 165Å thick film. The individual crystallite size is approximately 200Å.

An electron diffraction pattern of a 320Å thick gold film is given in figure 35 (b). The ring pattern is indicative of a polycrystalline film. The rings are sharply defined because of the large crystal size, and the squares of the radii are in the sequence 3, 4, 8, 11, which is characteris-

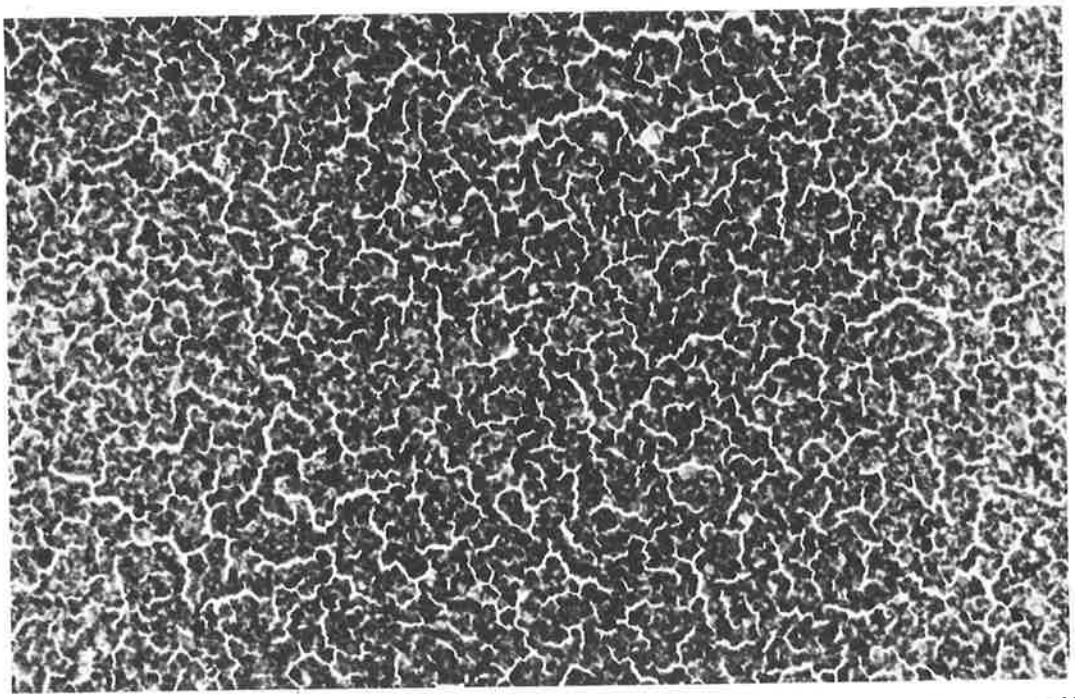

Neg. No. 1027

(a) 165 Å gold film on collodion. Mag. 50000X

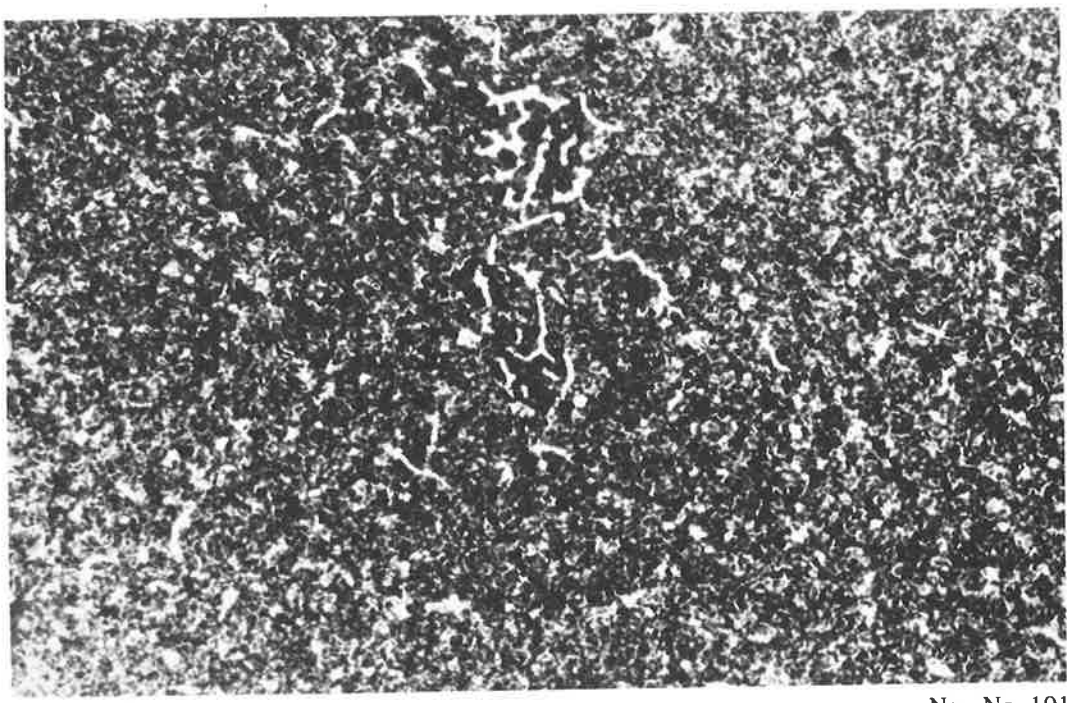

Neg. No. 1018

(b) 250 Å gold film on collodion. Mag. 50000X

Figure 34. Structure of gold films. 1

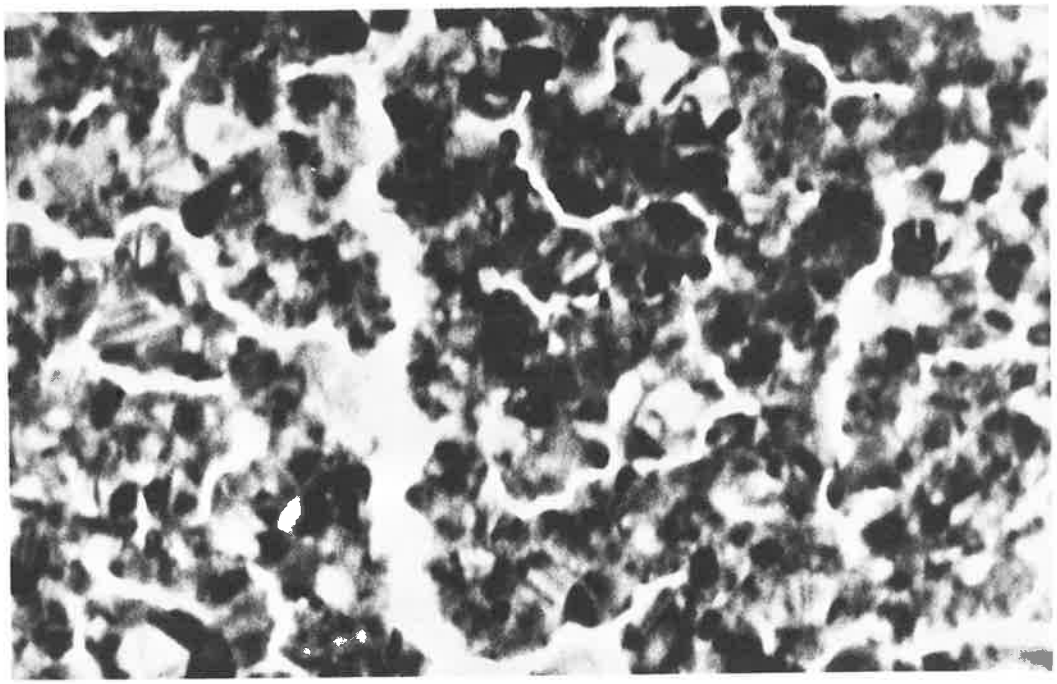

Neg. No. 1030

(a) 165 Å gold film on collodion substrate. Mag. 250000X

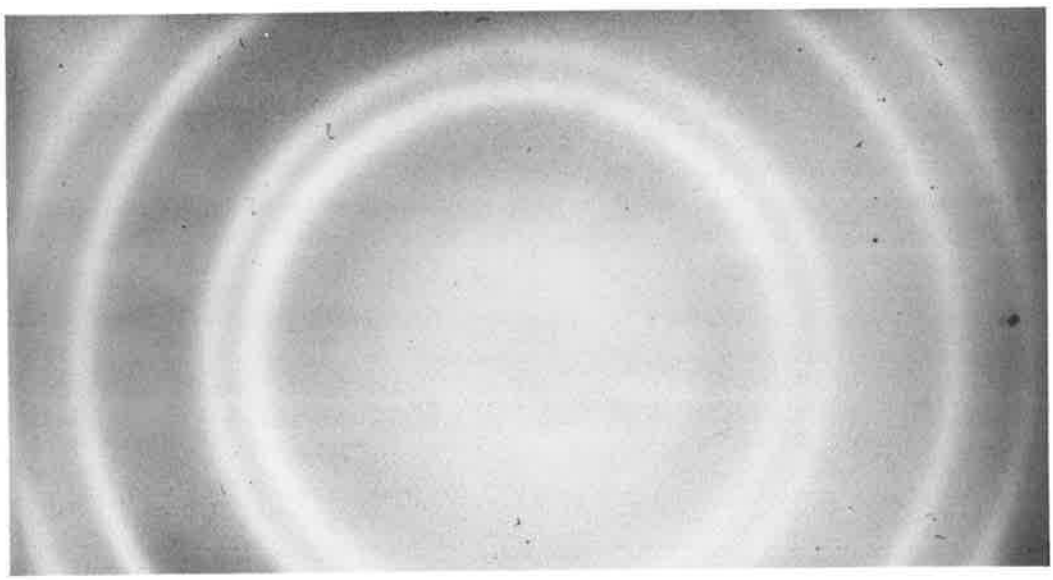

Neg. No. 1040

(b) Gold diffraction pattern

Figure 35. Structure of gold films. 2

tic of the expected face-centred cubic lattice. The rings appeared sharper in the electron microscope - the micrograph is overexposed. The diffuse background is a consequence of the collodion substrate.

The electron micrographs are identical in appearance to specimens prepared by Pashley et al on carbon substrates (ref. 22, figure 12). Similar structure has been observed for gold films deposited on to both borosilicate substrates (ref. 55), and rock salt substrates at room temperature (ref. 23).

Three important observations with the electron microscope have shed light on the infrared absorber characteristics of gold films :

(a) A change in crystal structure is often observed soon after exposure to the electron beam. This phenomenon has also been noted in early work by Levinstien (ref. 26). Crystal re-orientation is caused by beam heating, and is an indirect confirmation of the postulate of "current aging" discussed in Section 7.2.

(b) There is clear evidence of the influence of deposition rate on film properties. Thus a film formed by very slow deposition became electrically conducting at roughly twice the thickness of films prepared in the normal manner. The film was, however, similar in appearance to the thinner films, indicating a preferred upward growth. When conduction commenced the film was, at that stage, almost a perfect infrared reflector.

(c) The characteristic "fissures" in the micrograph, figure 34 (a), were observed to be areas of mechanical weakness in the gold films. Films were seen to fracture along these fissures under the action of the electron beam, suggesting a stress concentration. This structure is typical of films having maximum infrared absorption, and thus it imposes a limitation on the operating temperature of gold films on

collodion substrates.

It is not surprising that it is difficult to prepare gold films of precisely determined electrical characteristics. The slightest change in growth pattern may cause, for films of the same thickness and optical properties, a difference in sheet resistance of many orders of magnitude.

The discontinuous nature of thin gold films must account, at least in part, for the reduced film density noted in Section 7.1. This is an immediate consequence of the fact that the Tolansky interferometer measures the average thickness of thin films.

10.4 Structure of nichrome films

The structure of nichrome films has been investigated in several laboratories, the best known work being that by Bricknell et al (ref. 56). These author's postulated that the films are composed of nickel rich islands separated by a continuous chromium oxide skin. The island size was approximately 100Å, whilst the individual crystallites were less than 10Å in diameter. This is in agreement with our earlier discussion of the influence of oxidation on the formation of nickel and nichrome films (Section 9.3). The author has found no evidence, from his own study of nichrome films in the electron microscope, of a structure in contradiction to this general description.

Figure 36 (a) shows an electron micrograph of a nichrome film on a collodion substrate. The film is seen to consist of a fine island structure, some of larger size and thicker (higher contrast). The most notable difference from the work of Bricknell et al is that the island size is much smaller - only the largest has a dimension of approximately 100Å. This is not surprising, as the Bricknell study applies to cleaved rock salt substrates at a substrate temperature of 270°C. Because of the inherent complexity of the structure of nickel-chromium films, and the

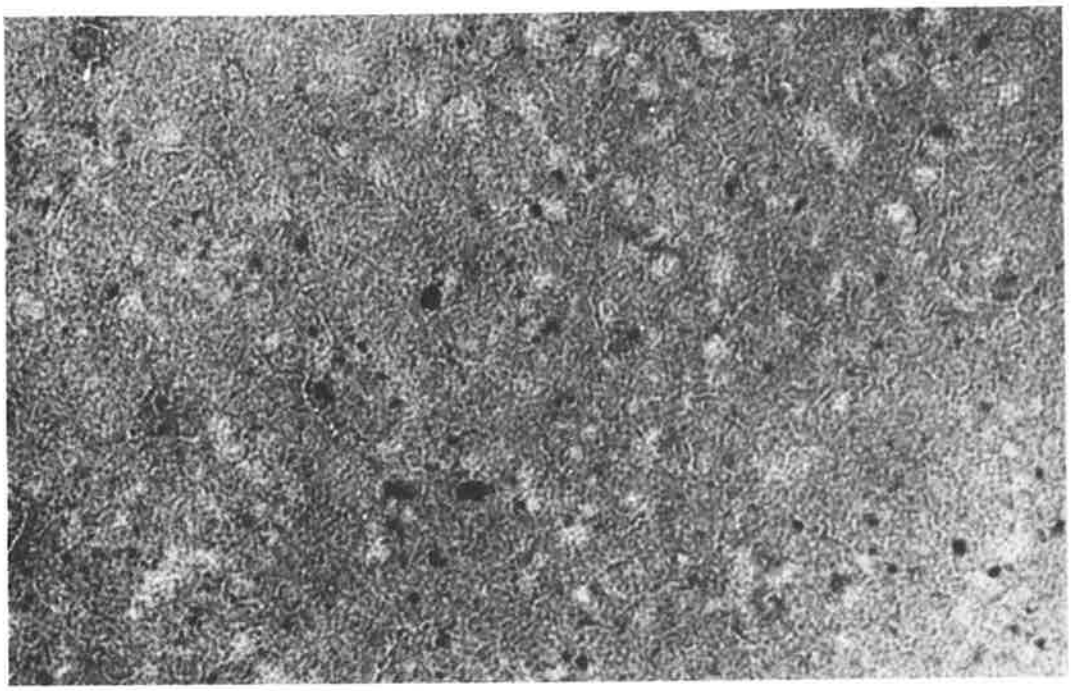

Neg. No. 987

(a) 140 Å nichrome film on collodion. Mag. 100000X

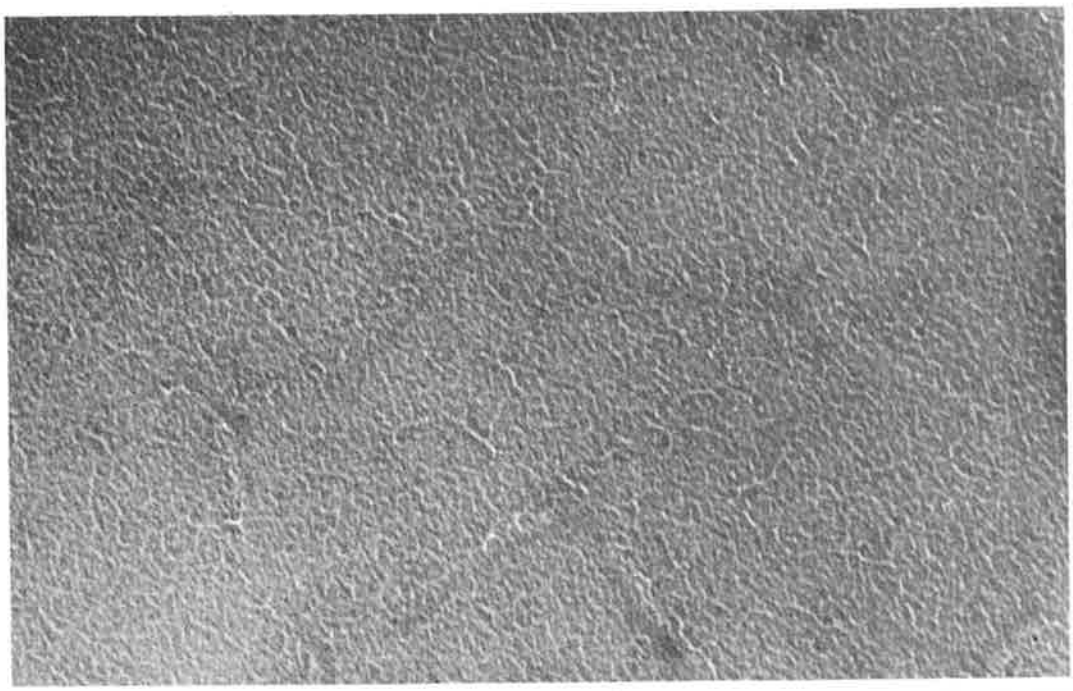

Neg. No. 972

(b) 125 Å nichrome film on collodion. Mag. 200000X

Figure 36. Structure of nichrome films

ample descriptions reported in the literature, no effort was made to extend this study.

Figure 36 (b) shows a thin (200Ω per square) nichrome film on a formvar substrate, at high magnification. This micrograph is of interest because of the evidence of both "filamentary" structure and the larger scale "cellular" structure in the polymer film.

10.5 Structure of nickel films

The examination of nickel films in the electron microscope was hampered by the difficulty of preparing specimens which were totally free of structural influence from the polymer substrate. This problem was also experienced with nichrome films. In general, it was found that films of sheet resistance of less than 200Ω per square showed some sign of damage from the deposition process, and almost invariably revealed the characteristic substrate structure. High power conventional microscopy has shown that thicker nickel films prepared by electron beam deposition on 3mm grid carriers were usually buckled or partially destroyed. A similar result was observed for platinum and chromium films. Because of more effective heat sinking, the grid carrier specimens survived deposition, whereas the larger specimens prepared for optical measurement were often destroyed.

The structure of a nickel film of thickness 350Å deposited on to a collodion substrate is illustrated in figure 37 (a). The film is seen to be finely granulated, the maximum size of the crystallites being approximately 50Å. Because of this fine structure it was often difficult to achieve an accurate focus. A similar "pepper pattern" appearance was also observed for chromium and platinum films.

Neugebauer (refs. 34, 57) found that for 100Å thick nickel films on glass substrates, there was no evidence of aggregations into islands,

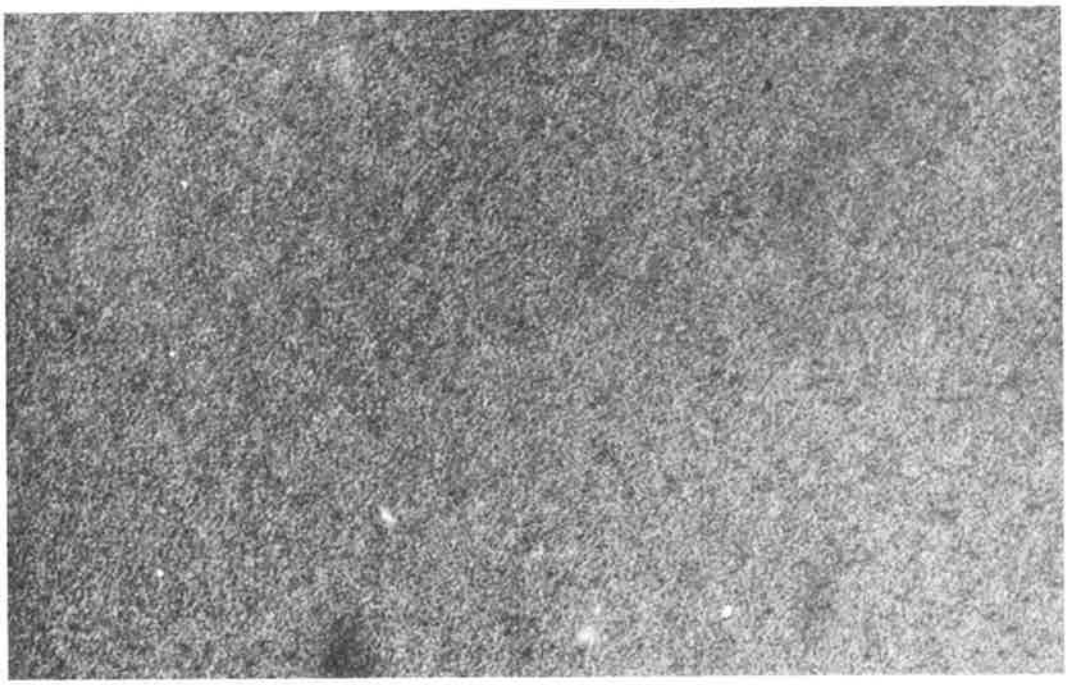

Neg. No. 1038

(a) 350 Å nickel film on collodion. Mag. 100000X

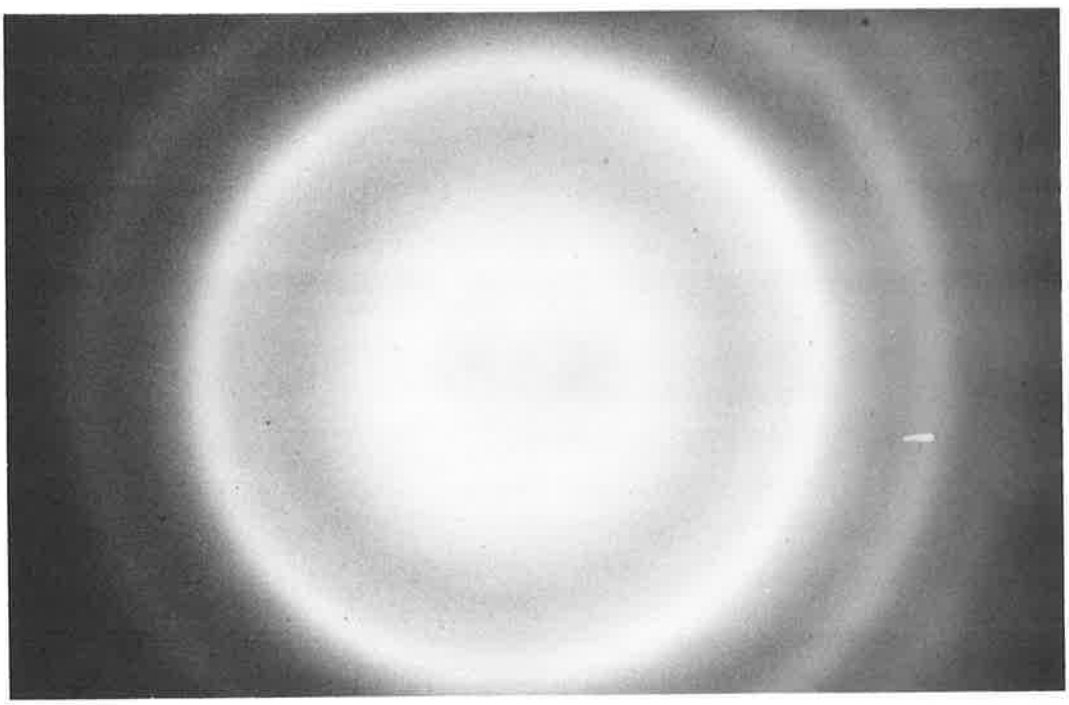

Neg. No. 1048

(b) Electron diffraction pattern of partially oxidized nickel film

Figure 37. Structure of nickel films

and the films appeared continuous. These films were prepared in ultra high vacuo. Fleet (ref. 33) found a crystallite size of 60Å for glass and silica substrates at room temperature. Levinstien (ref. 26) also observed a finely crystalline structure for nickel on collodion substrates. These latter results are in agreement with the author's recent study. On the other hand, Sennett and Scott (ref. 27) noted an aggregated structure for films on formvar substrates. These authors shadowed their specimens to demonstrate that aggregation was not caused by electron beam interaction, but may have overlooked the possibility of structural anomalies introduced by the extremely thin formvar substrates.

Electron diffraction patterns for nickel films on formvar and collodion substrates were not as sharp as that of gold (figure 34), indicating either a small crystallite size or a crystallite size significantly different from island dimensions. The ring radii confirm the face-centred cubic lattice for nickel. An electron diffraction study of a thick semi-insulating film prepared at a slow deposition rate (figure 37 (b)) indicated a change in the ring pattern which, from a study of the reports by several authors on artificial thermal aging of metal films, would suggest the presence of an oxide phase. A quantitative analysis was not carried out.

The influence of stress in nickel films is apparent in the micrograph figure 38. The micrograph shows an imperfection in a nickel film on a formvar substrate. The tear in the film probably originates from a flaw in the substrate, and the weakening (of the substrate) has caused the nickel film to part, presumably under the influence of beam heating. The substrate can be seen stretched across the gap in the film, and the stress is clearly tensile. This observation would appear to support the proposed mechanism for stress in nickel films discussed in Section 9.4,

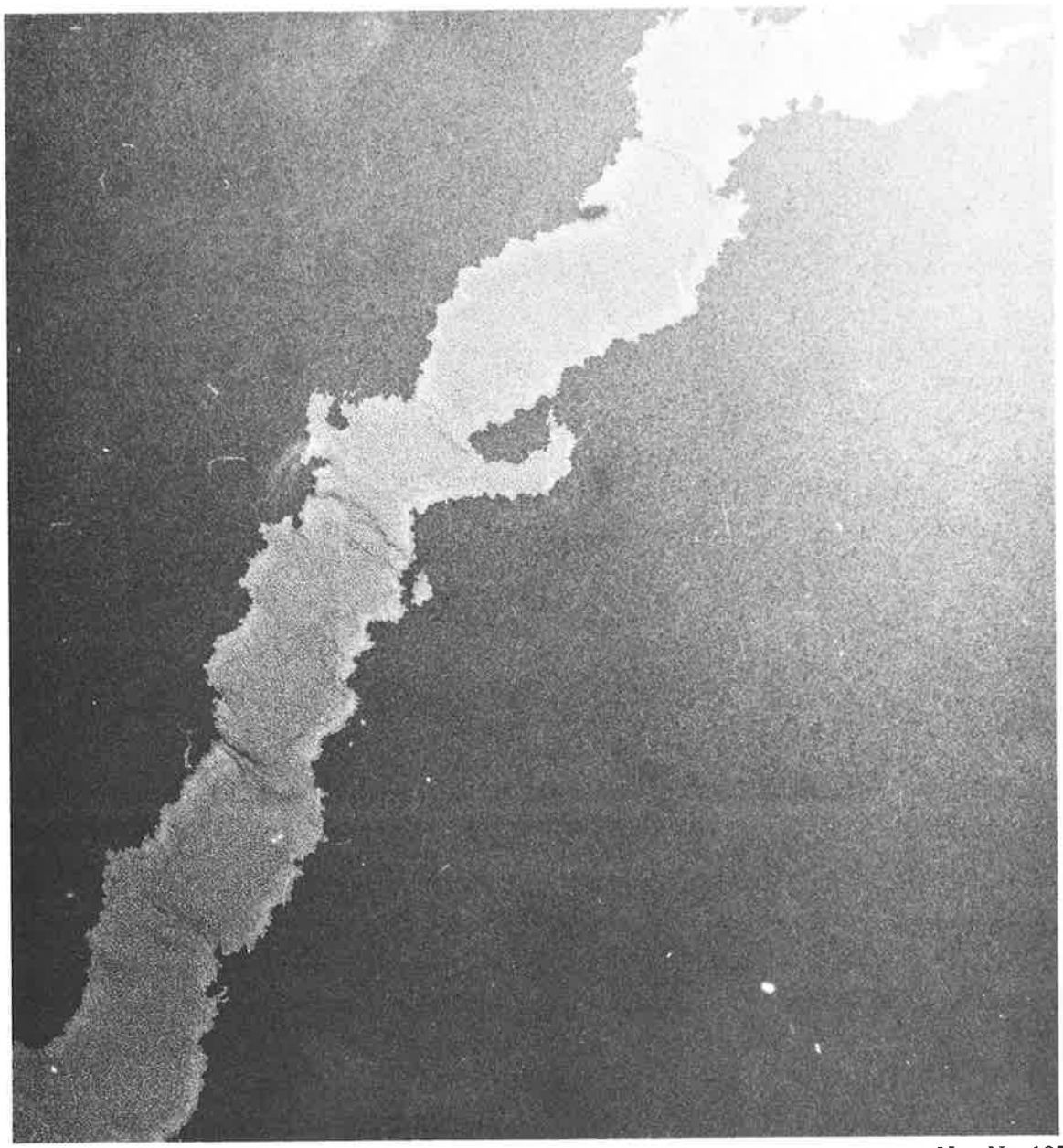

Neg. No. 1074

195 Å nickel film. Mag. 50000X

Figure 38. Stress in nickel film on formvar substrate

although it should be noted that we have found no evidence of gross imperfections in the "stress-relieved" films.

A further examination of figure 38 reveals the fine filamentary structure in the formvar substrate, described earlier in Section 10.2. The characteristic fine-grain structure of the nickel film is also clearly discerned.

10.6 Relationship between structure and film properties

This study has afforded considerable evidence, albeit of a qualitative nature, of the relationship between film structure (as observed in the electron microscope) and the various film properties discussed in preceding sections.

Electron microscope examinations have enabled us to explain, with increased confidence, the reasons for the failure of the electrical-optical relationships for gold absorber films, and also the change in film properties with deposition parameters.

The study of the structure of the higher melting point evaporants has tended to confirm our evaluations of the suitability of these materials as infrared absorbers, notably that small crystallite size is conducive to a more predictable absorber, and that a much thinner film can be realised.

The problem of stress in thin films of higher melting point materials has been clarified.

When we take the observed physical properties of the thermoplastic substrates into consideration, we may deduce that future research should proceed along the following lines :

(a) We should seek a new substrate film, which is capable of withstanding a higher temperature and does not swell or stretch. A thermoplastic material such as polyacryonitrile, which can be partially pyrolised

without change in composition, may be suitable. Alternatively, a "cross-linked" material may prove to be satisfactory.

(b) The film should be cooled during deposition, e.g., radiation cooling to either a dewar or thermoelectric cooler.

(c) Cooling of the film will not reduce, and indeed may enhance, film stress. Therefore we must seek a stress release mechanism. Our experience would indicate that high voltage "current aging" during the initial coalescence phase may be appropriate. Stress relief may also be inherent in the electron beam deposition process, provided that an improved substrate material is available.

(d) In order to reduce oxidation and to realise the smallest possible crystallite size, the deposition rate should be increased, and preparations carried out in a higher vacuum. Unfortunately, there is a practical limit to rate of roughly $2000\text{Å}.m^{-1}$, set by the acceptable monitoring time.

Finally, we have the satisfaction of justification of our earlier predictions on the structure of the selected infrared absorber materials. We are now able to proceed with confidence to the study of new and probably superior absorber materials such as platinum and palladium. These materials are readily prepared by means of electron beam deposition.

11. MEASUREMENT OF THERMAL PROPERTIES

Measurements were made of the temperature coefficient of resistance, temperature rise, thermal rise time and thermal spread of metal absorber films. A radiometer test apparatus has been constructed for the measurement of thermal properties of thin films. This instrument comprises a motor-scanned sample stage, a fast-response infrared radiometer and a miniature blackbody cavity. Unfortunately the apparatus is still in the developmental stage and precision measurements are not yet available. All thermal measurements reported

in this thesis were carried out using various indirect experimental techniques, whereby temperature rises were generated by Joule heating in the absorber film. Thus radiant power was simulated by an electrical analogue.

11.1 Theory of the electrical analogue technique

In all of the techniques described in this section, radiant energy absorption was simulated by the application of a d.c. or pulsed voltage to a specially shaped absorber element. This in no way complicates the theoretical analysis. The only change to the derivations of Section 2 is that the absorbed power, ΔP, appearing in the expression for maximum temperature rise (equation(20)) takes the form :

$$\Delta P = I^2 R \qquad (119)$$

where I is the average current passing through the element, and R is the average resistance of the element.

11.1.1 Thermal spread

Thermal spread can be measured by passing a steady current through an appropriately shaped element, then scanning the specimen with a high resolution radiometer. The magnitude of the temperature rise need not be known; however, if the radiometer is calibrated, then a direct measurement of temperature rise can be recorded during the scan.

11.1.2 Thermal rise time

Thermal rise time can only be measured directly with the above instrumentation if the response time of the radiometer detector is very much smaller than the time to be observed. If,however, the element is pulsed, then the thermal time constant can be determined by measurement of the change in resistance with temperature. The actual temperature again need not be known but if the temperature coefficient of resistance is measured, then the average temperature

can be determined during the same experiment.

Let us assume that a current, I, is applied to the absorber element from a voltage supply of output resistance R_L. As the temperature of the element rises through Joule heating, its resistance, R, increases by an increment ΔR (the metal film has a positive temperature coefficient of resistance), and the voltage drop, V, across the element rises by an increment ΔV. The voltage rise is given by

$$\Delta V = \frac{R_L \Delta R \, V_o}{(R+\Delta R+R_L)(R+R_L)}$$

$$= \frac{R_L \Delta R \, I}{R+\Delta R+R_L} \quad , \tag{120}$$

where Vo is the source voltage. If the average temperature rise, ΔT_a is small, then

$$\Delta R = R\alpha\Delta T_a \tag{121}$$

where α is the temperature coefficient of resistance ($^oK^{-1}$). If we make R_L very much larger than R (i.e., a constant current source), then

$$\Delta V \simeq \frac{RR_L}{R+R_L} \, I\alpha\Delta T_a$$

$$\simeq RI\alpha\Delta T_a \tag{122}$$

This is the rise in voltage over a period which is long compared to the thermal rise time (we assume that the pulse length is much larger than the rise time). The time dependent voltage rise is simply

$$\Delta V \simeq RI\alpha\Delta T_a \, (1-\exp(-t/\tau)) \tag{123}$$

where τ is the thermal rise time.

Thus measurement of the voltage rise yields a value of the

thermal rise time for the absorber film. If the thermal spread is small compared to the element dimensions, τ is just the time constant given by equation (26). Otherwise, τ is the rise time corresponding to the average temperature rise, and can be computed from the theory of Section 2.3.3.

If the temperature coefficient of resistance of the absorber film is known, the average temperature rise can be determined during the same experiment from equation (121).

11.2 Specimen preparation

The specimens prepared for the measurement of thermal properties were briefly described in Section 5.3.6. Absorber films were deposited on to 850Å thick collodion membrane substrates. Substrates were mounted on either 25 mm o.d. x 20 mm i.d. epoxy annuli or 25 mm diameter slotted epoxy discs. Evaporation masks were shaped to provide metal specimen films of size 12.5 mm long x 2.5 mm wide for the annuli or 2.5 mm square for the slotted discs. We would expect the temperature rise and thermal rise time for the large elements to approach the maximum values determined by radiation loss only. However, for the smaller elements, conduction loss to the film mount will reduce the magnitudes of the temperature rise and rise time, depending on the value of the thermal spread constant.

Some relevant parameters of the eight specimens selected for study are listed in Table 4. It will be noted that resistance is given as ohm per square, R_s, whereas the actual resistance of the large specimens is $5R_s$.

TABLE 4

SPECIMENS FOR THERMAL MEASUREMENTS

Specimen number	Absorber type	Length (mm)	Thickness (Å)	Emissivity	Resistance (Ω per square)
G9	gold	12.5	160	.45	65
G21	gold	2.5	165	.45	124
A13	nichrome	12.5	230	.47	46
A15	nichrome	2.5	200	.47	205
C23	nickel	12.5	273	.30	40
C24	nickel	12.5	142	.40	83
E30	nickel	2.5	135	.47	230
E31	nickel	2.5	165	.47	100

11.3 Temperature coefficient of resistance

Temperature coefficient of resistance was measured for nickel, nichrome and gold absorber films. The specimens were placed in an environmental test chamber and film resistance was monitored as a function of chamber temperature.

The absorber specimens were inserted in a Wheatstone bridge circuit. The bridge difference voltage, corresponding to a change in specimen resistance with temperature, was measured with a P.A.R. Model HR-8 lock-in amplifier. The 10 kHz bridge voltage was provided by the amplifier's internal reference source. Specimen resistance was determined from the resistance required to null the Wheatstone bridge circuit. The resistance standard was a precision decade shunt. Temperature coefficient of resistance was then determined from the relationship

$$\alpha = \frac{1}{R} \frac{\Delta R}{\Delta T} \qquad (^{o}C)^{-1} \tag{124}$$

An immediate difficulty was encountered when measurements were made of the resistance of the specimens listed in Table 4. Accurate null readings could not be obtained because of an excessive noise level. The noise was found to be caused by fluctuations in the resistance of the specimens. The fluctuations were greatest for the 12.5 mm absorber films, and reliable measurements of the temperature coefficient of resistance could not be obtained for these specimens. This problem was not evident when measurements were made of the resistance of either very small absorber elements or of metal films deposited on to glass substrates. There appears to be little doubt that the excess noise level is caused by the "strain gauge" effect.

Because of the above difficulty, only limited data were obtained of the temperature coefficient of resistance of the eight selected specimens listed in Table 4. The temperature coefficient of 2.5 mm gold and nickel absorber specimens was found to lie in the range 0.5 to 1.0 x 10^{-3} $^{o}C^{-1}$. The temperature coefficient of a nichrome specimen was less than 0.5 x 10^{-3} $^{o}C^{-1}$.

A new series of experiments has been commenced to determine the temperature coefficient of resistance of 0.2 mm x 0.05 mm gold and nickel bolometer elements. The results obtained so far indicate that the temperature coefficients of films of similar thickness to the specimens listed in Table 4 lie within the range of values given above.

The bulk temperature coefficient of resistance of gold and nickel is approximately 4 x 10^{-3} $^{o}C^{-1}$ and 6 x 10^{-3} $^{o}C^{-1}$ respectively. The lower values observed for thin films are to be expected, and indeed are predicted by the Fuchs-Sondhiemer theory (Section 3.5). It is of interest to note that measurements made on nickel films yield further information on the influence of film oxidation. Thus Reale (ref. 58)

has measured a temperature coefficient of $1.2 \times 10^{-3}\ ^{o}C^{-1}$ for nickel films of thickness 2000Å to 5000Å, and has deduced that the oxide content of these films is approximately 3.5%. The method of preparation was not stated in the reference. However, the trend is clear : in addition to "size effect", film oxidation contributes to a decreased temperature coefficient of resistance.

11.4 Measurement of thermal rise time

A relatively simple technique was devised for the measurement of thermal rise time. This technique makes use of the electrical analogue discussed in Section 11.1.2.

A test current was applied to the specimen film from a Data-pulse Model 100A pulse generator, and the voltage drop across the specimen was displayed on a Tektronix Type 564B plug-in storage oscilloscope. The vertical deflection plug-in unit was a Type 3A9 differential amplifier. This amplifier has a high common-mode-rejection-ratio, ranging from 300 at 10 Hz to 200000 at 1 kHz. The measurement circuit was arranged such that the specimen formed one arm of a Wheatstone Bridge. A precision decade shunt was inserted in a second arm of the bridge, and the voltage drop across this shunt (the 'reference' voltage) was applied to the alternate channel of the amplifier. The two remaining resistances in the bridge were of equal magnitude, and were used to set the test current. Thus, when operated in the differential mode, the oscilloscope displayed the bridge difference voltage, the desired waveform being achieved by adjusting the reference channel voltage. The oscilloscope time base was externally triggered from the pulse generator.

The specimen was evacuated to 2×10^{-6} torr. A 100 ms or 250 ms square wave (chosen so that the period was large compared to the

observed rise time) was applied to the measurement circuit. The test current was set to a suitable peak value, usually 1.0 to 2.0 mA. With the amplifier in the differential mode, the reference voltage was adjusted to display a null at the trailing edge of the pulse. A typical waveform is illustrated in figure 39(a). Figure 39(a) represents thermal decay, the leading edge corresponding to the incremental resistance ΔR in equation 121. This display was preferred to the rising waveform, shown in figure 39(b), because of greater null stability.

The display was photographed using a Tektronix Type C-12 oscilloscope camera and the thermal rise time determined as the time to which the waveform decayed to 1/e of the initial value. At least two measurements were made of each specimen, yielding an estimated accuracy of ± 0.05 time base divisions (e.g., ± 1 ms for 20 ms/div).

This technique was found to be a rapid and sensitive method of estimating the thermal time constant of infrared absorber and bolometer detector elements. Because of the low signal levels, particular care was required to minimize pick-up and earth loops.

11.4.1 Theoretical predictions

The thermal rise time was computed for each specimen from the theory of Section 2. We should recall that the measured rise time approximates the simple time constant, given by equation (26), only when the element size is large compared to the thermal spread constant, i.e., for radiation loss only. When conduction loss becomes significant, the rise time must be computed from the time dependent equations given in Section 2.3.3. The selection of the 1/e ordinate as the reference for rise time measurements is useful for comparison purposes, but should not be taken to imply a simple exponential law. Equation (123) is thus an approximation.

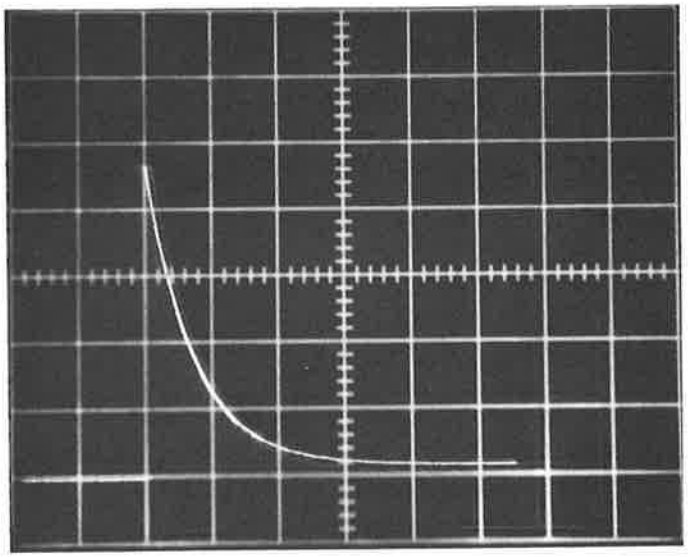

(a) Thermal decay

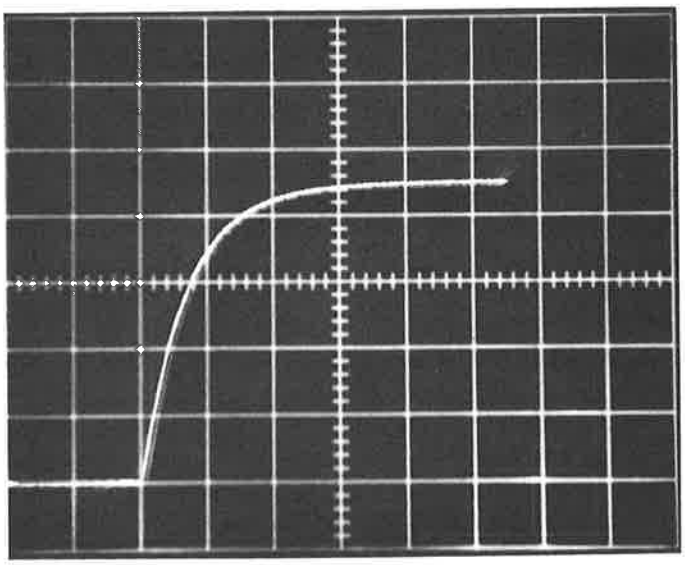

(b) Thermal rise

Specimen C24
Scale: 50 ms/div (horizontal)
500 μV/div (vertical)

Figure 39. Thermal rise time measurement. Oscilloscope display

The rise time was determined by computer computation of the time dependent average temperature rise, initially by assuming the bulk properties listed in Table 1. The remaining relevant parameters (determined experimentally) are listed in Table 4. The computed rise time was then compared with the experimentally determined value. Where necessary, the computation was repeated to determine the value of specific thermal capacitance (density and specific heat) and thermal conductivity required to effect agreement with the measured value.

11.4.2 Influence of background temperature variations

An accurate measurement of the background temperature, T_o, was not made; however, this should not be significantly different to room temperature. The average laboratory temperature (controlled to ± 2°C) was 295°K. The computer program provides for a fixed value of T_o of 300°K; thus an error will occur in the determination of rise time. It can be readily shown from equations (6) and (26) that the maximum error from this cause in the calculation of rise time is approximately 5%, and in this case the computed value will be lower than the actual value. A similar error will be incurred in the estimation of temperature rise.

11.4.3 Influence of the linear radiation loss law

The assumption of a linear radiation loss law also leads to errors in the computation of both temperature rise and thermal rise time. From equations (2), (5) and (6) it is easily shown that for a temperature rise of 10°K above a background at 300°K, the maximum error is again approximately 5%, but here the computed value will be higher than the actual value.

The author has concluded that the overall error due to the above considerations lies within the accuracy of measurement of thermal rise time, the two errors being compensatory.

11.4.4 Influence of an imperfect heat sink

In the analysis of the thermal properties of the selected specimen films, it is assumed that the epoxy mounts act as perfect heat sinks. In order to test this assumption, the thermal waveform was stored on the oscilloscope for a period of at least 2 minutes after applying the pulse bias. It was found that the temperature rose by at most 5% of the initial value, indicating slight heating of the epoxy mount; however, the error in rise time was within the accuracy of the measurement technique.

11.4.5 Influence of chamber pressure

A rise in chamber pressure has a dramatic effect on the observed thermal rise time. This observation is not unexpected, and is caused by the contribution of gaseous conduction and convective heat loss to the thermal surface conductance. At high chamber pressures these losses are much larger than radiation loss.

Careful measurements were made of temperature rise and thermal rise time as a function of chamber pressure. It was found that the temperature rise and rise time were constant (within measurement accuracy) at pressures less than 1×10^{-4} torr. From approximately 5×10^{-4} torr to 1.0 torr both parameters decreased rapidly, thenceforth falling slowly from 1.0 torr to atmospheric pressure. The following values for rise time (specimen E31) were typical :

Pressure	2×10^{-6} torr	rise time	32 ms
	1×10^{-2} torr		22 ms
	1×10^{-1} torr		8 ms
	1.0 torr		4 ms
	760 torr		2 ms

The temperature rise at atmospheric pressure was approximately 1/15 of that at 2×10^{-6} torr.

These observations clearly demonstrate the usual compromise between the sensitivity and speed of response of infrared detectors. Insofar as this project is concerned, it may be safely assumed that for pressures of less than 5×10^{-5} torr, radiation cooling is the only surface loss mechanism.

11.4.6 Dependence of rise time on film temperature

Thermal rise time was measured as a function of applied current, i.e. temperature rise. The rise time was found to be constant over the range of currents applied during the measurements, corresponding to a maximum temperature rise of $15^{o}C$ above the background temperature.

11.4.7 Gold films

Reasonable agreement was found between the measured rise times for large area gold films (represented by the 12.5 mm long specimens) and the computed values based on bulk parameters. Good agreement was achieved when the film density was taken to be 12.0 $g.cm^{-3}$ - the value estimated from the observed quartz crystal frequency shift during deposition. As expected, the rise time approached the theoretical time constant for radiation loss only, in agreement with the supposition that the specimen dimensions are much larger than the thermal spread constant.

The measured rise times for 2.5 mm specimens were in poor agreement with the computed values, including computations corrected for film density. The measured values were higher; hence we may suppose that the difference is due to reduced thermal conduction to the film mount. Computations indicate that a thermal conductivity of 1.0 to 1.5 $W(cm.^{o}C)^{-1}$, i.e., one-third to one-half the bulk value, yields the correct rise time. This result is in agreement with thermal spread measurements (see Section 11.5.3).

The time dependent average temperature rise in vacuo for a 2.5 mm specimen is illustrated in figure 40. The various computations discussed above are shown in the figure. The influence of thermal conduction loss is clearly indicated.

A summary of rise time measurements is given in Table 5. Three values of rise time are listed: the calculated rise time, τ_c, the rise time for radiation loss only, τ_r, and the measured rise time, τ_m. The computed values shown in the table are corrected for estimated metal film density, but are not corrected for thermal conductivity.

TABLE 5

SUMMARY OF THERMAL RISE TIME MEASUREMENTS

Specimen number	Absorber type	Estimated density ($g.cm^{-3}$)	τ_r (ms)	τ_c (ms)	τ_m (ms)
G9	gold	12.0	39	35	34
G21	gold	12.0	39	15	22
A13	nichrome	6.4	45	44	36
A15	nichrome	6.5	43	39	32
C23	nickel	6.5	74	70	63
C24	nickel	6.0	47	45	37
E30	nickel	4.0	37	30	31
E31	nickel	4.5	39	31	32

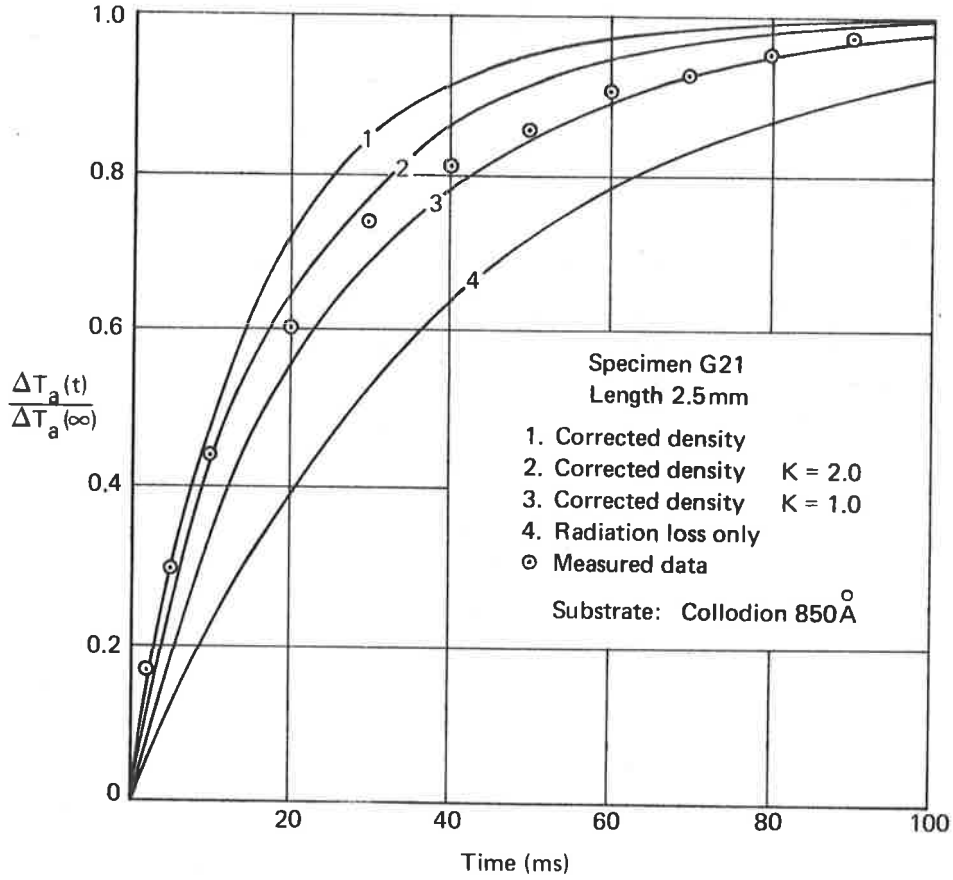

Figure 40. Thermal rise time for a gold absorber film

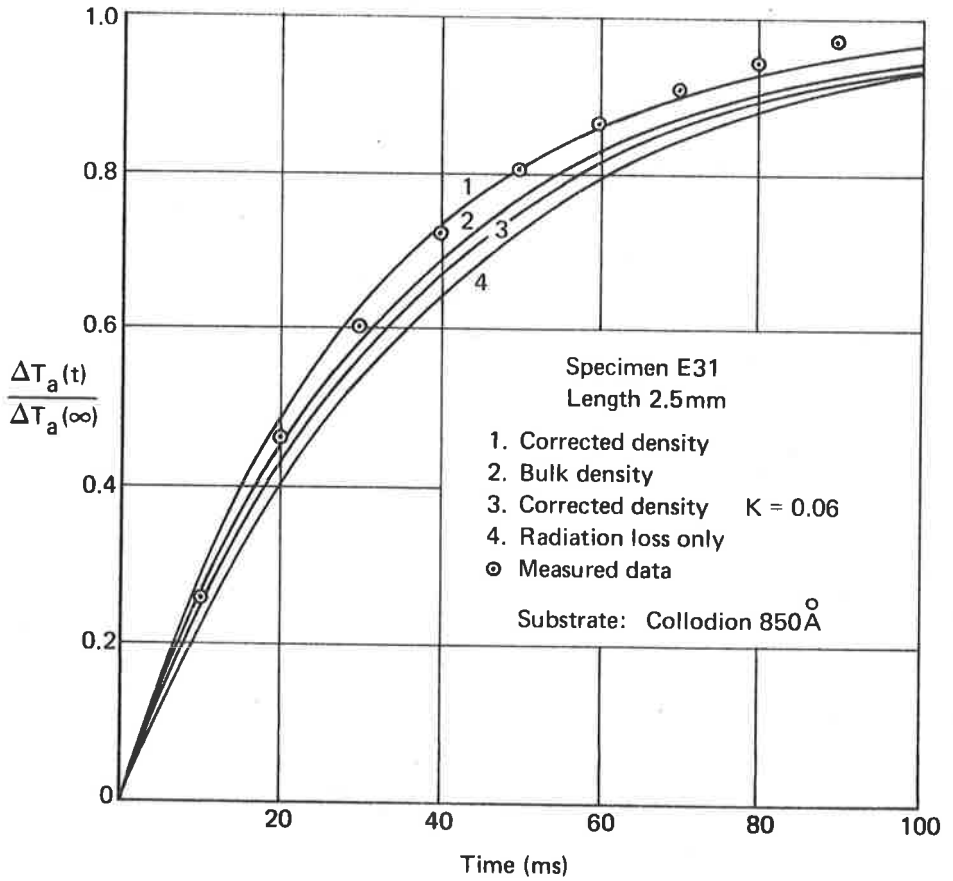

Figure 41. Thermal rise time for a nickel absorber film

11.4.8 Nichrome films

Measured rise times for two specimens are listed in Table 5. The measured rise times are seen to be 7 to 8 ms lower than the calculated values, which are based on the bulk value for thermal conductivity. It is worthy of note that the thickness of both specimen films is larger than films of the same sheet resistance prepared at an earlier stage of the research program (see Section 8), probably because of deposition in a poor vacuum. The composition and structure of these films is therefore uncertain.

11.4.9 Nickel films

Thermal rise time data for four nickel specimens are listed in Table 5. Reasonable agreement was again found between the measured rise times and the computed values, assuming a corrected film density derived from quartz crystal frequency shift data during deposition.

The time dependent average temperature rise in vacuo for a 2.5 mm long nickel film is illustrated in figure 41. The influence of the corrected density is clearly shown. It should be noted that this correction implies a decrease in thermal capacitance, a quantity which also includes the specific heat of the film. We cannot say with certainty that the decreased thermal capacitance is due to density alone, only that the evidence points to this conclusion; hence the specific heat is presumably not much different to the bulk value. Partial oxidation of the nickel film would not significantly alter the results because the density and specific heat of NiO are not greatly different

to nickel metal.

It will be noted in Table 5 that the computed rise times for the 12.5 mm specimens are larger than the measured values, whereas the predictions for the 2.5 mm specimens are smaller. However, when a correction is applied for thermal conductivity (deduced from thermal spread measurements), as shown in figure 41 for specimen E31, the computed rise time is increased. The corrected value for specimen E31 is 36 ms. This general trend is evident throughout the measured results, and is probably a consequence of the selection of 2.25 $J.cm^{-3}.^{o}C^{-1}$ for the product of density and specific heat of the collodion substrate. Examination of the published bulk data for cellulose nitrate shows that this product can vary from 1.7 to 2.7. A value of 1.9 to 2.0 is required to achieve agreement between the computed and measured rise times, for the specimens listed in Table 5.

In the light of the above discussion, it is significant that agreement between theory and experiment can be realised by applying corrections to the thermal capacitance and thermal conductivity of the metal absorber film alone. This implies that the thermal properties of the 850Å thick polymer substrate are not significantly reduced from the bulk values, a result borne out in earlier work by one of the author's associates (ref.2).

11.5 Measurement of thermal spread

Measurements were made of the thermal spread in gold, nickel and nichrome absorber films. The thermal spread constant, χ, was determined for each specimen and estimates were made of the thermal

conductivity. The measurement technique and experimental results are described below.

11.5.1 Thermal spread apparatus

Thermal spread was measured with a high-resolution scanning radiometer. This instrument was constructed in the author's laboratory (ref.59), and has been used in earlier research on thermal spread in thin membranes (ref.2). The infrared radiometer is comprised of an f/1, 4X magnification, monocentric optical system, a thermocouple detector and an 11.5 Hz mechanical chopper assembly. The specimen is mounted in a precision sample holder, which remains stationary during operation, and the entire radiometer assembly is made to move, by means of a small motor drive unit, in the horizontal direction. Optical focus and scan position can be accurately located by means of micrometer drums. The maximum scan amplitude is 3 mm. The scan rate is 165 $\mu m.min^{-1}$ and the optical resolution, measured in the specimen plane, is approximately 0.05 mm along the direction of the scan motion.

In the present experiments the detector output was connected to a P.A.R. Model HR-8 lock-in amplifier, with the amplifier phase-locked on to the chopper reference, and the output was displayed on a Goerz Minigor Type RE501 potentiometric chart recorder.

The entire radiometer assembly was mounted in a 30 cm (12 in) vacuum system and evacuated to a pressure of less than 5×10^{-5} torr. The specimen was heated by applying a d.c. voltage from a constant current power supply, and a

radiometer scan was then executed along the desired absorber axis. The resultant chart record represents a plot of steady state temperature rise versus scan distance.

11.5.2 Theoretical predictions

The steady state temperature rise was computed for each specimen from equations (13) and (17). Bulk thermal parameters listed in Table 1 were used in initial computations. The results were compared with radiometer records and the computations repeated to seek the value of the thermal spread constant, χ, required to effect agreement with experiment.

The analysis of the thermal spread characteristics of absorber films is considerably simplified if the length of the specimen is greater than 10χ. The thermal spread constant can then be determined from equation (19). This equation can be expressed in the form

$$\ell n(1-\Delta T/\Delta T_o) = -x/\chi \qquad (125)$$

Thus χ can be determined directly from the slope of the log plot of the radiometer records. The thermal conductivity, K, can then be estimated from equation (50). An examination of the radiometer chart record will immediately establish the validity of this technique for any given specimen.

When the above procedure cannot be applied, e.g. when the length of the specimen is less than 10χ and hence the mid-point temperature does not rise to the maximum value, ΔT_o, then the estimation of χ becomes more difficult. The simplest approach is to plot a family of curves, each curve corresponding to a given value of χ, then to seek the best fit with the measured data.

Examination of the radiometer scan records revealed that the

edge of the absorber film, where it contacted the epoxy mount, was not clearly defined, the temperature rise typically falling to zero at approximately 0.1 mm beyond the boundary. This effect may be attributed to :

(a) the resolution of the optical system (0.05 mm half width),

(b) an imperfect mechanical boundary, determined by the coarseness of the machining process, and

(c) an imperfect heat sink (see Section 11.4.4).

Poor boundary definition will doubtlessly affect the accuracy of the thermal spread computations. However, considerably greater sophistication in experimental technique would be required to achieve substantial improvement in accuracy.

11.5.3 Gold films

Radiometer scans were carried out for several 2.5 mm long absorber specimens. The estimated thermal spread characteristics for one specimen (G21) are shown in Table 6. In this table χ_c is the computed thermal spread constant, based on bulk parameters, and χ_m is the value determined by measurement.

Because of the high thermal conductivity of gold, the temperature rise at the centre of the 2.5 mm long specimens will not attain the maximum value given by equation (20); hence the thermal spread constant was deduced by seeking the best fit with computed temperature rise curves, as discussed in the preceding subsection. The results for specimen G21 are shown in figure 42. Agreement with theory is achieved for a thermal conductivity of approximately 1.0 $W(cm.^{o}C)^{-1}$, i.e. one-third of the bulk conductivity. This result is in accord with thermal rise time measurements. Published data for silver films (ref. 60) would

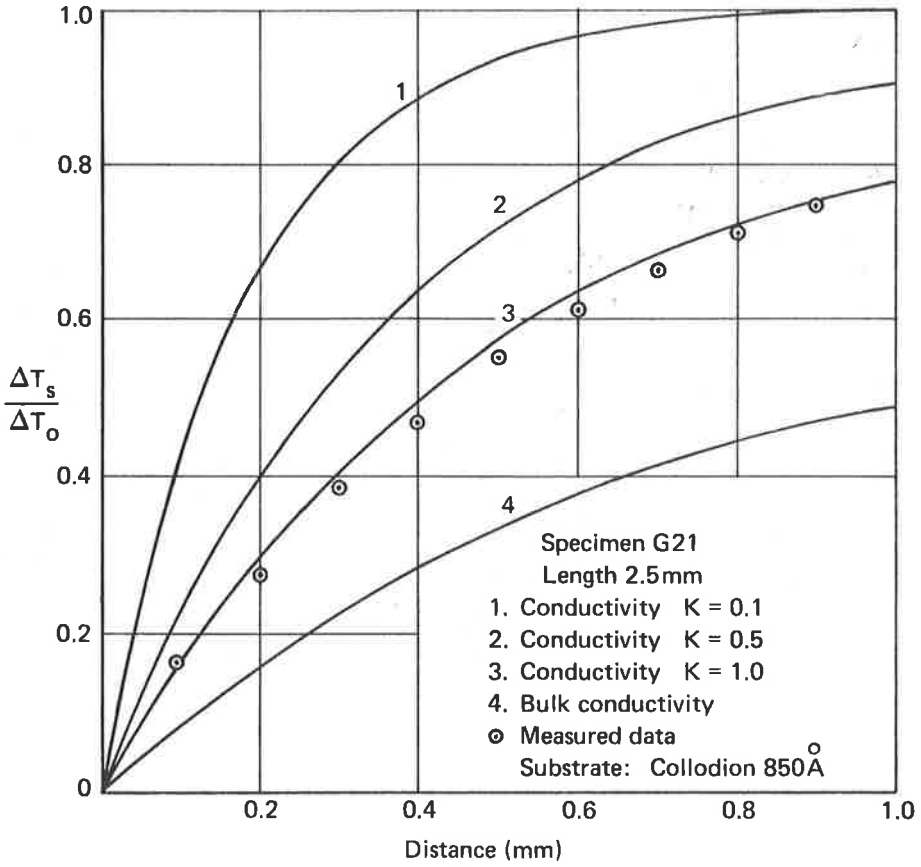

Figure 42. Steady state temperature rise. Gold absorber film

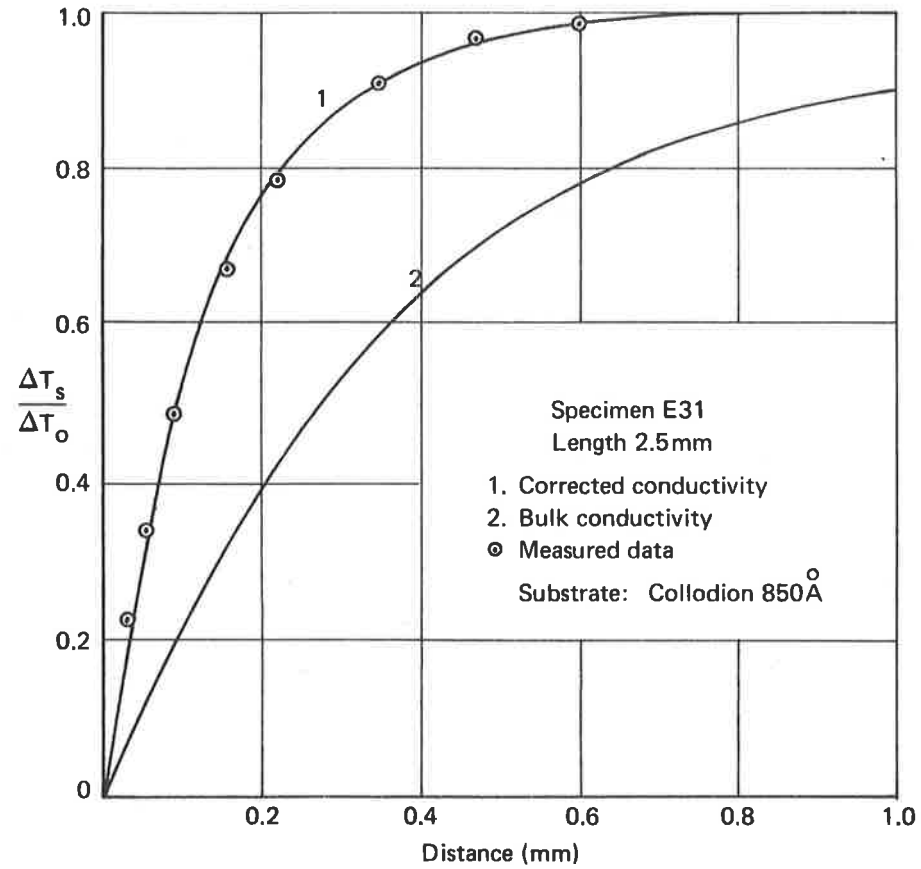

Figure 43. Steady state temperature rise. Nickel absorber film

suggest that the above value may be too high.

Special 10 mm long specimens were prepared in an unsuccessful attempt to determine a more accurate value of the thermal spread constant. The radiometer scan for all specimens showed an anomalous peak near the ends of the absorber film. This effect has been observed only for long gold films.

No predictable relationship has been found between the thermal conductivity and electrical conductivity of gold absorber specimens. This observation is not surprising, in view of the electrical properties of these films (Section 7.2).

TABLE 6

SUMMARY OF THERMAL SPREAD MEASUREMENTS

Specimen number	Absorber type	χ_c (μm)	χ_m (μm)	$W(cm.^{\circ}K)^{-1}$
G21	gold	949	550	1.0
A15	nichrome	207	102	0.02
E30	nickel	363	99	0.03
E31	nickel	400	143	0.06

11.5.4 Nichrome films

Thermal spread measurements were made for only one absorber specimen . The results are given in Table 6. The thermal spread constant was calculated from the slope of the log plot, as discussed in Section 11.5.2. Note that the thermal conductivity of the specimen is approximately one-fifth of the bulk value.

11.5.5 Nickel films

Radiometer scans were carried out for several nickel absorber specimens. Two specimens, E30 and E31, were studied in depth, with the results shown in Table 6. The thermal spread in nickel

absorber films was observed to be much smaller than predictions based on bulk thermal conductivity. This permitted the determination of the spread constant from the slope of the log plot (equation (125)). The thermal conductivity, estimated from equation (50), was found to be approximately one-tenth of the bulk value.

Figure 43 shows the computed steady state temperature rise for specimen E31. Also shown is experimental data derived from radiometer records. The computed temperature rise is plotted for both the bulk and thin film values of thermal conductivity, emphasising the decreased thermal spread in the thin film.

It is important to note that the lateral thermal conductance, Kt, of the nickel absorber is only 4 to 10 times larger than that of the 850Å thick collodion substrate. This is in marked contrast to the gold absorbers, where the substrate contribution is small. In reaching this conclusion, we have assumed that the thermal conductivity of the collodion film is the bulk value listed in Table 1. In fact earlier research carried out in the author's laboratory (ref. 2) indicate that the thermal conductivity is approximately half the value given in the table. Recent measurements suggest that the thermal conductivity may be slightly higher.

A definite relationship has been established between the thermal and electrical conductivities of nickel absorber films. Whilst we have not discussed the possibility of such a relationship in earlier sections of the thesis, the free electron theory of metals predicts that conduction electrons are mainly responsible for the transfer of heat in metals. In view of the success of the infrared optical theory for nickel absorber films, as represented by the

results shown in figure 30, we might suspect therefore that the thermal conductivity is also directly related to the measured electrical properties.

The Wiedemann-Franz law states that for a given temperature the ratio of thermal to electrical conductivity of a metal is a constant. This constant has been verified by experiment for bulk metals at room temperature. We would not, however, expect to find a constant proportionality between the thermal conductivity, K, and electrical conductivity, σ, of the nickel absorber films prepared in this study. We have seen that the ratio of the bulk to thin film conductivity, σ_o/σ for films of maximum absorption is at least 20. The magnitude of this ratio is a measure of the degree of film oxidation. Increased oxidation can lead to semi-conducting films, for which σ_o/σ is very large (and the infrared absorption small). On the other hand, the ratio of the bulk to thin film thermal conductivity, K_o/K, will have an upper bound set by the phonon contribution to the total conductivity. Thus we should seek a relationship of the form :

$$\frac{K_o}{K} = \xi\frac{\sigma_o}{\sigma} \qquad (126)$$

where ξ is not a constant, but decreases as the film departs from metallic behaviour.

Thermal spread measurements have indicated that for nickel absorber films of maximum absorptance

$$\xi \simeq 0.5$$

We would expect this value to increase for films of higher purity.

The above result is of particular significance, for it implies that the measured electrical conductivity of an absorber film is

also a measure of the thermal spread characteristics of the film. It would appear, however, that a predictable relationship is characteristic of finely crystalline films such as nickel and nichrome, and presumably other higher melting point metals. A definite relationship has not been found for gold absorber films.

11.6 Measurement of temperature rise

True temperature rise was determined from thermal spread measurements by calibrating the Thermal Spread Apparatus against a small blackbody cavity. The estimation of average temperature rise from rise time experiments was found to be inaccurate because of the uncertainty of the measured values of temperature coefficient of resistance (see Section 11.3).

Temperature rises extracted from the radiometer calibration data are apparent blackbody temperatures. To find the true temperature of the absorber film, we must solve a radiation exchange equation similar to that given in Section 6.3.1, noting that in this case the temperatures of specimen and blackbody are not the same. If the radiometer output is referenced to the ambient background - a zero output will be observed if the temperature of the blackened chopper blade is equal to background temperature - then a simple reduction gives :

$$\Delta T = \Delta T_{bb}/\varepsilon \qquad (127)$$

where ΔT_{bb} is the apparent blackbody temperature rise.

Several sources of error arise when we attempt to compare the computed temperature rise with the measured values. The following factors must be taken into consideration :-

(a) The use of both a linear radiation loss law and a constant background temperature in temperature rise computations (see Sections 11.4.2 and 11.4.3).

(b) The effect of an imperfect heat sink: the actual temperature will be slightly higher than the computed value (Section 11.4.4).

(c) The area of the absorber may be effectively smaller than that assumed in computations because of shadowing during deposition.

(d) Uncertainty in the blackbody calibration due to a temperature gradient along the electrically heated conical cavity.

(e) Transverse radiometer scans across gold absorber specimens indicate large apparent variations in emissivity. This cannot be accounted for by thinning at the edges of the films, and is possibly caused by structural changes induced by electrical current aging. Except at the edges, these variations have not been observed for nickel absorber specimens.

(f) We have assumed Lambertian radiation characteristics. This is a good approximation for many applications, but may lead to errors in the present computations.

It is clearly difficult to account fully for all of the above factors. To do so would require a far greater degree of sophistication in both theory and measurement. Factor (f) is, however, quite fundamental, and is worthy of further consideration.

The values of emissivity determined with the Emissivity Test Apparatus (Section 6.3) are effectively normal emissivities. These values are valid for the determination of true temperature rise from radiometer scans. However, the hemispherical emissivity should be used in the computation of thermal surface conductance (see Sections 2.1.1 and 3.1). We can calculate the hemispherical emissivity for a metal film absorber by integration of equation (74). This calculation gives a value of 1.18 for the ratio of normal to hemispherical emissivity, $\varepsilon_n/\varepsilon_h$, for films of optimum thickness and absorption ($\varepsilon_n = 0.5$). For thicker films the ratio

is larger; for thinner films the ratio is lower, and can be less than unity. We should bear in mind that the polymer substrate has not been taken into consideration.

Evidently the normal emissivity may be used with reasonable accuracy for the computation of small temperature rises. However, a significant error is likely for large temperature rises. The results of temperature rise measurements for four specimens are given in Table 7. The measured temperatures, ΔT_m, are mid-point values. A high power density has been applied in this experiment to accentuate the various errors discussed above. The computed temperature rise, ΔT_c, was determined from equation (18), and is corrected for the estimated hemispherical emissivity of the metal film.

TABLE 7

TEMPERATURE RISE MEASUREMENTS

Specimen number	Absorber type	Power density ($mW.cm^{-2}$)	ΔT_m (^oC)	ΔT_c (^oC)
G21	gold	13.4	29.5	24.2
A15	nichrome	12.7	30.0	26.3
E30	nickel	10.2	24.1	21.3
E31	nickel	7.4	18.1	15.9

In each case the measured temperature rise is higher than the computed value. Nevertheless, surprisingly good agreement is obtained, in view of the errors inherent in the present technique. It is of interest to note that the temperature rise was found to obey the fourth power radiation loss law, when measured as a function of applied heating current. This observation represents qualitative validation of the Joule heating technique for the measurement of thermal properties.

11.7 Summary of thermal properties

We have seen that both the thermal capacitance and lateral thermal

conductance of metal absorber films are significantly smaller than that of the bulk metal. The decreased thermal capacitance appears to be mainly attributable to a reduced film density, whereas the lateral conductance is explained by a lower thermal conductivity. These factors result in faster response times and higher temperature rises for absorbers of given size, thickness and optical characteristics, when operated in vacuo.

Analysis of the thermal properties of nickel absorber films raises an interesting and pertinent technical question. If, as discussed in Section 9.3, we prepare nickel films of higher purity, our absorber specimens will have a higher density, increased electrical and thermal conductivity, and a higher temperature coefficient of resistance. The main improvements in absorber characteristics will be greater stability and a decrease in film thickness; but the latter is unlikely to be much more than 25Å for films of optimum absorption. However, we have found that absorbers of sheet resistance 100 to 150 ohm per square, prepared by the present experimental techniques, have an acceptable electrical and optical stability, and will probably be capable of a larger temperature rise than specimens of higher purity. High purity may therefore be undesirable in some applications.

Finally we note that the thermal theory of infrared absorber films presented in Section 2 of the thesis is considered to be adequate for most practical purposes. We have found that the accuracy of prediction is largely determined by the accuracy with which we can specify the various physical parameters, e.g., emissivity, thermal capacitance, thermal conductivity, physical dimensions, etc. It is significant that the general conclusions drawn from the theoretical analysis of absorber elements in Section 2.7 are still valid. The quantitative

results have proved to be a useful guide in absorber research; and conversely, the results of the research studies may now be used to obtain more accurate predictions. Thus the calculated temperature rise given in Table 2 (page 26) for a 0.1 cm long nickel film would be realised in practice for a film of approximately one third of that length, due to reduced thermal conductivity. The initial prediction was nevertheless sufficiently accurate for comparative purposes.

12. CONCLUSIONS

In this thesis we have presented the results of a research study on the physics of absorption of infrared radiation in thin metallic films vacuum deposited on to polymer membrane substrates. The aim of this study was to investigate the thermal and infrared optical properties of thin metallic films, and to establish the relationship between these properties and the electrical conductivity, physical dimensions and structure, and conditions of preparation. Our ultimate intention was to deduce the desired physical parameters and optimum method of preparation of an efficient metallic absorber for use in thermal radiation detectors.

It is believed that in general terms the aims of the project have been achieved.

The thermal theory of infrared absorbers presented in Section 2 of the thesis has been used successfully to predict the temperature rise and thermal rise time of absorber films operated in vacuo. The accuracy of prediction is mainly dependent on the accuracy with which we can specify properties of materials in thin films, e.g., thermal capacitance, thermal conductivity, emissivity and thin film dimensions, especially thickness. The importance of smallest possible film thickness was confirmed by experiment. However, there is a thickness limit for individual metals, imposed by the requirements for infrared absorptance. We have found that in order to achieve maximum

absorptance in the thinnest possible film, we need to use higher melting point metals. In addition, it is clearly desirable that the polymer substrate be as thin as practicable. Indeed the substrate is responsible for the major contribution to the thermal rise time.

A predictable relationship has been found between the thermal conductivity and electrical conductivity of nickel and nichrome films. A similar relationship has not been observed for gold absorber films, and it is believed that this latter result will, in general, be characteristic of coarsely crystalline, lower melting point metals.

The optical theory of Section 3 predicts a maximum absorptance (emissivity) of 0.5 when the sheet resistance of the metal film is 189 ohm per square. The maximum value of absorptance was confirmed by experiment for all metals studied. However, whereas there was good experimental agreement with the predicted optical-electrical relationship for nickel and nichrome, there was no systematic relationship for gold. On the other hand, the absorptance of gold films is strongly dependent on thickness. Again we conclude that this is characteristic of coarsely crystalline metals.

A study of film structure described in Section 10 confirms our predictions, based on established nucleation and growth phenomena (Section 4), of both the characteristic structure of a given metal and the influence of structure on film properties. In particular, metals having a melting point higher than about $1350^{o}K$ will form finely crystalline deposits on ambient temperature amorphous substrates. These films, provided they are chemically inert, will have more predictable thermal and optical properties than films of lower melting point metals and will be thinner for the same value of absorptance.

Deposition parameters have a marked influence on the characteristics of metallic infrared absorbers. In general, the best absorbers are prepared at a high deposition rate in a pressure of 10^{-6} torr or better. This observation

applies especially to metals such as nickel, which are prone to oxidation.

The author has concluded that the most suitable thin film absorbers are prepared from high melting point metals. The choice of metals is, unfortunately, limited (see Section 4.4); furthermore intrinsic stress may be high in thin films of these metals, imposing a serious technical difficulty when deposited on to fragile substrates. The nickel films prepared in this research project meet many of the requirements specified for the optimum infrared absorber. It is believed that platinum is the most promising metal for further investigation.

13. ACKNOWLEDGEMENTS

The author wishes to express his appreciation to his Internal Tutor, Dr S.G. Tomlin, and External Tutor, Mr N.K. Jones, for their assistance in the preparation of this thesis. Mr Jones who, as Principal Officer of the author's Research Group, was responsible for the overall supervision of this task, has offered much valuable advice from his wide experience in the field of infrared detection.

The author is indebted to Mr M.R. Meharry for many helpful discussions and constructive criticisms, and particularly for assistance with the precision alignment of optical instrumentation.

Mr J.R. Waller has rendered invaluable technical assistance during the project. He is responsible for all specimen preparations carried out in the ancillary vacuum coating unit, and must take the credit for certain specialised experiments, notably the measurement of temperature coefficient of resistance, the preparation of nickel specimens for stress analysis, and the investigation of the electrical properties of gold films.

Routine preparation of polymer membrane substrates was carried out by Mrs J.M. Jansen.

Finally, the author acknowledges the assistance afforded by other members of the technical staff, and supporting effort provided by the Electronic Section, Drawing Office and Mechanical Workshop.

REFERENCES

1. Carslaw H.S. and Jaeger J.C. — "Conduction of Heat in Solids" (Oxford, Oxford University Press, Second Edition, 1959)

2. Meharry, M.R. — Internal W.R.E. Report, 1964

3. Smith, R.A., Jones F.E. and Chasmar R.P. — "The Detection and Measurement of Infra-red Radiation" (Oxford, Clarendon Press, 1957)

4. Wolfe, W.L. — "Handbook of Military Infrared Technology" (Washington, U.S. Government Printing Office, 1965), Chapter 1

5. Bleaney, B.I. and Bleaney, B. — "Electricity and Magnetism" (Oxford, Clarendon Press, 1959)

6. Slater, J.C. — "Quantum Theory of Molecules and Solids Vol. 3". Insulators, Semiconductors and Metals. (New York, McGraw-Hill, 1967)

7. Hadni, A. — "Essentials of Modern Physics Applied to the Study of the Infrared" (Oxford, Pergamon, 1967)

8. Heavens, O.S. — "Optical Properties of Thin Solid Films" (London, Butterworth, 1955)

9. Vasicek, A. — "Optics of Thin Films" (Amsterdam, North-Holland, 1960)

10. Hadley, L.N. and Dennison, D.M. — "Reflection and Transmission Interference Filters" Jnl. Opt. Soc. Am., Vol. 37, No. 6, p.451, June 1947

11. Hilsum, C. — "Infrared Absorption of Thin Metal Films" Jnl. Opt. Soc. Am., Vol. 44, No. 3, p.188, March 1954

12. Fuchs, K. — "The Conductivity of Thin Metallic Films According to the Electron Theory of Metals" Proc. Cambridge Phil. Soc., Vol. 13, p.100, 1938

13. Sondhiemer, E.H. — "The Mean Free Path of Electrons in Metals" Advances in Physics, Vol. 1, No. 1, p.1, January 1952

14. Chopra, K.L. — "Thin Film Phenomena" (N.Y., McGraw-Hill, 1969)

15. Soffer, S. — "Evaluations of Expressions for the Electrical Resistivity in Thin Plane Samples", Jnl. Appl. Phys., Vol. 36, p.3947, 1965

16. Rhodin, T.N., and Walton, D. "The Use of Thin Films in Physical Investigations", J.C. Anderson, Ed. (N.Y., Academic Press, 1966) p.187

17. Hirth, J.P. and Pound, G.M. "Heterogeneous Nucleation on Substrates" (In "Condensation and Evaporation", Oxford, Pergamon, 1963)

18. Lewis, B. and Campbell, D.S. "Nucleation and Initial Growth Behaviour of Thin Film Deposits", Jnl. Vacuum Sci. and Tech., Vol. 4, No. 5, p.209, 1967.

19. Lewis, B. "Bond Energy Formulations of Heterogeneous Nucleation Theory", Thin Solid Films, Vol. 1, p.85, 1967

20. Neugebauer, C.A. "Condensation, Nucleation and Growth of Thin Films", in "Handbook of Thin Film Technology", L.I. Maissel and R. Glang (Eds), (N.Y., McGraw-Hill, 1970)

21. Pashley, D.W. "The Nucleation, Growth, Structure and Epitaxy of Thin Surface Films", Adv. in Physics, Vol. 14, No. 55, p.327, July 1965

22. Pashley, D.W., et al "The Growth and Structure of Gold and Silver Deposits Formed by Evaporation Inside an Electron Microscope", Phil. Mag., Vol. 10, No. 103, p.127, July 1964

23. Chopra, K.L. & Randlett, M.R. "Influence of Deposition Parameters of the Coalescence Stage of Growth of Metal Films", Jnl. Appl. Phys., Vol. 39, No. 3, p.1874, February 1968

24. Komnik, Yu. F. "Characteristic Condensation Temperatures of Thin Films", Soviet Phys - Solid State, Vol. 6, No. 10, p.2309, April 1965

25. Kosevich, V.M. et al "The Form of Metallic Condensate Particles in the Initial Stages of Growth", Soviet Phys - Solid State, Vol. 6, No. 11, p.2591 May 1965

26. Levinstein, H. "Growth and Structure of Thin Metallic Film Jnl. Appl. Phys., Vol. 20, p.306, April 1949

27. Sennett, R.S. & Scott, G.D. "The Structure of Evaporated Metal Films and Their Optical Properties", Jnl. Opt. Soc. Am., Vol. 40, No. 4, p.203, April 1950

28. Chopra, K.L. et al "Electrical Resistivity of Thin Single Crystal Gold Films", Jnl. Appl. Phys.,

Vol. 34, No. 6, p.1699, June 1963

29. Belser, R.B. "Electrical Resistance of Thin Metal Films Before and After Artificial Aging by Heating", Jnl. Appl. Phys., Vol. 28, No. 1, p.109, January 1957

30. Chopra, K.L. "Influence of Electric Field on the Growth of Thin Metal Films", Jnl. Appl. Phys., Vol. 37, No. 6, p.2249, May 1966

31. Herman, D.S. and Rhodin, T.N. "Electrical Conduction Between Metallic Microparticles" Jnl. Appl. Phys., Vol. 37, No. 4, p.1594, March 1966

32. Hill, R.M. "Electrical Conduction in Discontinuous Metal Films" Contemp. Phys., Vol. 10, No. 3, p.221, 1969

33. Fleet, S.G. Mullard Res. Lab. Rep., 466, 1963

34. Neugebauer, C.A. "Structural Aspects of the Magnetization in Ultrathin Ferromagnetic Films" Z. Angew Phys., Vol. 14, No. 4, p.182, April 1962.

35. Glang, R. "Vacuum Evaporation" Ch. 1 of Handbook of Thin Film Technology (N.Y., McGraw-Hill, 1970)

36. Holland, L. "Vacuum Deposition of Thin Films" (London, Chapman and Hall, 1956)

37. Unvala, B.A. and Grigson, C.W.B. "Precision Electron Bombardment Furnace for High Purity Evaporation of Silicon" Proc. Fifth Electron Beam Symposium, Boston, Mass., P.168, 1963

38. Gillespie, F.C. "Vacuum Evaporation Experiences with a Ring-type Electron Beam Gun" Vacuum, Vol. 22, No. 7, p.255, July 1972

39. Hill, P.J. W.R.E. Technical Report (unpublished)

40. Tolansky, S. "Multiple-Beam Interferometry of Surface Films" (London, Oxford University Press, 1948)

41. Schartz, B. and Schwartz, N. (Editors) "Optimization of the Tolansky Technique For Thin Film Thickness Measurement", in Measurement Techniques for Thin Films (N.Y., Electrochemical Society, 1967)

42. Bennett, H.E., Bennett, J.M. and Ashley, E.J. "Infrared Reflectance of Evaporated Aluminium Films" Jnl. Optical Soc. Am., Vol. 52, No. 11, p.1245, November 1962

43. Liddiard, K.C. "Research Studies on Metal Film Infrared Bolometer Detectors" W.R.E. Technical Note, in preparation

44. Alderson, R.H. and Ashworth, F. "Vacuum-Deposited Films of Nickel Chromium Alloy" Br. Jnl. Appl. Phys., Vol. 8, p.208, May 1957

45. Degenhart, H.J. and Pratt, I.H. "Thickness and Composition of Nickel-Chromium Films" Trans. 10th Nat. Vac. Symp., p.480 (N.Y., MacMillan, 1963)

46. Siddall, G. and Probyn, B.A. "Vacuum-Deposited Metal Film Resistors" Br.Jnl. Appl. Phys., Vol. 12, p.668, December, 1961

47. Wied, O.J. and Berner, W.E. "The Dependence of the Electrical Characteristics of Ni-Cr Thin Films on Evaporation Parameters" Trans. Third Int. Vac. Congress, Vol. 2, Pt. 1, p.59, 1965

48. Caruso, S.V. and Dettaye, R.F. "Properties of Vacuum-Deposited Thin-Film Nichrome Resistors" Proc. Second NASA Microelectronics Symp., p.101, 1966.

49. Ziman, J.M. "Electrons and Phonons" (Oxford, Clarendon Press, 1960)

50. Neugebauer, C.A. and Webb, M.B. "Electrical Conduction Mechanism in Ultrathin, Evaporated Metal Films" Jnl. Appl. Phys., Vol. 33, No. 1, p.74, January 1962

51. Hoffman, R.W. "Mechanical Properties of Thin Condensed Films" in Physics of Thin Films, Vol. 3, (N.Y., Academic, 1963)

52. Campbell, D.S. "Mechanical Properties of Thin Films" Ref. 35, Ch. 12

53. Klokholm, E. and Berry, B.S. "Intrinsic Stress in Evaporated Metal Films" Jnl. Electrochem. Soc., Vol. 115, No. 8, p.823, August 1968

54. Kay, D.H. (Editor) "Techniques for Electron Microscopy" (Oxford, Blackwell, 2nd Ed., 1965)

55. Morris, J.E. "Resistance Changes of Discontinuous Gold Films in Air", Thin Solid Films, Vol. 5, p.339, 1970

56. Bricknell, R.W. et al — "The Structure of Vacuum Condensed Ni-Cr Films" Microelectronics and Rel., Vol. 3, p.61, 1964.

57. Neugebauer, C.A. — "Saturation Magnetization of Nickel Films of Thickness Less Than 100Å" Phys. Rev., Vol. 116, No. 6, p.1441, 15 December, 1959.

58. Reale, C. — "Electrical Properties of Vacuum Deposited Nickel Films", Phys. Letters, Vol. 24A, No. 3, p.145, 30 January, 1967.

59. Meharry, M.R. & Brown, D.H. — "A Scanning Radiometer for Measuring Thermal Spread in Thin Membranes", W.R.E. Internal Technical Report.

60. Abrosimov, V.M. et al — "Investigation of the Thermal Conductivity of Thin Metallic Films", Soviet Phys. - Solid State, Vol. 11, No. 2, p.427, August, 1969.

TABLE OF SYMBOLS

A	area	cm^2
	interferometer absorption	-
C	thermal capacitance	$J.^oK^{-1}$
	visual contrast	-
E	electric field	$N.C^{-1}$
	energy	J or eV
F	Fabry coefficient of fineness	-
G	thermal surface conductance	$W.^oK^{-1}$
H	irradiance	$W.cm^{-2}$
I	fringe intensity	$W.sr^{-1}$
	electric current	A
K	thermal conductivity	$W.cm^{-1}.^oK^{-1}$
M	molar mass	$g.mol^{-1}$
N	radiance	$W.cm^{-2}.sr^{-1}$
	evaporant impingement rate	$cm^{-2}.s^{-1}$
	gas impingement rate	$cm^{-2}.s^{-1}$
	free electron concentration	cm^{-3}
	adsorption site surface density	cm^{-2}
	adatom surface density	cm^{-2}
P	radiant power	W
R	electrical resistance	Ω
	distance in space	cm
	deposition rate	$cm.s^{-1}$
	deposition rate per unit thickness	$cm^{-2}.s^{-1}$
	interferometer reflection	-
S	stress	Pa
T	temperature	^oK or ^oC
	interferometer transmission	-

V	potential	V
W	radiant emittance	$W.cm^{-2}$
	fringe half width	Å
Y	Young's Modulus	Pa
Δ	as prefix, incremental values of above physical quantities	
a	absorber radius	cm
	fringe displacement	Å
b	fringe separation	Å
c	specific heat	$J.g^{-1}.{}^{o}K^{-1}$
	wave velocity in free space	universal constant
d	distance or thickness	cm
	wedge spacing	cm
e	electronic charge	universal constant
f	frequency	Hz
g	collision frequency	s^{-1}
h	Plank's constant	universal constant
	height	cm
k	Boltzmann constant	universal constant
	absorption index	-
ℓ	length	cm
m	electronic mass	universal constant
n	refractive index	-
	fringe order	-
p	pressure	torr
	specularity parameter	-
r	radius	cm

t	time	s
	thickness	Å or μm
v	volume	cm^3
	electron velocity	$cm.s^{-1}$
α	infrared absorptance	-
	temperature coefficient of resistance	$^oC^{-1}$
	coefficient of linear expansion	$^oC^{-1}$
ε	emissivity	-
	permittivity	-
θ	angle	degree
κ	diffusivity	-
	ratio of thickness to mean free path	-
λ	wavelength	Å or μm
	mean free path of electrons	Å
μ	permeability	-
	reciprocal of thermal spread constant	μm^{-1}
ν	vibrational frequency	s^{-1}
ξ	conductivity constant	-
ρ	density	$g.cm^{-3}$
	infrared reflectance	-
σ	Stefan-Boltzmann constant	universal constant
	electrical conductivity	$\Omega^{-1}.cm^{-1}$
τ	rise time, dwell time, time constant, or characteristic lifetime	s
	infrared transmittance	-
χ	thermal spread constant	μm
ω	angular frequency	$rad.s^{-1}$

Notes : (a) Symbols conform to British Standards, except in radiometry where the symbols are based on widely accepted notation. This has caused duplication in some instances, a situation which is aggravated by the several disciplines demanded in the project. Care has been taken to avoid duplication in the same sections of the thesis.

(b) Wide use is made of subscripting to distinguish between various values of the same physical quantity, and to avoid confusion between different physical quantities.

(c) The Greek symbol Δ is used as a prefix to denote incremental values of the physical quantities in the Symbol Table.

(d) SI units are used throughout, except that length is expressed in cm in accord with common practice in infrared technology. Consequently, mass is given in g, density in $g.cm^{-3}$.